

REPORT DOCUMENTATION PAGE

Form Approved
OMB No. 0704-0188

Public reporting burden for this collection of information is estimated to average 1 hour per response, including the time for reviewing instructions, searching existing data sources, gathering and maintaining the data needed, and completing and reviewing the collection of information. Send comments regarding this burden estimate or any other aspect of this collection of information, including suggestions for reducing this burden, to Washington Headquarters Services, Directorate for Information Operations and Reports, 1215 Jefferson Davis Highway, Suite 1204, Arlington, VA 22202-4302, and to the Office of Management and Budget, Paperwork Reduction Project (0704-0188), Washington, DC 20503.

1. AGENCY USE ONLY (Leave blank)		2. REPORT DATE July 18, 1997		3. REPORT TYPE AND DATES COVERED Final Technical Report 15 Aug 95 to 31 Jan 97	
4. TITLE AND SUBTITLE DURIP 95/ ULTRA HIGH PRECISION DIAGNOSTIC HIGH TEMPERATURE LABORATORY				5. FUNDING NUMBERS F49620-95-1-0483	
6. AUTHOR(S) Professor Golam M. Newaz					
7. PERFORMING ORGANIZATION NAME(S) AND ADDRESS(ES) Mechanical Engineering Department Wayne State University Detroit, MI 48202					
9. SPONSORING/MONITORING AGENCY NAME(S) AND ADDRESS(ES) AFOSR/NA 110 Duncan Ave, Suite B 115 Bolling AFB, DC 20332-8050				10. SPONSORING/MONITORING AGENCY REPORT NUMBER F49620-95-1-0483	
11. SUPPLEMENTARY NOTES					
12a. DISTRIBUTION AVAILABILITY STATEMENT Approved for public release; distribution unlimited.				12b. DISTRIBUTION CODE	
13. ABSTRACT (Maximum 200 words) The DURIP grant was used to develop an efficient high temperature laboratory with high precision instruments to make deformation and load measurements in high temperature materials including advanced composites. The laboratory has been successfully developed in Mechanical Engineering Department at Wayne State University under the direction of Professor Golam Newaz - who was the PI of the program. Based on the capability developed, the laboratory can be considered a national resource as extensive capabilities have been integrated with existing facilities in Advanced Composites Research Laboratory at Wayne State University. High temperature testing capabilities include evaluation of mechanical and thermomechanical capabilities up to 2200 F with an induction heating system that is interfaced with modern MTS 810 servohydraulic equipment. Polymeric, ceramic and metal matrix composites including superalloys with thermal barrier coatings can be tested for material properties, fatigue and fracture performance.					
14. SUBJECT TERMS				15. NUMBER OF PAGES	
				16. PRICE CODE	
17. SECURITY CLASSIFICATION OF REPORT Unclassified		18. SECURITY CLASSIFICATION OF THIS PAGE Unclassified		19. SECURITY CLASSIFICATION OF ABSTRACT Unclassified	
				20. LIMITATION OF ABSTRACT UL	

AFOSR-TR-97

C347

DTIC QUALITY INSPECTED 3

Standard Form 298 (Rev. 2-89) (EG)
Prescribed by ANSI Std. Z39-18

FINAL REPORT
ON
DURIP95/ULTRA HIGH PRECISION DIAGNOSTIC HIGH TEMPERATURE
LABORATORY

(AFOSR GRANT # F49620-95-1-0483)

to

Air Force Office of Scientific Research
Bolling AFB
Washington D.C.

from

Professor Golam M. Newaz
Principal Investigator
Mechanical Engineering Department
Wayne State University
Detroit, MI 48202

July 18, 1997

19971006 151

DTIC QUALITY INSPECTED 3

PROJECT SUMMARY

The DURIP grant was used to develop an efficient high temperature laboratory with high precision instruments to make deformation and load measurements in high temperature materials including advanced composites. The laboratory has been successfully developed in Mechanical Engineering Department at Wayne State University under the direction of Professor Golam Newaz - who was the PI of the program. Based on the capability developed, the laboratory can be considered a national resource as extensive capabilities have been integrated with existing facilities in Advanced Composites Research Laboratory at Wayne State University. High temperature testing capabilities include evaluation of mechanical and thermomechanical capabilities up to 2200 F with an induction heating system that is interfaced with modern MTS 810 servohydraulic equipment. Polymeric, ceramic and metal matrix composites including superalloys with thermal barrier coatings can be tested for material properties, fatigue and fracture performance. For aerospace engine applications, a wide variety of material systems with high temperature performance can be evaluated in our laboratory. Another critical competency achieved was in the area of post-test evaluation. An excellent microscopy facility has been developed that can be utilized to interrogate material damage development, progressive cracking, any plastic deformation, material defects and failure modes. An optical microscope with all necessary polishing facilities and photomicrography is now available to investigate deformation and failure in high temperature materials. We are now in the implementation stage to equip our laboratory with a Hopkinson Pressure Bar with high temperature capabilities. With the combined high temperature testing capabilities, the research and teaching environment at WSU shows great promise with regard to advanced high temperature material testing capabilities. With our capabilities we have attracted research dollars from other Air Force

programs through Small Business organizations to the tune of \$300K. There is now additional requests to funding agencies of about \$700K that utilizes the capability of the laboratory. A Ph. D. was granted and there are three Ph.D. students currently utilizing the equipment. A strong educational base has been created as well due the development of this laboratory. The DURIP95 award was for \$275,000. We have expended a total of \$274,261.02 for the program.

The overall high temperature testing capabilities in Mechanical Engineering Department at Wayne State University adds a new strength in educational and research capability of the department. Professor Newaz's expertise is in the area of damage evolution assessment, mechanism-based constitutive response modeling, fatigue and fracture evaluation with emphasis on experimental techniques. The DURIP95 grant was utilized to develop a combined educational and research capability that will continue to help the PI for a long time to come in his research career. Instruments purchased under the DURIP program are listed in the purchase orders enclosed.

A recent professional resume of the PI is attached to show the impact of this laboratory on research accomplishments of the PI including publications. The laboratory is considered vital and without the facilities, attracting research dollars would not be possible. A number of representative publications are also attached which were a direct result of the availability of the instruments in the laboratory.


The laboratory was instrumental for Dr. Saied Nusier to obtain his Ph.D. in February, 1997. Current graduate students include, Mr. M. Abdel-Haq and Mr. Ke Zhang who are utilizing the high temperature laboratory for their thesis work.

LIST OF INSTRUMENTS ORDERED

16. Imprint De,


rector Authorization

Federal Fair Purchase Acquisition

 Wayne State University

三三三

1. Contact for further information: Name/Telephone No./Address Audra L. Duffer 577-3835 Rm. 2109 Mechanical Engineering		Date Prepared 4/1/96	
2. Requisitioner Golam Newaz 577-3877 Rm. 2135 Mechanical Engineering		Required Delivery 5/1/96	
3. Deliver to: (Building, Room No., Attention of) Golam Newaz Rm. 2135 Engineering Bldg.		4. Commodity Selection <input type="checkbox"/> Optional <input checked="" type="checkbox"/> Major Vendor Selection <input type="checkbox"/> Optional <input checked="" type="checkbox"/> Major For Purchase Amount of \$100,000 or more, reverse side of this form MUST be completed.	
5. Suggested Source: Ameritherm, Inc. 39 Main Street Scottsville, NY 14546 FAX # (716) 889-4030 ATTN: Rick Bausch		6. Ship to: Wayne State University 540 E. Canfield	
7. Quantity		8. Part No. and Description	
1	Ameritherm Model #XP7.5/450, 7.5 kW output solid state induction power supply on 220V/3 phase.		9. Cost <input type="checkbox"/> Estimated <input type="checkbox"/> Firm 10. Unit Cost Total \$28,200 \$28,200
1	Loop powered isolator mounted on the 4-20 mA input circuit in the power supply.		\$ 550 \$ 550
	Travel & Living Expenses for installation of equipment.		N/C N/C
	Please Note: Purchase of the installation and start up service will extend the standard one year warranty to two full years. Warranty to cover parts and labor for any defects in material and factory workmanship.		\$1,000.00 \$1,000.00
	Quotation Attached		\$29,750
		11. Purchase Amt.	\$28,750
		12. Est. Fgt. Chg.	\$ 150
		13. Total Amt.	\$28,900

Approved by _____ Date _____		FOR PURCHASING USE ONLY	
15. Imprint Dept. Authorization Card AGCS-18-31244 U.S. AIR FORCE 7495209510-83.0000 HIGH VACUUM & PRECISION GOLAN NEWAZ 08/14/96		20. Vendor Selection Method Code: Other: Vendor: ULTRA DIAGNC 08/14/96	
		21. I.D. Coding Ship to Coding Vendor I.D.	
		23. Quote 24. Terms 25. Delivery 26. F.O.B. 27. Buyer 28. Order No. 29. Date Placed 30. Date Typed	
		G003093 19. Received Purchasing 	



Federal Fur Purchase Requisition

Wayne State University for Purchase of Capital Equipment of \$500.00 or More.

(003091

16. Imprint Del. rector Authorization

17. Account Distribution/Commitment Info:
Account No. Amount

Committed by

Dept. Date

14. Equipment Purchase of \$500.00 or more using Federal Funds: I certify that the equipment requested is needed and have ascertained to the best of my knowledge that no similar equipment is available to me for full or shared usage.

P.I. Authorization

Date

Special Approval

- ☐ Computer Services Center
- ☐ Facilities Planning & Management
- ☐ General Counsel
- ☐ General Services
- ☐ Management Info. Support Center
- ☐ Media Services
- ☐ Office of Research and Sponsored Program Services
- ☐ Other (Specify)

Approved by

Date

15. Imprint Del. Authorization Card

Acct: 3-31224

2001 DAMAGE
VISHS BY
DR. GOL

372

1. Contact for further information: Name/Telephone No./Address

Audra L. Duffer 577-3835 Rm. 2109 Mechanical Engineering

2. Requisitioner Telephone No. Dept./Address

Golan Newaz 577-3877 Rm. 2135 Mechanical Engineering

3. Deliver to: (Building, Room No., Attention of)

Golan Newaz Rm. 2135 Engineering Bldg.

5. Suggested Source:

Telephone No.

6. Ship to: Wayne State University

MTS Systems Corp.

2600 Telegraph Rd., Suite 140 (810) 334-2772 540 E. Canfield

Bloomfield Hills, MI 48302 FAX # (810) 334-3784

ATTN: Robert J. George

7. Quantity

8. Part No. and Description

9. Cost ☐ Estimated ☐ Firm

10. Unit Cost Total

MTS 858 System

\$65000.00 \$65000.00

*See Quotation for Specifications

*Please Note: Dr. Newaz will contact MTS for delivery time. MTS should not deliver immediately.

ENTERED
5/13/96
D.C.

11. Purchase Amt. \$65000.00
12. Est. Fgt. Chg. \$150.00
13. Total Amt. \$65150.00

FOR PURCHASING USE ONLY

20. Vendor Selection Method

23. Quote

24. Terms

25. Delivery

26. F.O.B.

27. Buyer

28. Order No.

29. Date Placed

30. Date Typed

31. I.D. Coding

32. Ship to Coding

33. Vendor I.D.

34. Date Placed

35. Date Typed

36. Ship to Coding

37. Vendor I.D.

38. Date Placed

39. Date Typed

40. Ship to Coding

41. Vendor I.D.

42. Date Placed

43. Date Typed

44. Ship to Coding

45. Vendor I.D.

46. Date Placed

47. Date Typed

48. Ship to Coding

49. Vendor I.D.

50. Date Placed

51. Date Typed

52. Ship to Coding

53. Vendor I.D.

54. Date Placed

55. Date Typed

56. Ship to Coding

57. Vendor I.D.

58. Date Placed

59. Date Typed

60. Ship to Coding

61. Vendor I.D.

62. Date Placed

63. Date Typed

64. Ship to Coding

65. Vendor I.D.

66. Date Placed

67. Date Typed

68. Ship to Coding

69. Vendor I.D.

70. Date Placed

71. Date Typed

72. Ship to Coding

73. Vendor I.D.

74. Date Placed

75. Date Typed

76. Ship to Coding

77. Vendor I.D.

78. Date Placed

79. Date Typed

80. Ship to Coding

81. Vendor I.D.

82. Date Placed

83. Date Typed

84. Ship to Coding

85. Vendor I.D.

86. Date Placed

87. Date Typed

88. Ship to Coding

89. Vendor I.D.

90. Date Placed

91. Date Typed

92. Ship to Coding

93. Vendor I.D.

94. Date Placed

95. Date Typed

96. Ship to Coding

97. Vendor I.D.

98. Date Placed

99. Date Typed

100. Ship to Coding

101. Vendor I.D.

102. Date Placed

103. Date Typed

104. Ship to Coding

105. Vendor I.D.

106. Date Placed

107. Date Typed

108. Ship to Coding

109. Vendor I.D.

110. Date Placed

111. Date Typed

112. Ship to Coding

113. Vendor I.D.

114. Date Placed

115. Date Typed

116. Ship to Coding

117. Vendor I.D.

118. Date Placed

119. Date Typed

120. Ship to Coding

121. Vendor I.D.

122. Date Placed

123. Date Typed

124. Ship to Coding

125. Vendor I.D.

126. Date Placed

127. Date Typed

128. Ship to Coding

129. Vendor I.D.

130. Date Placed

131. Date Typed

132. Ship to Coding

133. Vendor I.D.

134. Date Placed

135. Date Typed

136. Ship to Coding

137. Vendor I.D.

138. Date Placed

139. Date Typed

140. Ship to Coding

141. Vendor I.D.

142. Date Placed

143. Date Typed

144. Ship to Coding

145. Vendor I.D.

146. Date Placed

147. Date Typed

148. Ship to Coding

149. Vendor I.D.

150. Date Placed

151. Date Typed

152. Ship to Coding

153. Vendor I.D.

154. Date Placed

155. Date Typed

156. Ship to Coding

157. Vendor I.D.

158. Date Placed

159. Date Typed

160. Ship to Coding

161. Vendor I.D.

162. Date Placed

163. Date Typed

164. Ship to Coding

165. Vendor I.D.

166. Date Placed

167. Date Typed

168. Ship to Coding

169. Vendor I.D.

170. Date Placed

171. Date Typed

172. Ship to Coding

173. Vendor I.D.

174. Date Placed

175. Date Typed

176. Ship to Coding

177. Vendor I.D.

178. Date Placed

179. Date Typed

180. Ship to Coding

181. Vendor I.D.

182. Date Placed

183. Date Typed

184. Ship to Coding

185. Vendor I.D.

186. Date Placed

187. Date Typed

188. Ship to Coding

189. Vendor I.D.

190. Date Placed

191. Date Typed

192. Ship to Coding

193. Vendor I.D.

194. Date Placed

195. Date Typed

196. Ship to Coding

197. Vendor I.D.

198. Date Placed

199. Date Typed

200. Ship to Coding

201. Vendor I.D.

202. Date Placed

203. Date Typed

204. Ship to Coding

205. Vendor I.D.

206. Date Placed

207. Date Typed

208. Ship to Coding

209. Vendor I.D.

210. Date Placed

211. Date Typed

212. Ship to Coding

213. Vendor I.D.

214. Date Placed

215. Date Typed

216. Ship to Coding

217. Vendor I.D.

218. Date Placed

219. Date Typed

220. Ship to Coding

221. Vendor I.D.

222. Date Placed

223. Date Typed

224. Ship to Coding

225. Vendor I.D.

226. Date Placed

227. Date Typed

228. Ship to Coding

229. Vendor I.D.

230. Date Placed

231. Date Typed

232. Ship to Coding

233. Vendor I.D.

234. Date Placed

235. Date Typed

236. Ship to Coding

237. Vendor I.D.

238. Date Placed

239. Date Typed

240. Ship to Coding

241. Vendor I.D.

242. Date Placed

243. Date Typed

244. Ship to Coding

245. Vendor I.D.

246. Date Placed

247. Date Typed

248. Ship to Coding

249. Vendor I.D.

250. Date Placed

251. Date Typed

252. Ship to Coding

253. Vendor I.D.

254. Date Placed

255. Date Typed

256. Ship to Coding

257. Vendor I.D.

258. Date Placed

259. Date Typed

260. Ship to Coding

261. Vendor I.D.

262. Date Placed

263. Date Typed

264. Ship to Coding

265. Vendor I.D.

266. Date Placed

267. Date Typed

268. Ship to Coding

269. Vendor I.D.

270. Date Placed

271. Date Typed

272. Ship to Coding

273. Vendor I.D.

274. Date Placed

275. Date Typed

276. Ship to Coding

277. Vendor I.D.

278. Date Placed

279. Date Typed

280. Ship to Coding

281. Vendor I.D.

282. Date Placed

283. Date Typed



Federal Funds Purchase Requisition

G'011635

Wayne State University for Purchase of Capital Equipment of \$500.00 or More.

Print Dean/Director Authorization

1. Contact for further information: Name/Telephone No./Address

Andra L. Duffer 577-3835 Rm. 2109 Mechanical Engineering

Date Prepared

8/28/96

2. Requisitioner Telephone No. Dept/Address

Golan Newaz 577-3877 Rm. 2135 Mechanical Engineering

Required Delivery Date(s)

9/28/96

3. Deliver to: (Building, Room No., Attention of)

Golan Newaz Rm. 2135 Engineering Bldg.

4. Commodity Selection:

☐ Optional ☒ Mandatory

Vendor Selection:

☐ Optional ☒ Mandatory

For Purchase Amount of \$2500 or more, reverse side of part one MUST be completed.

PURCHASING USE ONLY

7. Quantity	8. Part No. and Description	9. Cost	10. Unit Cost	11. Estimated Total	12. Firm Total
1	#EX60F3 Microscope Stand for Reflected/Transmitted Light for Olympus B-Max modular system.	\$ 431.20	\$ 431.20	\$ 431.20	\$ 431.20
1	#5-UL110 12V/100W Halogen Light source	\$ 431.20	\$ 431.20	\$ 431.20	\$ 431.20
1	#5-UL111 12V/100W Halogen Light source w/long cord	\$ 28.16	\$ 112.64	\$ 112.64	\$ 112.64
4	#8-C406 12V/100W Halogen Bulb	\$ 14.96	\$ 29.92	\$ 29.92	\$ 29.92
2	#UYCP-11 UYCP Power cord	\$ 519.20	\$ 519.20	\$ 519.20	\$ 519.20
1	#5-UR510 4-place Universal Cassette Module	\$ 618.64	\$ 618.64	\$ 618.64	\$ 618.64
1	#5-UR520 Universal Optical Module	\$ 2725.36	\$ 2725.36	\$ 2725.36	\$ 2725.36
1	#3-U183 Super Widefield Trinocular Observation Tube	\$ 2062.72	\$ 2062.72	\$ 2062.72	\$ 2062.72
1	#3-U803 Double Port Tube				

*Continued on Attached Sheet

*Quote Attached

*Please Note: Credit given to P070752

for returned equipment.

FOR PURCHASING USE ONLY

20. Vendor Selection Method

Code:

Other:

Vendor:

23. Quote

24. Terms

25. Delivery

26. F.O.B.

27. Buyer

28. Order No.

29. Date Placed

30. Date Typed

G 011635

19. Received Purchasing

Account Distribution/Commitment Info: Amount

Typed by

Date

Equipment Purchase of \$500.00 or more using Federal Funds: I certify that the equipment requested is needed and have ascertained to the best of my knowledge that no similar equipment is available to me for full or shared usage.

Authorization

Date

Special Approval

Computer Services Center

Facilities Planning & Management

General Counsel

General Services

Management Info. Support Center

Media Services

Office of Research and Sponsored Program Services

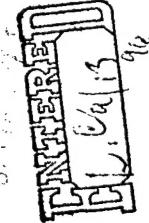
Other (Specify)

Signed by

Date

Print Dept. Authorization Card

See Attached Sheet



Purchase Requisition # G011635 (con't)

<u>Quantity</u>	<u>Part No. & Description</u>	<u>Unit Cost</u>	<u>Total</u>
2	#2-U500H Eyepiece	\$ 212.96	\$ 425.92
1	#U-R255 Brightfield/Darkfield Quintuple Nosepiece	\$ 578.16	\$ 578.16
1	#4-U113 Rectangular Mechanical Stage for Olympus B-MAX microscopes	\$ 401.28	\$ 401.28
1	#6-U110 Abbe Condenser	\$ 122.32	\$ 122.32
1	#U-M501 Brightfield Beamsplitter Cube	\$ 134.64	\$ 134.64
1	#U-M503 Darkfield Beamsplitter Cube	\$ 165.44	\$ 165.44
1	#1-UR522 Universal Plan Fluorite 5x Transmitted Brightfield	\$ 727.00	\$ 727.00
1	#1-UR523 Universal Plan Fluorite 10x Transmitted Brightfield	\$ 999.00	\$ 999.00
1	#1-UR525 Universal Plan Fluorite 20x Transmitted Brightfield	\$1185.00	\$1185.00
1	#1-UR530 Universal Plan Fluorite 50x Transmitted Brightfield	\$1486.00	\$1486.00
1	#1-UR534 Universal Plan Fluorite 100x Transmitted Brightfield	\$2287.00	\$2287.00
1	#2-U504 10x helical superwidefield eyepiece	\$ 290.40	\$ 290.40
1	#U-P210 Polarizer Slider	\$ 439.12	\$ 439.12
1	#U-P219 Analyzer for polarized light	\$ 613.36	\$ 613.36
1	#U-P110 Polarizer for Transmitted light	\$ 154.88	\$ 154.88
1	#9-U573 Filter Slider	\$ 52.80	\$ 52.80
1	#9-U571 Filter Slider	\$ 52.80	\$ 52.80
1	#9-U579 Filter Slider	\$ 18.48	\$ 18.48
1	#U-P200 DIC Prism Slider	\$2492.16	\$2492.16
1	#9-U520 IF550 Filter Slider	\$ 72.16	\$ 72.16
1	#9-B323 45mm diameter Interference Green Filter	\$ 102.96	\$ 102.96
1	#U-P212 POLARIZER TINT PLATE (530NM)	\$ 791.12	\$ 791.12
1	#9-U510 Filter Slider	\$ 45.76	\$ 45.76
1	#7-U311 AUTO EXPOSURE CONTROL BOX	\$3937.12	\$3937.12

<u>Quantity</u>	<u>Part No. & Description</u>	<u>Unit Cost</u>	<u>Total</u>
1	#7-U301 AUTO EXPOSURE BODY-PM30	\$2544.08	\$2544.08
1	#2-U730 3.3X Photoeyepiece	\$ 227.92	\$ 227.92
1	#7-U510 Camera Adapter	\$ 195.36	\$ 195.36
1	#7-U530 35mm Camera Back for DX Coded Film	\$ 752.40	\$ 752.40
1	#7-U620 Adapter for front mounting of Large Format Camera Backs.	\$ 938.96	\$ 938.96
1	#7-U640 Intermediate Adapter for 4" x 5" Large Format Film Holder.	\$ 511.28	\$ 511.28
1	#617878 Polarid "545" sheet film holder	\$ 234.08	\$ 234.08
1	#7-U840 Bright Frame Focusing Viewfinder	\$ 510.40	\$ 510.40
1	#D63BXC Diagnostic Instruments 0.63X C-Mount	\$ 263.12	\$ 263.12

*Olympus Microscopes and accessories are warranted from date of purchase for five (5) years of mechanical and optical components and one (1) year on electrical and electronic components. The Olympus AX70, IX70, and IX50 Microscopes and Microtomes are warranted for one (1) year from the date of purchase on all components. All other accessories, parts or equipment not manufactured by LECO are covered to the extent of warranty provided by the original manufacturer.



Federal Funds Purchase Requisition
for Purchase of Capital Equipment of \$500.00 or More.

G 011634

6. Imprint Dean/Director, Authorization Engineering

Wayne State University

1. Contact for further information: Name/Telephone No./Address
Audra L. Duffer 577-3835 Rm. 2109 Mechanical Engineering

2. Requisitioner
Golam Newaz 577-3877 Rm. 2135 Mechanical Engineering

3. Deliver to: (Building, Room No., Attention of)
**ET Concepts, Inc.
234 Shelford Way
Beavercreek, OH 45440
ATTN: Norman Frey**

4. Commodity Selection:
☐ Optional ☒ Mandatory

5. Suggested Source:
**ET Concepts, Inc.
234 Shelford Way
Beavercreek, OH 45440
ATTN: Norman Frey**

6. Ship to: Wayne State University
540 E. Canfield

Date Prepared
1/23/97

Required Delivery Date(s)
2/23/97

17. Account Distribution/Commitment Info:

Account No. 33/244-6110

Amount 16824.75

Committed by

Dept.

Equipment Purchase of \$500.00 or more
Using Federal Funds: I certify that the
equipment requested is needed and have
ascertained to the best of my knowledge
that no similar equipment is available to
me for full or shared usage.

P.I. Authorization

Golam Newaz 1/24/97

18. Special Approval

- ☐ Computer Services Center
☐ Facilities Planning & Management
☐ General Counsel
☐ General Services
☐ Management Info. Support Center
☐ Media Services
☐ Office of Research and Sponsored Program Services
☐ Other (Specify)

Approved by

Date

15. Imprint Dept. Authorization Card

Acct. #3-31244

FOR PURCHASING USE ONLY

G 011634

19. Received Purchasing

20. Vendor Selection Method

Code:
Other:
Vendor:

23. Quote

24. Terms

25. Delivery

26. F.O.B.

27. Buyer

28. Order No.

29. Date Placed

30. Date Typed

PURCHASING USE ONLY

Unit Cost

9. Cost ☐ Estimated ☐ Firm

10. Unit Cost

11. Purchase Amt. \$16,750.00

12. Est. Fgt. Chg. \$ 54.75

13. Total Amt. \$16,804.75

Special test oven for MTS System test frame

1

8. Part No. and Description

*Quote Attached

16. Imprint Dean/Director Authorization
OFFICE OF ENGINEERING
[Signature]
11/24/97

17. Account Distribution/Commitment Info:
Account No. 331244-6170 Amount 26850.00
Committed by [Signature] Date 11/24/97
Dept.

14. Equipment Purchase of \$500.00 or more using Federal Funds: I certify that the equipment requested is needed and have ascertained to the best of my knowledge that no similar equipment is available to me for full or shared usage.

P.I. Authorization Date
John Newaz 1/24/97

18. Special Approval
☐ Computer Services Center
☐ Facilities Planning & Management
☐ General Counsel
☐ General Services
☐ Management Info. Support Center
☐ Media Services
☐ Office of Research and Sponsored Program Services
☐ Other (Specify)

Approved by Date

15. Imprint Dept. Authorization Card
Acct. #3-31244

[Signature]

Wayne State University
Federal Funds Purchase Requirement
for Purchase of Capital Equipment of \$500.00 or More.

G U I I 0 3 2

1. Contact for further information: Name/Telephone No./Address
Audra L. Duffer 577-3835 Rm. 2109 Mechanical Engineering
2. Requisitioner Telephone No. Dept/Address
Golam Newaz 577-3877 Rm. 2135 Mechanical Engineering
3. Deliver to: (Building, Room No., Attention of)
Golam Newaz Rm. 2135 Engineering Bldg.
4. Requested Source: Telephone No. Ship to: Wayne State University
ABB Autoclave Systems, Inc. 540 E. Canfield
3721 Corporate Drive (614) 891-2732
Columbus, OH 43231 FAX # (614) 891-4568
ATTN: Richard T. Muzyka

7. Quantity	8. Part No. and Description	9. Cost 10. Unit Cost 11. Estimated 12. Total	13. Unit Cost 14. Total
1	One standard model #CIP42260 cold isostatic press	\$25,470	\$25,470
1	One kit of recommended spare parts #SPCIP42260-P1.	\$1,300	\$1,300
	*Quote Attached		

11. Purchase Amt. \$26,770
12. Est. Fgt. Chg. \$80
13. Total Amt. \$26,850

20. Vendor Selection Method
23. Quote
24. Terms
25. Delivery
26. F.O.B.
27. Buyer
28. Order No.
29. Date Placed
30. Date Typed

19. Received Purchasing
G 011632

Wayne State University for Purchase of Capital Equipment of \$500.00 or More.

18. Imprint Dean/Director Authorization

COLLEGE OF ENGINEERING

Requisitioner

Golam Newaz 577-3877 Rm. 2135 Mechanical Engineering Bldg.

Deliver to: (Building, Room No., Attention of)

Golam Newaz Rm. 2135 Engineering Bldg.

Suggested Source:

Ross Engineering Associates, Inc.

237 South Bayshore Drive (904) 678-7880

Valparaiso, FL 32580

ATTN: C. Allen Ross

Ship to: Wayne State University

540 E. Canfield

Account No. 331244 6110

Amount 60,100

Committed by

Dept.

Date 11/24/97

14. Equipment Purchase of \$500.00 or more

using Federal Funds: I certify that the

equipment requested is needed and have

ascertained to the best of my knowledge

that no similar equipment is available to

me for full or shared usage.

P.I. Authorization

Date 11/24/97

18. Special Approval

☐ Computer Services Center

☐ Facilities Planning & Management

☐ General Counsel

☐ General Services

☐ Management Info. Support Center

☐ Media Services

☐ Office of Research and Sponsored Program Services

☐ Other (Specify)

Approved by

Date

15. Imprint Dept. Authorization Card

Acct. #3-31244

Signature

19. Received Purchasing

G 011630

FOR PURCHASING USE ONLY

23. Quote

24. Terms

25. Delivery

26. F.O.B.

27. Buyer

28. Order No.

29. Date Placed

30. Date Typed

21. I.D. Coding

Ship to Coding

Vendor I.D.

20. Vendor Selection Method

Code:

Other:

Vendor:

19. Received Purchasing

G 011630

FOR PURCHASING USE ONLY

23. Quote

24. Terms

25. Delivery

26. F.O.B.

27. Buyer

28. Order No.

29. Date Placed

30. Date Typed

21. I.D. Coding

Ship to Coding

Vendor I.D.

20. Vendor Selection Method

Code:

Other:

Vendor:

19. Received Purchasing

G 011630

FOR PURCHASING USE ONLY

23. Quote

24. Terms

25. Delivery

26. F.O.B.

27. Buyer

28. Order No.

29. Date Placed

30. Date Typed

21. I.D. Coding

Ship to Coding

Vendor I.D.

20. Vendor Selection Method

Code:

Other:

Vendor:

19. Received Purchasing

G 011630

FOR PURCHASING USE ONLY

23. Quote

24. Terms

25. Delivery

26. F.O.B.

27. Buyer

28. Order No.

29. Date Placed

30. Date Typed

21. I.D. Coding

Ship to Coding

Vendor I.D.

20. Vendor Selection Method

Code:

Other:

Vendor:

19. Received Purchasing

G 011630

FOR PURCHASING USE ONLY

23. Quote

24. Terms

25. Delivery

26. F.O.B.

27. Buyer

28. Order No.

29. Date Placed

30. Date Typed

21. I.D. Coding

Ship to Coding

Vendor I.D.

20. Vendor Selection Method

Code:

Other:

Vendor:

19. Received Purchasing

G 011630

FOR PURCHASING USE ONLY

23. Quote

24. Terms

25. Delivery

26. F.O.B.

27. Buyer

28. Order No.

29. Date Placed

30. Date Typed

21. I.D. Coding

Ship to Coding

Vendor I.D.

20. Vendor Selection Method

Code:

Other:

Vendor:

19. Received Purchasing

G 011630

FOR PURCHASING USE ONLY

23. Quote

24. Terms

25. Delivery

26. F.O.B.

27. Buyer

28. Order No.

29. Date Placed

30. Date Typed

21. I.D. Coding

Ship to Coding

Vendor I.D.

20. Vendor Selection Method

Code:

Other:

Vendor:

19. Received Purchasing

G 011630

FOR PURCHASING USE ONLY

23. Quote

24. Terms

25. Delivery

26. F.O.B.

27. Buyer

28. Order No.

29. Date Placed

30. Date Typed

21. I.D. Coding

Ship to Coding

Vendor I.D.

20. Vendor Selection Method

Code:

Other:

Vendor:

19. Received Purchasing

G 011630

FOR PURCHASING USE ONLY

23. Quote

24. Terms

25. Delivery

26. F.O.B.

27. Buyer

28. Order No.

29. Date Placed

30. Date Typed

21. I.D. Coding

Ship to Coding

Vendor I.D.

20. Vendor Selection Method

Code:

Other:

Vendor:

19. Received Purchasing

G 011630

FOR PURCHASING USE ONLY

23. Quote

24. Terms

25. Delivery

26. F.O.B.

27. Buyer

28. Order No.

29. Date Placed

30. Date Typed

21. I.D. Coding

Ship to Coding

Vendor I.D.

20. Vendor Selection Method

Code:

Other:

Vendor:

19. Received Purchasing

G 011630

FOR PURCHASING USE ONLY

23. Quote

24. Terms

25. Delivery

26. F.O.B.

27. Buyer

28. Order No.

29. Date Placed

30. Date Typed

21. I.D. Coding

Ship to Coding

Vendor I.D.

20. Vendor Selection Method

Code:

Other:

Vendor:

19. Received Purchasing

G 011630

FOR PURCHASING USE ONLY

23. Quote

24. Terms

25. Delivery

26. F.O.B.

27. Buyer

28. Order No.

29. Date Placed

30. Date Typed

21. I.D. Coding

Ship to Coding

Vendor I.D.

20. Vendor Selection Method

Code:

Other:

Vendor:

19. Received Purchasing

G 011630

FOR PURCHASING USE ONLY

23. Quote

24. Terms

25. Delivery

26. F.O.B.

27. Buyer

28. Order No.

29. Date Placed

30. Date Typed

21. I.D. Coding

Ship to Coding

Vendor I.D.

20. Vendor Selection Method

Code:

Other:

Vendor:

19. Received Purchasing

G 011630

FOR PURCHASING USE ONLY

23. Quote

24. Terms

25. Delivery

26. F.O.B.

27. Buyer

GULLB33

Federal Funds Purchase Requisition for Purchase of Capital Equipment of \$500.00 or More.

Wayne State University

16. Imprint Dean/Director Authorization

OFFICE OF ENGINEERING

1/24/97

418

33/244-6110

17. Account Distribution/Commitment

Account No. 381305

Committed by

Date 1/24/97

14. Equipment Purchase of \$500.00 or more using Federal Funds: I certify that the equipment requested is needed and have ascertained to the best of my knowledge that no similar equipment is available to me for full or shared usage.

P.I. Authorization

Date 1/24/97

18. Special Approval

☐ Computer Services Center
☐ Facilities Planning & Management
☐ General Counsel
☐ General Services
☐ Management Info. Support Center
☐ Media Services
☐ Office of Research and Sponsored Program Services
☐ Other (Specify)

Approved by

Date

15. Imprint Dept. Authorization Card

Acct. #3-31244

Vendor:

20. Vendor Selection Method

23. Quote

24. Terms

25. Delivery

26. F.O.B.

27. Buyer

28. Order No.

29. Date Placed

30. Date Typed

1. Contact for further information: Name/Telephone No./Address

Audra L. Duffer 577-3835 Rm. 2109 Mechanical Engineering

2. Requisitioner

Golam Newaz 577-3877 Rm. 2135 Mechanical Engineering

3. Deliver to: (Building, Room No., Attention of)

Golam Newaz Rm. 2135 Engineering Bldg.

4. Commodity action:

☐ Optional
☐ Mandatory
☐ Vendor Selection:
☐ Optional
☐ Mandatory
For Purchase Amount of \$2500 or more, reverse side of part one MUST be completed.

5. Suggested Source:

VWR Scientific

P.O. Box 66929

Chicago, IL 60666

6. Ship to: Wayne State University

540 E. Canfield

7. Quantity

8. Part No. and Description

#11378-513 Balance, Galaxy, Mod. GT410

#53880-026 Press, Carver Model M 25Ton

9. Cost

10. Unit Cost

11. Purchase Amt.

12. Est. Fgt. Chg.

13. Total Amt.

19. Received Purchasing

G 011633

FOR PURCHASING USE ONLY

21. I.D. Coding

Shir Coding

Vendor I.D.

PURCHASING DEPARTMENT - DETAIN 7 VENDOR

PHYSIOLOGIC NEUTRALITY, DETAIL 7 V 2 1 2 0

**PROFESSIONAL RESUME OF PI SHOWING CONTRACTS AND
PUBLICATIONS**

WAYNE STATE UNIVERSITY

PROFESSIONAL RECORD

Name: Golam Newaz
Office Address: 2135 Mechanical Engineering
Telephone No: (313) 577-3877

DEPARTMENT: Mechanical Engineering

PRESENT RANK & DATE OF RANK: Professor (January 1, 1995)

CITIZEN OF: United States of America

EDUCATION:

High School: Dhaka College, Dhaka, Bangladesh
Baccalaureate: Nuclear Engineering, Texas A&M University
Graduate: M.S.-Theoretical & Applied Mechanics, University of Illinois @ Urbana-Champaign
Ph.D.: Theoretical & Applied Mechanics, University of Illinois @ Urbana-Champaign
Postgraduate: N/A
Licensure: N/A
Certification: N/A

FACULTY APPOINTMENTS AT OTHER INSTITUTIONS: N/A

PROFESSIONAL SOCIETY MEMBERSHIP(S):

Member, American Society of Mechanical Engineers, 1987-present
Member, American Society of Testing and Materials, 1982-present
Member, American Society for Composites, 1993-present
Member, U.S. Japan Council on Composites, 1992-present

HONORS/AWARDS: Best Paper Award, Society of Plastics Industry Annual Technical Conference, 1983.

BIOGRAPHICAL CITATIONS: Not Checked

I. TEACHING

A. Years at Wayne State:

1. ME 772 Advanced Mechanics of Composites, Winter 1995, Winter 1996, Winter 1997.
2. ME 795 Delamination in Advanced Composites-Directed Study, Winter 1995

3. ME 572 Mechanics of Composite Materials, Fall 1995
4. ME 562 Fracture Mechanics in Engineering Design, Fall 1996

B. Years at Other Colleges/Universities:
University of Illinois @ Urbana-Champaign
TAM 110 Engineering Statics, Fall 1977
TAM 110 Engineering Statics, Winter 1978
TAM 210 Engineering Dynamics, Fall 1978
TAM 110 Engineering Statics, Winter 1979
TAM 110 Engineering Statics, Fall 1979

C. Courses Taught at Wayne State in Last Five Years:

1. Undergraduate: BE 206 Problem Solving & Design
2. Graduate: ME 772 Advanced Mechanics of Composites, Winter 1995
ME 795 Delamination in Advanced Composites (Directed Study), Winter 1995.
ME 572 Mechanics of Composite Materials, Fall 1995
ME 562 Fracture Mechanics in Engineering Design, Fall 1996.
3. Graduate Professional School: N/A

D. Essays/Theses/Dissertations Directed:

M.S. Theses:

1. "Analysis of Mixed-Mode Crack Growth in CMC", M. Krishnappa, July 1996.
2. "Evaluation of Innovative Strain-Gage Application to Polymer Test Samples", S. Sterbenz, October 1996.

Ph.D. Dissertations:

1. "Damage Accumulation and Failure in TBC", S.Q. Nusier, Feb. 1997.

II. RESEARCH

A. Research in Progress:

1. Inelastic Deformation Mechanisms in Metal Matrix Composites in Compression
2. Damage Accumulation Mechanisms in Thermal Barrier Coated Superalloys
3. Analysis of Mixed-Mode Crack Growth in Ceramic Matrix Composite
4. Crushing & Energy Absorption in Composite Tubes
5. Tribological Behavior of Cylinder Liner Materials

B. Funded Research in Last Five Years

1. "Inelastic Deformation Mechanisms in Metal Matrix Composites in Compression", G. Newaz-Principal Investigator, AFOSR, \$319,000 over two years, Feb. 1993-Dec. 1994.
2. "Life Prediction of Ceramic Matrix Composite", G. Newaz-Principal Investigator, Air Force Materials Directorate, PRDA IV Program with Pratt & Whitney and UTRC, \$550,000 over three years, Oct. 1993-present.
3. "Thermomechanical Fatigue of Metal Matrix Composites", G. Newaz and B. Majumdar Co-Principal Investigators, NASA NRA Program, \$154,000 over two years, January 1993-December 1994.
4. "Isothermal Fatigue Mechanisms in Metal Matrix Composite", G. Newaz and B. Majumdar Co-Principal Investigators, NASA NRA Program, \$140,000 over one year, January 1992-December 1992.
5. "Inelastic Deformation Mechanisms under Monotonic Loading in Metal Matrix Composites", G. Newaz and B. Majumdar Co-Principal Investigators, NASA NRA Program, \$125,000 over one year, January 1991-December 1991.
6. "Delamination Growth in Ceramic Matrix Composites", G. Newaz-Principal Investigator, GE/NASA EPM Program, \$84,000 over 1.5 years, January 1994-present.
7. "Damage Accumulation Mechanisms in Thermal Barrier Coatings", G. Newaz-Principal Investigator, AFOSR, \$240,000 over three years, March 1995-present.
8. "Life Prediction of Ceramic Composites", G. Newaz-Principal Investigator, Battelle/U.S. Air Force, \$39,500, August 1995-December 1996.
9. "High Temperature Laboratory Development", G. Newaz-Principal Investigator, AFOSR DURIP Grant, \$275,000, June 1995-February 1997.
10. "Design Tool for Oxidation in TBC", G. Newaz-Principal Investigator, RAI/U.S. Army, \$24,500, January 1996-December 1996.
11. "Dual Applications of MMC: Phase I", G. Newaz-Principal Investigator, RAI/U.S. Air Force, \$21,000, June 1995-May 1996.
12. "Damage Tolerance of PMC", G. Newaz-Principal Investigator, \$21,000, RAI/U.S. Air Force, January 1996-December 1996.
13. "Dual Applications for MMC: Phase II", G. Newaz-Principal Investigator, \$224,000, RAI/U.S. Air Force, June 1996-May 1998.
14. "REU Program-Summer Internship", Co-PI-G. Newaz and R.F. Gibson, Ford Motor Company, \$20,000, 1996.
15. "REU Program-Summer Internship", Co-PI-G. Newaz and R.F. Gibson, Ford Motor Company, \$16,500, 1997.
16. "Advances in Composites Manufacturing Workshop", Co-PI - G. Newaz and R.F. Gibson, National Science Foundation, \$19,161, 1997.

17. "Fatigue Methodology for Short-Fiber Composites", G. Newaz - Principal Investigator, Automotive Composites Consortium (Ford/GM/Chrysler), \$33,900, 1997

III. PUBLICATION

A. Scholarly Books Published

1. Newaz, G.M., (with Sierakowski, R.L.), "Damage Tolerance of Advanced Composites", Technomic Publishing Co., Lancaster, PA, 1995.

B. Chapters Published

1. Newaz, G.M., "Polymer Composites", in Materials Science and Technology Series, VCH, Weinham, Germany, 1994.
2. Newaz, G.M., "Mechanical Behavior of Metal Matrix Composites", in Advances in Metal Matrix Composites, in press, S. Mall and T. Nicholas, Editors, Technomic Publication Co., Lancaster, PA, 1997.

C. Editorships of Book/Proceedings

1. Newaz, G.M., "Delamination of Advanced Composites", Technomic Publishing Co., Lancaster, PA, 1993.

D. Journal Articles Published

Refereed Journals

1. Newaz, G.M., Nusier, S.Q., and Chaudhury, Z.A., 1996, "Damage Accumulation Mechanisms in Thermal Barrier Coatings", accepted for publication in ASME J. of Engineering Materials and Technology, 1997.
2. Chaudhury, Z.A., Newaz, G.M., Nusier, S.Q., and Ahmed, T., "Interfacial Damage in EB-PVD Thermal Barrier Coatings Due to Thermal Cycling", in press, J. of Materials Science and Engineering, 1996.
3. Nusier, S.Q., and Newaz, G.M., "Analysis of Interfacial Cracks in a TBC/Superalloy System Under Thermomechanical Loading", accepted for publication in the ASME J. of Engineering for Gas Turbines and Power, 1997.
4. Newaz, G.M., and Bonora, N., "Fatigue Life Modeling of Hybrid CMC", ASTM STP 1309, Amer. Soc. for Testing and Materials, 1996.
5. Rahman, M. and Newaz, G.M., "Elastostatic Surface Displacements of a Half-Space Reinforced by a Thin Film Due to an Axial Ring Load", in press, International Journal of Engineering Science, 1996.
6. Bonora, N., and Newaz, G.M., "Modeling Damage Evolution in a Hybrid Ceramic Matrix Composite Under Static Tensile Load", in press, ASME J. of Engineering Materials and Technology, 1997.

7. Bonora, N., and Newaz, G.M., "Low-Cycle Fatigue Life Estimation for Ductile Metals Using a Nonlinear Continuum Damage Mechanics Model", accepted for publication in International J. of Solids and Structures, 1997.
8. Newaz, G.M., and Majumdar, B.S., "In-Phase Thermomechanical Fatigue of MMC Deformation Response and Progressive Damage Mechanisms", ASTM STP 1274, 264, (1996).
9. Newaz, G.M., "Constitutive Response and Deformation Mechanisms in Unidirectional MMC Under Compression", ASTM STP 1274, 278, (1996).
10. Newaz, G.M., Majumdar, B.S., Brust, F.W., "Inelastic Deformation Mechanisms in SCS-6/Ti 15-3 MMC Lamina Under Compression", ASTM STP 1258, (1996).
11. Newaz, G.M., and Majumdar, B.S., "Failure Modes in Transverse MMC Lamina Under Compression", J. of Materials Science & Letters, UK, 12: 551-552, (1993).
12. Newaz, G.M., and Majumdar, B.S., "A Comparison of Mechanical Response of MMC at Room and Elevated Temperatures", J. of Composites, Science & Technology, UK, 50: 85-90, (1993).
13. Newaz, G.M., Majumdar, B.S. and Brust, F.W., "Thermal Cycling Response of Quasi-Isotropic Metal-Matrix Composite", J. of Eng. Materials and Technology, Vol. 114, #2, 156-161, (1992).
14. Newaz, G.M., Majumdar, B.S., "Fatigue Crack Initiation Around Holes in MMC", Engineering Fracture Mechanics, Vol. 42, #4, 699-711, 1992.
15. Uralil, F.S., Newaz, G.M., and Lustiger A., "Processing Effects and Damage Tolerance in PEEK Composites", appeared in the J. of Polymer Composites, 12: 35-51, (1991).
16. Lustiger A., and Newaz, G.M., "Interlaminar Failure and Craze Growth in PEEK Composites Under Cyclic Loading", J. of Composite Materials, Vol. 24, 175-187, Feb. 1990.
17. Lustiger, A., and Newaz, G.M., "Processing and Structural Optimization of PEEK Composites: Mechanical Response and Morphology", Journal of Polymer Composites, Vol. 11, #1, 65-75, (1990).
18. Newaz, G.M. and Mall S., "Relaxation-Controlled Delamination Growth in Advanced Thermoset and Thermoplastic Composites Under Fatigue Loading at Elevated Temperature", Journal of Composite Materials, Vol. 23, #2, 133-145, (1989).
19. Newaz, G.M., and Walsh, W.J., "Interrelationship of Damage and Strain in Particulate Composites", J. of Composite Materials, Vol. 23, #4, 326-336, (1989).
20. Newaz, G.M., and Ahmad, J., "A Simple Technique for Measuring Mode I Delamination Energy Release Rate in Polymetric Composites", Engineering Fracture Mechanics, Vol. 3, #4, 541-552, (1989).

21. Newaz, G.M., and Yung, J.Y., "Modeling Split Crack Growth Behavior in Unidirectional Composites Under Fatigue Loading", Engineering Fracture Mechanics, Vol. 29, #4, 483-495, (1988).
22. Newaz, G.M., "On the Validity of Orthotropic Fracture Model for Advanced Thermoplastic Composites", Engineering Fracture Mechanics, Vol. 29, #1, 19-26, (1988).
23. Newaz, G.M., Lustiger, A., and Yung, J.Y., "Delamination Growth Under Cyclic Loading in Thermoplastic Composites at Elevated Temperature", ASTM STP 1044, Advances in Thermoplastic Matrix Composite Materials, Newaz, G.M., Editor, 263-278, (1988).
24. Rodriguez, E.L., and Newaz, G.M., "Effect of Surface Treatment on Sandfilled Composites", J. of Polymer Composites, Vol. 9, #1, 93-102, (1988).
25. Newaz, G.M., "Microstructural Aspects of Crack Propagation in Filled Polymers", Fractography of Modern Engineering Materials, ASTM STP 948, Eds., Masters, J.E. and Au, J.J., 17-188, (1987).
26. Newaz, G.M., "A Fractographic Investigation of Fatigue Damage in Carburized Steel", Fractography of Modern Engineering Materials, ASTM STP 948, Eds., Masters, J.E. and Au, J.J., 3-33, (1987).
27. Mall, S., and Newaz, G.M., "Effect Filler Size and Matrix Ductility on Fracture Toughness of Polyester Composite", J. Reinforced Plastics and Composites, 6, (2), 138-152, (April 1987).
28. Newaz, G.M., "Fracture in Particulate Composites", J. Matls. Science Letters, 5, 71-72, (1986).
29. Newaz, G.M., "Tensile Behavior of Clay-Filled Polyester Composites", J. Polymer Composites, Vol. 7, #3, 176-181, (1986).
30. Newaz, G.M., "Evaluation of Interphasial Toughness in Unidirectional Composites", J. Polymer Composites, 7, 6, 421-425, (1986).
31. Newaz, G.M., "Fatigue Damage Growth Rate in Unidirectional Composites in Flexural Loading", J. Matl. Science Letters, 4, 197-199, (1985).
32. Newaz, G.M., "On Interfacial Failure in Notched Unidirectional Glass/Epoxy Composites", J. Composite Materials, 19 (3), 276-286, (May 1985).
33. Newaz, G.M., "A Quantitative Assessment of Debonding in Unidirectional Composites Under Long-Term Loading", J. Reinforced Plastics and Composites, 4, 354-364, (October 1985).
34. Newaz, G.M., "Influence of Matrix Material on Flexural Fatigue Performance in Unidirectional Composites", Composite Science and Technology-An International Journal, Vol. 24, #3, 199-214, (1985).
35. Newaz, G.M., "Transverse Toughness as a Material Characterization Parameter for Unidirectional Composites", SAMPE Quarterly, 15, (2), 20-26, (1984).

36. Newaz, G.M., "Analysis of Flexural Fatigue Damage in Unidirectional Composites", High Module Fiber Composites in Ground Transportation and High Volume Applications, Edited by D.W. Wilson, ASTM STP 873, 51-64, (1983).
37. Joneja, S.K. and Newaz, G.M., "Influence of Defects on Fracture Toughness and Impact Characteristics of a Hybrid Composite System: Polyester/Glass Fiber and Sand", Effect of Defect in Composite Materials, Edited by D.J. Wilkins, ASTM STP 836, 1-11, (1982).

E. Paper Published in Conference Proceedings

Refereed Papers

1. Newaz, G.M., "Compressive Response of MMC", Durability of Composite Marterials, Editor, R.C. Wethrehold, MD., Vol. 51, American Society of Mechanical Engineers, 13-28, (1995).
2. Newaz, G.M., Brust, F.W., Jarmon, D.C., and Cairo, R.R., "Mechanical Response Modeling Dual Fiber CMC", to be presented at the American Ceramic Society Annual Meeting, Cocoa Beach, Florida, January 12-14, 1994.
3. Newaz, G.M., and Majumdar, B.S., "Deformation and Damage Mechanisms in MMC Under Isothermal and TMF Loading", presented at the ASTM Symposium, Montreal, May 16-17, 1994.
4. Newaz, G.M., Majumdar, B.S., and Brust, F.W., "Inelastic Deformation Mechanisms in Ti 15-3/SCS-6 Lamina Under Compression", Invited Paper, ASTM Symposium on Life Prediction of Titanium Composites" (to appear in an ASTM STP), Hilton Head, S. Carolina, March 22-24, 1994.
5. Newaz, G.M., "Evaluation and Modeling of Mechanical Response and Strength of MMC in Compression", presented at the Air Force Mechanics Composites Review Meeting, Dayton, OH, Dec. 7-8, 1993.
6. Newaz, G.M., "Inelastic Response of Off-Axis MMC Lamina", presented at the 6th Meeting of National Institute for Mechanics and Life Prediction of Composites (NIC), Cleveland, OH, November 3, 1993.
7. Newaz, G.M., "Deformation and Failure of High Temperature Metal Matrix Composites", Keynote Speaker, Italian Group of Fracture (IGF9), Rome, Italy, June 1993.
8. Newaz, G.M., "Compression Behavior of Unidirectional MMC", Invited Paper, Air Force, Titanium Metal Matrix Composite Workshop II, LaJolla, CA, June 1993.
9. Newaz, G.M., "Comparison of Inelastic Deformation in Transverse Lamina under Tension and Compression", Invited Lecture in MEET'N 93-Joint ASME-ASCE-SEM Meeting, Charlottesville, VA, June 7-8, 1993.

10. Newaz, G.M., and Majumdar, B.S., "Damage and Plasticity in MMC: Implications on Constitutive Modeling", proceedings of the Ninth International Conference on Composite Materials (ICCM-9), Madrid, Spain, July 12-16, 1993.
11. Sierakowski, R. and Newaz, G.M., "Damage Tolerance in Advanced Composites: A Review of Key Elements", proceedings of the 8th American Society for Composites Annual Conference, Cleveland, OH, October 17-19, 1993.
12. Brust, F.W. and Newaz, G.M., "Computational Micromechanics Modeling of Loading-Unloading Response in MMC in Compression", proceedings of the 8th American Society for Composites Annual Conference, Cleveland, OH, October 17-19, 1993.
13. Brust, F.W., Newaz, G.M., and Majumdar, B.S., "Damage Development in Metal Matrix Composites Including Plasticity and Creep Effects", presented at the 8th International Conference on Fracture (ICF8), Kiev, Ukraine, June 8-14, 1993.
14. Newaz, G.M., and Majumdar, B.S., "Deformation and Failure Mechanisms in MMC", ASME AD-Vol. 22/AMD. Vol. 122, 55 (1992).

IV. SERVICE

- A. Administrative Appointments at WSU: N/A
- B. Administrative Appointments at Other College/Universities: N/A
- C. Committee Assignments in Last Five Years: N/A
- D. Positions Held in Professional Associations: None
- E. Membership in Private or Public Agencies Related to Discipline: None
- F. Professional Consultation

Lockheed	1990-present
US Navy	1989-1994
Pratt & Whitney	1992-present
Sealy	1994
- G. Journal/Editorial Activity

Editorial Board-ASTM Journal of Testing Evaluation
Editorial Board-Advanced Performance Materials, Kluwer Publications
- H. Other Professional Related Service:

Member:	ASME Materials Division/Symposia Organizer
Member:	ASME Aerospace Division/Symposia Organizer

**REPRESENTATIVE PUBLICATIONS AS AN OUTCOME UTILIZING THE
DURIP HIGH TEMPERATURE PRECISION DIAGNOSTICS LABORATORY**

*To be presented at Amer. Soc. for Composites Conference
Densborn, Oct, 1997
In review: J. of Composite Materials*

Analysis of Quasi-Isotropic MMC Using Iosipescu Shear Test

*K. Zhang and G. M. Newaz
Mechanical Engineering Department
Wayne State University
Detroit, Michigan*

*and
S. Chandu and J. Ahmad
Research Applications, Inc.
Dayton, Ohio*

ABSTRACT

The shear constitutive response and deformation mechanisms under Iosipescu test for a quasi-isotropic, $[0/+45/-45/90]_s$ laminate made from TMIETAL 21S/SCS-6 MMC were investigated using a combination of mechanical measurement, microstructure analysis and finite element method. The objectives were to evaluate the material response using the Iosipescu test and attempt to establish Iosipescu test as a reasonable routine measurement for properties under shearing loading for Quasi-isotropic MMCs. Shear induced inelastic deformation is dominant due to plasticity which is associated with slip bands and damage which includes matrix grain boundary cracks, reaction zone cracks, debonding and fiber cracks. The prediction for the constitutive response using finite element analysis fits test data very well. The correlation of predicted results with experimental data shows that Iosipescu shear test is a valid method to investigate shear properties of quasi-isotropic MMC laminates.

INTRODUCTION

Considerable research to date has been conducted in characterizing silicon-carbide (SiC) fiber-reinforced titanium composites to understand their monotonic behavior (Sun and Chen 1989; Pindera, 1989; Sun *et al.* 1990; Newaz and Majumdar, 1991; Majumdar and Newaz, 1992; Newaz and Majumdar, 1993; Brust, Majumdar and Newaz, 1993; Newaz and Majumdar, 1994; Gao and Zhao, 1995; Allen Jones and Boyd, 1994; Newaz, Majumdar and Brust, 1996; Newaz and Zhang, 1996). One important aspect is a continuing effort to understand and model the composite's constitutive response and failure conditions.

Constitutive modeling and inelastic deformation mechanisms have been studied extensively for longitudinal and transverse MMC laminates. However, little attention has been paid to investigate the constitutive response of pure shearing loading on MMCs, especially for the differently oriented ply-stacked laminate, its inelastic deformation mechanisms and the evolution of damage to failure. Furthermore, properties and constitutive response under pure shearing loading for MMCs using a reliable test technique has not been identified to date.

A variety of test methods are available for introducing shear stresses in unidirectional

fiber MMCs. However, all of the tests have inherent deficiencies or disadvantages. The most uniform shear strain-stress state can be achieved in a MMC by applying torsional loading to a thin-walled tube specimen. However, such specimens are expensive requiring special fixtures and process techniques. The Iosipescu Test standard as explained in ASTM D 5379M-93 is recommended for in-plane shear testing specimens with unidirectional, cross-ply, woven composite and short-fiber composites. Tests on MMCs of continuous fibers are not within the scope of the standard. Iosipescu test has been conducted with various composites (Adams and Lewis 1995; Pindera, Ifju and Post, 1990; Swanson, Messick and Toombes, 1985; Morton *et al.*, 1992). For continuous fiber MMCs, especially oriented ply-stacked MMCs, some limited analysis has been performed as well (Santhosh and Ahmad, 1992; Chandu, Ahmad and Newaz, 1997).

For metal matrix composites, the tubular specimens can be quite expensive. Testing of tubes also requires specially designed fixtures (Swanson, Messick and Toombes, 1985). Off-axis tensile tests are not ideal for generating shear properties for titanium based metal matrix composites because of the relatively strong interaction of the transverse normal stress and shear stress at all possible angles due to the nature of orthotropy in a single ply. Also, off-axis tests are not applicable for multi-ply oriented laminates. The most reasonable approaches for shear testing of MMCs appear to be the Iosipescu test and $[\pm 45]_s$ tension test. The specific advantage of the Iosipescu shear test is the ability to develop pure shear stresses in a line zone between the two notches in the specimen. For ± 45 tension test, the shear properties are estimated after manipulating tension strain data in the normal and transverse directions. In this test, the plies in the lamina are subjected to both transverse normal and shear stresses.

EXPERIMENTAL APPROACH

The material for testing was Ti 15-3/SCS-6 composite of 8-ply unidirectional for off-axis tension test and 8-ply quasi-isotropic $[0/+45/-45/90]_s$ lay-up for Iosipescu shear tests, approximately 0.00785-inch thick each ply with a fiber volume fraction of approximately 0.34. The SCS-6 (SiC) fiber diameter is approximately 140 μm .

The test specimens were cut from an electric-discharge machining (EDM) technique and then mechanically polished after EDM machining to remove any damage associated with the machining. Monotonic loading was applied at room temperature. All specimens were tested in the as-fabricated condition, i.e., no heat-treatment was performed prior to the testing.

The dimensions of a specimen with a test fixture and a strain gage (Micro-measurements, A2P-08-C085C-500) designed for pure shear strain measurement is shown in figure 1. The tests were performed at MTS test machine with an Iosipescu fixture. The strain data came from the strain gage and the stress data from the loading value divided by the cross section area between the notch tips. The specimens were loaded to a different deformation levels then unloaded to zero to investigate the constitutive response in both elastic and inelastic regimes and to determine how consistent are the elastic shear modulus, yielding and hardening tendency. Unloading from different loading levels, the zero-load strain offset, plasticity versus damage effects in nonlinear regime can be analyzed. In order to obtain information about shear failure of 8-ply quasi-isotropic $[0/+45/-45/90]_s$ Ti 15-3/SCS-6 composite, one of the specimens was loaded until its

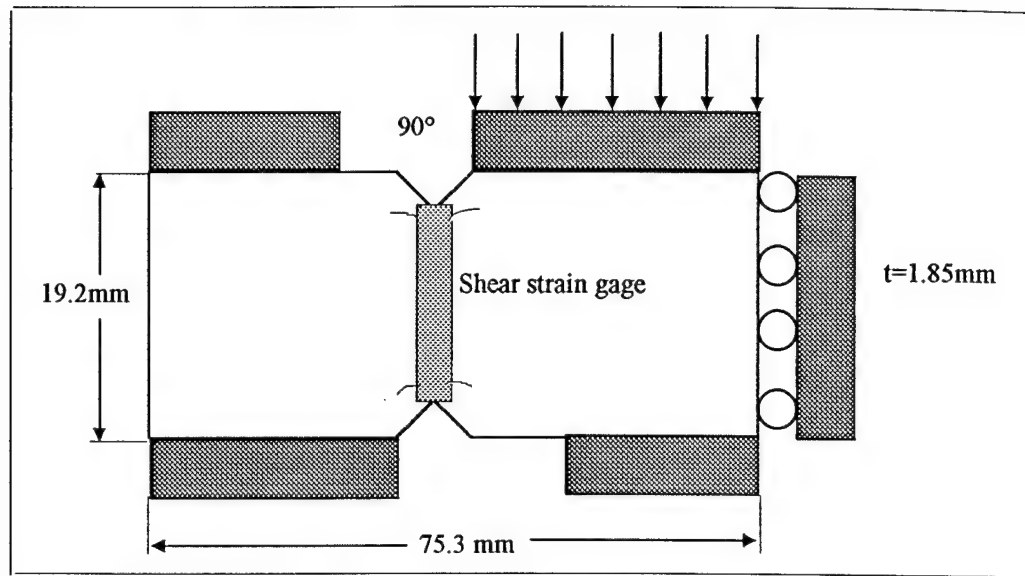


Figure 1. Dimensions of an Iosipescu test specimen with strain gage under loading fixture.

failure. Following mechanical testing, specimens were sectioned using a diamond wafering blade; debonding and fiber cracking can be significant during machining if adequate care is not taken during sectioning. Specimens were metallographically polished up to the first set of fibers. Specimens were etched using Kroll's reagent, which was found to be effective in revealing matrix damage and slip bands

RESULTS AND DISCUSSION

MECHANICAL BEHAVIOR

TABLE I shows the Iosipescu test results for specimens OH3-2, OH3-4, OH3-8 and OH3-12. It can be seen that the apparent yield stress was in the range of 200 MPa to 270 MPa and the corresponding yielding strain ranged from 0.0038 to 0.005.

TABLE I IOSIPESCU SHEAR TEST RESULTS

Specimen Number	Elastic Shear Modulus (GPa)	Maximum Stress (MPa)	Maximum Strain	Apparent Yield Stress (MPa)	Apparent Yield Strain	Unload Strain Offset	Failure Stress (MPa) / Failure Strain
OH3-2	55	757	0.021	270	0.0045	X	757/0.021
OH3-4	48	434	0.01	250	0.005	0.0004	X
OH3-8	54	559	0.014	200	0.0038	0.0017	X
OH3-12	48	659	0.017	250	0.005	0.0028	X

The elastic shear modulus are within 48 MPa to 55 MPa. Specimen OH3-2 failed with notched region pure shear stress reaching 757 MPa and strain reaching to 0.021.

Figure 2 shows the shear response for these specimens. For specimen OH3-4 the maximum shear stress was 434 MPa with maximum shear strain reaching 0.01. The specimen then was unloaded to zero. The curve shows that (a) there was no obvious turning point between elastic and inelastic regimes though the curve slope began decreasing gradually after about 250MPa. This was also the case for the other specimens; (b) the unloading slope decreased and zero-load strain offset are due to associated damage and plasticity respectively. The nonlinearity of the unloading curve near zero-load might be caused by damage closure. Figure 3 is a photo-micrograph of etched specimen OH3-4 in the notched zone (strain gage covered zone). There were apparent cracks along grain boundaries and the fiber and matrix bonding reaction zone. Stiffness loss experienced in the unloading curve is due to damage in the net section area of the specimen.

For specimen OH3-8, the maximum shear stress applied was 559 MPa with corresponding maximum shear strain up to 0.014. The specimen was then unloaded to zero. The curve shows a consistent tendency as that of OH3-4 except in the unloading period. The zero-load strain offset means that plasticity took a dominant role in the inelastic deformation regime. Figure 4 illustrates obvious matrix slip bands in etched OH3-8 specimen. These slip bands are associated with the plastic deformation mechanism.

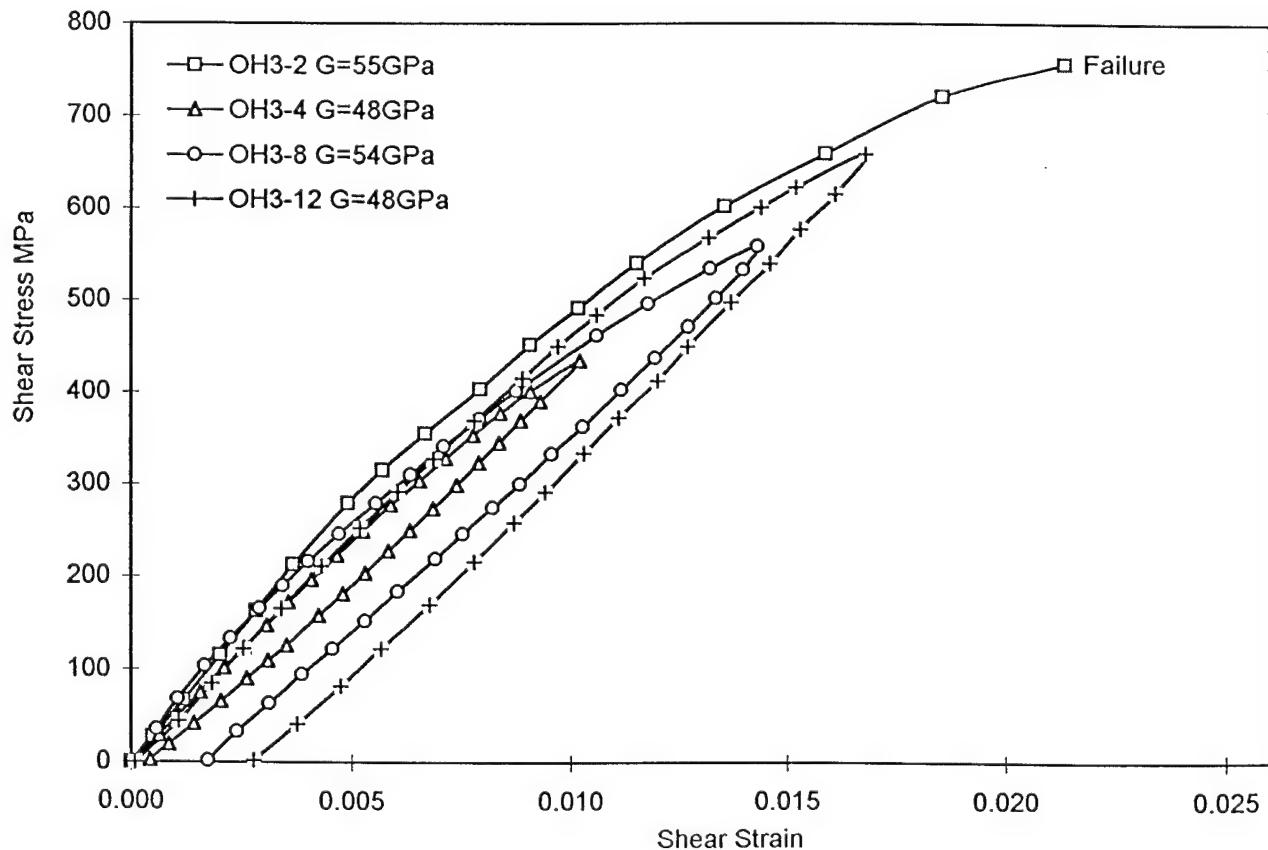


Figure 2. Mechanical response for Iosipescu test specimens of Quasi-isotropic laminate made of TMIETAL 21S/SCS-6 MMC.

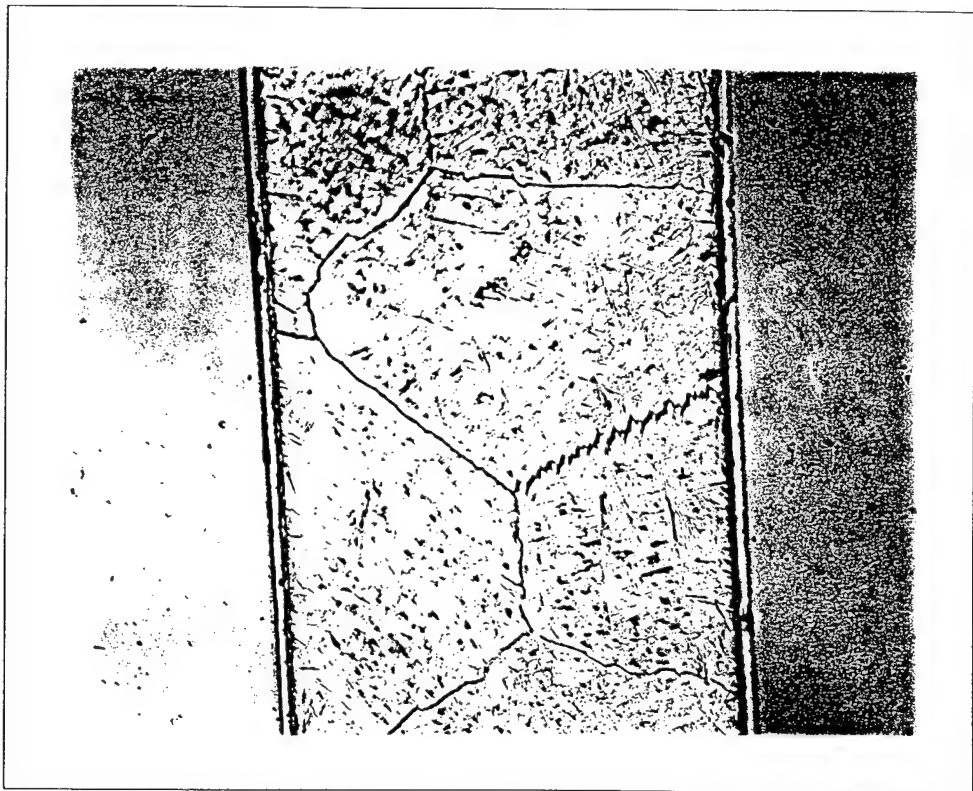


Figure 3. Etched microstructure (x500) of specimen OH3-4 in strain gage covered zone, cracks along grain boundaries and bonding reaction zone.

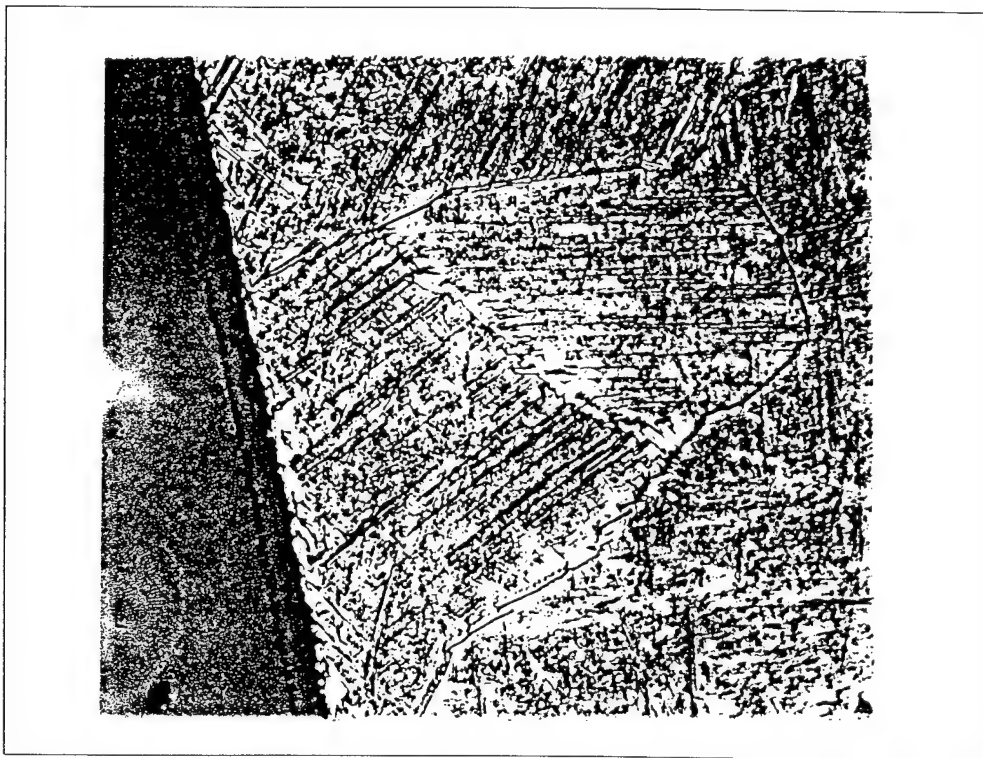


Figure 4. Etched microstructure (x1000) of specimen OH3-8, slip bands initiated from grain boundaries and bonding reaction zones.

CONSTITUTIVE RESPONSE MODELING

For the $[0/+45/-45/90]_s$ laminate, each laminae of the TMIETAL 21S/SCS-6 MMC is treated as an anisotropic ply. The laminate properties depend on the individual plies. In the model, each ply is modeled as a separate layer and connected to other plies through common nodes. The model is based on a plane stress analysis. In the inelastic range, the deformation becomes much more complex and the hardening effects are significant. It is necessary to determine inelastic equivalent stress, σ_e , like what we have in the case of homogenous plastic deformation. With a formulation regarding σ_e , we can relate our test data (monotonic tension test, for instance) to our analysis. Here we have according to Sun (1989):

$$\sigma_e = \left[\frac{3}{2} (\sigma_{22}^2 + 2 a_{66} \sigma_{12}^2) \right]^{1/2} \quad (1)$$

where, σ_e represents equivalent inelastic stress and 1 represents fiber direction, 2 is 90° of the fiber direction (transverse). σ_{22} represents the transverse stress of a MMC laminae. σ_{12} represents the in-plane shear stress. σ_{11} represents stress in the fiber direction.

Sun (Sun *et al.*, 1990) assumed that only the transverse normal stress σ_{22} and in plane-shear stress σ_{12} of composite contribute to inelastic deformation. Whereas the longitudinal (fiber direction) σ_{11} stress does not affect inelastic deformation though it contributes to elastic deformation. This is in fact not true. The nonlinear deformation starts after the tension stress reached approximately 1100 MPa (Majumdar and Newaz 1992). But here we can take Sun's assumption as an approximation to simplify our calculation. With Sun's equation if we relate it to the 90° tension test data (Newaz and Zhang, 1997) as yield and hardening reference in an analysis, then for this situation (transverse loading), $\sigma_{12}=0$, and Sun's formula becomes:

$$\sigma_e = \left[\frac{3}{2} \sigma_{22}^2 \right]^{1/2} \quad (2)$$

This case, the apparent yield stress is

$$\sigma_e = \sigma_y = 250 \text{ MPa (test data)} \quad (3)$$

For off axis monotonic tension test.

$$\sigma_{11} = \sigma_x \cos^2 \theta \quad (4)$$

$$\sigma_{22} = \sigma_x \cos \theta \sin \theta \quad (5)$$

$$\sigma_{12} = \sigma_x \sin^2 \theta \quad (6)$$

at $\theta = 10^\circ$ we have

$$\sigma_{11} = 0.970 \sigma_x \quad (7)$$

$$\sigma_{22} = 0.030\sigma_x \quad (8)$$

$$\sigma_{12} = -0.171\sigma_x \quad (9)$$

Putting these value into Sun's formula, we get:

$$\sigma_e = \left[\frac{3}{2} ((0.970\sigma_x)^2 + 2 a_{66} (-0.171\sigma_x)^2) \right]^{1/2} \quad (10)$$

where x is loading direction, and θ is the angle between fiber direction and loading direction.

From the test data (Newaz and Zhang, 1997), the apparent yield stress for 10° tension loading at x direction is $\sigma_x = 850$ MPa. Whereas with transverse tension test we already know that yielding equivalent stress is 250 MPa. With this information, we can get a_{66} which is approximately about 1.46. For MMC inelastic deformation includes not only plastic but damage - matrix grain boundary cracks, fiber and matrix bond separation and fiber cracks-effect too. Therefore, we should take both effects into the account in determining parameter a_{66} . We can modify Sun's model by choosing a suitable value of a_{66} . In Sun's paper (Sun *et al.*, 1990) $a_{66} = 0.5$ was chosen to fit the yield stress test curve of different angles of off-axis monotonic tension tests for SCS-6/Ti-6-4 MMC. But for $[0/+45/-45/90]_s$ laminate, shear test model in which the plies stacked have different orientation, the situation is more complicated. Analysis also shows that in different elements of the model either transverse tension stresses or transverse compression stresses is in effect in addition to shear stresses. And different stress state combination has different yield and hardening condition. From test data the transverse compression yield stress (750 MPa in Newaz, Majumdar and Brust, 1996) is much higher than the transverse tension yield stress (250 MPa in Newaz and Zhang, 1997). Here we can still use equation (1) for both tension and compression occasions, but choose $a_{66} = 0.4$, $\sigma_y = 250$ MPa (yield) for a case when $\sigma_{22} > 0$ in an element; choose $b_{66} = 0.5$, $\sigma_y = 750$ MPa (yield) for a case when $\sigma_{22} < 0$ in an element. During the analysis we use FORTRAN subroutine to check each element in different plies to see whether $\sigma_{22} > 0$ or $\sigma_{22} < 0$ to determine the field parameter and then apply tension hardening condition or compression hardening condition to the element accordingly. We used the transverse (90°) monotonic tension and compression test data as the hardening reference for the analysis.

FINITE ELEMENT ANALYSIS RESULTS

We used ABAQUS code to simulate a monotonic loading Iosipescu shear test for TMIETAL 21S/SCS-6 MMC $[0/+45/-45/90]_s$ laminate. Figure 5 shows the comparison of the constitutive responses between the FEA predication and the tested specimen OH3-8. The calculated response comes from the center portion elements of the notch zone (strain gage covered zone) of the surface layer, it is found that if the elements were taken from the 80% of the central portion between two notch tips, then the calculated curves can fit the test results well, otherwise the calculated response may be lower than the measured value. It can be seen that the calculated result fits the test data very well. Unlike the testing response, the calculated unloading stiffness, remained the same as the loading one. This is because the FEA model did

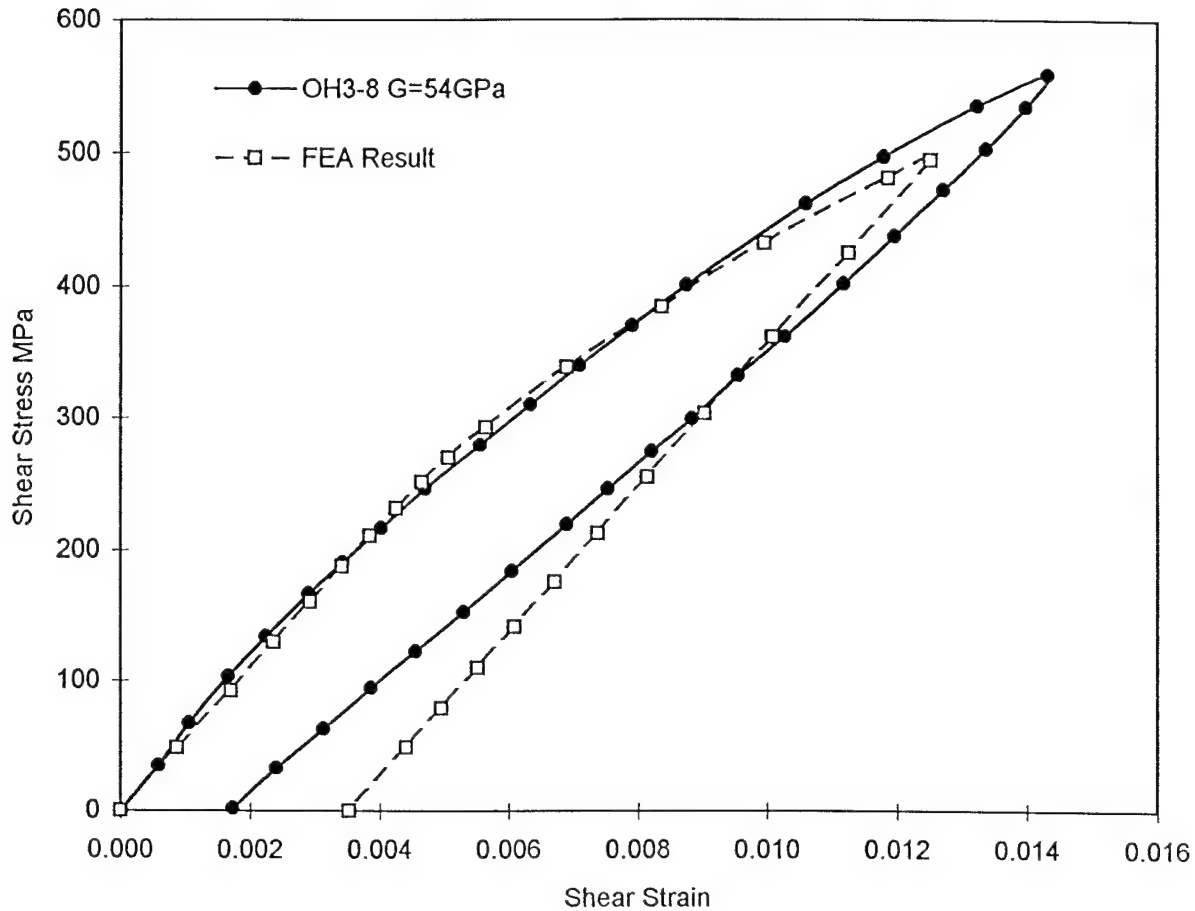


Figure 5. Comparison of analysis prediction and test measured constitutive shear response for Quasi-isotropic laminate made of the TMIETAL 21S/SCS-6 MMC.

not take the damage closure effect into the unloading analysis.

With the model surface color stress contours (they can not be clearly shown in white and black) for σ_x and τ_{xy} (x coincident with fiber direction) show that there is a small red color stress concentrated area on the edge next to a notch tip, its location is approximately the same as it was mentioned previously which caused the surface fiber fractures in specimen OH3-4 and further initiated failure in specimen OH3-2. The color contour also shows σ_x along fiber direction within the area exceeded 1900 MPa, Referring to Majumdar and Newaz, 1991, specimen under 0° tension loading failure at about 1500 MPa to 1800 MPa. This can explain why there were fiber fractures in the area of the surface layer of specimen OH3-4 and OH3-8.

It should be pointed out that Sun did not take the fiber direction inelastic deformation and neither the damage effects into his model. Therefore, when finite element model for MMC based on this assumption is limited to shear strain < 0.01 , the calculation may provide good prediction. Errors may increase when the shear strain is larger than this limit.

CONCLUSIONS

1. Iosipescu shear test provides a reasonable method for measurement of shear constitutive response of MMC material.
2. Iosipescu shear test has very good reproducibility in terms of overall properties and mechanical behavior. Iosipescu test can be recommended as a routine measurement to obtain MMC material linear and nonlinear shear properties at room temperature. Finite element analysis model for MMC Iosipescu test using Sun's assumption as an approximation plus a subroutine to check the stress state to determine the transverse tension or compression stress and then applying different yielding and hardening criterion can obtain satisfactory result for the case of shear strain < 0.01 .
3. Sun's effective stress model for plastic deformation was successfully used for prediction of experimental data. The basic input for finite element analysis required 0° tension, 90° transverse tension and compression data. Shearing coefficient a_{66} was assumed to be generated by manipulating off-axis tension test data. However a_{66} obtained by this way included neither damage effect nor fiber direction inelastic effect, and the subsequently determined a_{66} can not perform a good enough prediction in the analysis. Furthermore one parameter a_{66} is not enough to interpret the difference between transverse tension and compression constitutive responses. So a better way is to assume two trial shearing parameter a_{66} and b_{66} to interpret transverse tension and transverse compression of a laminae respectively. The values of a_{66} and b_{66} are dependent of the property of the material.
4. At an early stage of shear inelastic deformation (strain < 0.01), damage effect play an important role. This can be seen by the compliance change in the unloading curve. The damage mechanism was associated with matrix grain boundary crack and cracks along the fiber and matrix reaction zone. When shear deformation increases, plasticity becomes a primary inelastic deformation mechanism which is associated with slip bands in the matrix.

ACKNOWLEDGEMENT

Funding for this research was obtained through an Air Force Phase II subcontract from Research Application, Inc., Centerville, OH.

REFERENCES

- Adams, D.F., and Lewis, E.Q., 1995, "Experimental Strain Analysis of The Iosipescu Shear Test Specimen," *Experimental Mechanics*, 352-360.
- Allen, D. H., Jones, R. H., and Boyd, J. G., 1994, "Micromechanical Analysis of A Continuous Fiber Metal Matrix Composite Including The Effects of Matrix Viscoplasticity and Evolving Damage," *J. Mechanics And Physics of Solids*, 42: 505-29.
- Brust, F. W., Majumdar, B. S., and Newaz, G. M., 1993, "Constitutive Response Analysis of Metal Matrix Composites via the Unit Cell Model," *ASTM Symposium on Composite Materials*, Pittsburgh.

Chandu, S., and Ahmad, J., and Newaz, G. M., 1997, "Detailed Interpretation of Off-Axis and Iosipescu Test Data On Metal Matrix Composites," to appear in the J. of Reinforced Plastics & Composites.

Gao, Z., and Zhao, H., 1995, "Life Predictions of Metal Matrix Composite Laminates Under Isothermal and Nonisothermal Fatigue," J. Composite Materials 29 No. 9:1142-68.

Majumdar, B. S., and Newaz, G. M., 1992, "Inelastic Deformation of Metal Matrix Composite: Plasticity and Damage Mechanisms," Philosophical Magazine A, Vol. 66, No. 2, 187-212.

Morton, J., Ho, H., Tsai, M.Y. and Farly, G. L., 1992, "An Evaluation of the Iosipescu Specimen for Composite Materials Shear Property Measurement," J. Composite Materials, 26 (5), 708-750.

Newaz, G. M., and Majumdar, B. S., 1991, "Deformation and Failure Mechanism in Metal Matrix Composites," The Winter Annual Meeting of The America Society of Mechanical Engineers, Atlanta, Georgia, AD Vol. 22, 55-65.

Newaz, G. M., Majumdar, B. S., and Brust, F. W., 1992, "Thermal Cycling Response of Quasi-isotropic Metal Matrix Composites," ASME J. Eng. Materials and Technology, 114, 156-61.

Newaz, G. M., and Majumdar, B. S., 1994, "A Comparison of Mechanical Response of MMC At Room Temperature and Elevated Temperature," J. of Composites Science and Tech., 50.

Newaz, G. M., Majumdar, B. S., and Brust, F. W., 1996, "Inelastic Deformation Mechanisms in SCS-6/Ti 15-3 Metal Matrix Composite (MMC) Lamina Under Compression," Life Prediction Methodology for Titanium Matrix Composites, ASTM STP 1253, W. S. Johnson, J. M. Larsen, and B. N. Cox, Eds., American Society for Testing and Materials, 208-230.

Newaz, G. M. and Zhang, K., 1997 "Inelastic Response of Off-axis MMC Lamina," American Materials Science of Technology, submitted to ASME J. of Eng. Mat. & Technology.

Pindera, M. J., 1989, "Shear Testing of Fiber Reinforced Metal Matrix Composites," Metal Matrix Composites: Analysis, and Failure Modes ASTM STP 1032, W. S. Johnson, Ed., American Society for Testing and Materials, Philadelphia, 19-42

Pindera, M.J., Ifju, P. and Post, D., 1990, "Iosipescu Shear Characterization of Polymeric and Metal Matrix Composite," Experimental Mechanics, 30 (1), 101-108.

Santhosh, U. and Ahmad, J., "Metal Matrix Composite Response Under Biaxial Loading," Constitutive Behavior of High Temperature Composites, MD-Vol. 40, Majumdar, B. S., and Newaz, G. M., and S. Mall editors, ASME 1992.

Sun, C.T., 1989, "Modeling Continuous Fiber Metal Matrix Composite as an Orthotropic Elastic-Plastic Material," Metal Matrix Composites; Testing, Analysis, and Failure Modes, ASTM STP 1032, W.S. Johnson, Ed., American Society for Testing and Materials, Philadelphia, 148-160.

Sun, C. T., Chen, J. L., Sha, G. T., and Koop, W. E., 1990, "Mechanical Characterization of SCS-6/Ti-6-4 Metal Matrix Composite," J. of Composite Materials, Vol. 24, 1029-1059.

Swanson, S.R., Messick, M. and Toombes, G.R., 1985, "Comparison of Torsion Tube and Iosipescu In-Plane Shear Test Results for Carbon Fiber-Reinforced Epoxy Composite," Composites, 16 (3), 220-224.

ANALYSIS OF INTERFACIAL CRACKS IN A TBC/SUPERALLOY SYSTEM UNDER THERMO-MECHANICAL LOADING

S. Q. Nusier and G. M. Newaz¹
Mechanical Engineering Department
Wayne State University
Detroit, Michigan 48202

ABSTRACT

In thermal barrier coatings (TBC) residual stresses develop during cool down from processing temperature due to the thermal expansion mismatch between the different layers (substrate, bond coat, and TBC). These residual stresses can initiate microcracks at the bond coat/TBC interface and can lead to debonding at the bond coat/TBC interface. The effect of voids or crack like flaws at the interface can be responsible for initiating debonding and accelerate the oxidation process. Effect of oxidation growth between bond coat and the ceramic layer (TBC) can be modeled as volume increase. In this work we represent this change in volume as an induced pressure across the interface. Mixed-mode fracture analysis of a thin circular delamination in an-axisymmetrically multi-layer circular plate is developed. Geometrical nonlinearity is included in the analysis, since we have a large deflection case. The elastic deformation problem of a circular plate subjected to a clamped boundary condition at the edge delamination, an out of plane pressure load, and a compressive stress due to thermal mismatch between different layers, was solved numerically using a Rayleigh-Ritz method. The strain energy release rate was evaluated by means of the path-independent J-integral. The numerical results of this problem based on the energy method were verified using the finite element method. Both method correlate well in predicting the energy release rate for Mode I and Mode II, deflection, and postbuckling solutions. The energy release rate G , for both Mode I and Mode II using virtual crack extension method were evaluated. The specimen was cooled down from processing temperature of 1000 °C to 0 °C. The variation of the properties as a function of temperature were used for analysis. It was found that the use of temperature dependent properties in contrast to constant properties provide significantly different values of J-integral and G .

INTRODUCTION

Thermal barrier coatings (TBCs) provide thermal insulation and the bond coat provides oxidation resistance at high temperature to high temperature alloy substrates. Plasma-sprayed zirconia-yttria ceramic layer with a nickel-chromium-aluminum-yttrium bond coat on a substrate made of nickel-based superalloy (Chang, et al., 1987) is a common superalloy/TBC system. Application of these superalloy/TBC systems can be found in both aerospace and land-based gas turbine engines. In automotive applications, the piston head for diesel engine is coated to achieve longer life time and higher performance in terms of fuel reduction and power. However, these coatings have durability problems, due to the material and thermal mismatch between the coating and the metallic substrate. Thermal residual stresses develop during cool down from processing temperatures in TBC/metallic substrate. Environmental effects, specifically oxidation, create additional residual stresses due to the growth of an oxide layer causing additional material mismatch between the oxide surface and the TBC. These

¹Author receiving all communication

residual stresses may initiate microcracks such as debonding and radial cracks and can have profound effect on the response of the TBC and interfacial damage accumulation and failure. Their understanding is essential to predict the behavior of the coatings and their performance. The processing technique itself may produce voids or elongated flaws such as air bubble along the interfaces, which may initiate debonding.

Thermal fracture of multilayer ceramic thermal barrier coatings was studied by Takeuchi and Kokini (1994). Controlled experiments along with finite element modeling were used. Their work showed that surface cracks are formed as a result of tensile stresses that are created following stress relaxation in the TBC at steady-state high temperatures. The effect of a transient thermal load on a coating which is bonded to a cylindrical substrate was studied by Hornack and Kokini (1988). Finite element method was used to obtain a solution for a circumferential edge crack normal to the coating. Their analysis showed that smaller heat transfer rates result in smaller stress intensity factors. The finite element method has been used in conjunction with a numerical interface fracture mechanics model to investigate the structural response of coated brittle materials subjected to normal and shear loads, by Oneil and Wayne (1994). They examined how flaw orientation affects crack propagation through the coating, interface, and substrate. A comparison between the uncoated and coated substrate has shown that cracks are strongly influenced toward interfaces because of the preferred release of critical strain energy. Interfacial fracture in bimetals often is due to a combination of Mode I and Mode II crack growth. A finite element model to calculate the Mode II stress-intensity factors was developed by Van der Zande and Grootenboer (1986). The optimum size for a so-called singular element has been determined. Ahmad (1993) provides micromechanics based fracture analysis and correlation of experimental data for metal-ceramic and other interfaces. Suo (1995) studied wrinkles which induce interfacial stress and cause voiding. A linear bifurcation analysis has been carried out when wrinkles just start. The oxide scale thickens slowly at a higher temperature, until the compressive stress generated by oxidation and cooling causes it to spall off. The strain energy release rate components G_I and G_{II} in Mode I and Mode II at the tip of an interface crack in a bimaterial plate under tension in a direction normal to the interface were evaluated using finite element analysis and modified crack closure integral (MCCI) technique by Dattaguru, et al. (1994). The finite element results for all the models show increasing Mode II dominance as $\Delta a \rightarrow 0$. An elastoplastic solution for the interface crack with contact zones was studied by Aravas and Sharma (1991). It was shown that the elastic asymptotic solutions based on the assumption of a closed crack tip predicted material interpenetration. Also, it was shown that the asymptotic solution is separable in r and θ at the crack tip. Singular thermal stress fields in bonded viscoelastic quarter planes are studied by Blanchard and Ghoniem (1989). It was shown that the order of the singularity generally increases with time. Singular stress and heat flux fields at the tip of the crack in a general nonhomogeneous material are studied by Jin and Noda (1994). It was found that the crack-tip field singularities and angular distributions are the same as those in the homogeneous material. New domain integrals for axisymmetric interface crack problems are derived by Nahta and Moran (1993). The effect of crack front curvature is shown to play an important role in the derivation of the integrals.

Descriptions of residual stresses and their influence on mechanical failure of the coating were studied by Evans, et al., (1983). The mechanics of the delamination and spalling of compressed films or coatings has been analyzed using a combination of fracture mechanics and post-buckling theory by Evans and Hutchinson (1984). The phenomenon of delamination buckling and growth in a time dependent radial compressive load is analyzed by Boltega and Maewal (1983). An iterative procedure based on the fourth-order Runge-Kutta integration formula is used to generate a family of nondimensionalized postbuckling solutions of von Karman's nonlinear plate theory by Yin (1985). A mixed-mode fracture analysis combining nonlinear thin-plate stress solutions with crack-tip elasticity results has been developed to account for local variations of G_I , G_{II} , and G_{III} in thin-film debond problems associated

with large film deformations by Chai (1990). A shaft-loaded blister test has been developed by Wan and Mai (1995) to measure the interfacial energy of a thin flexible polymeric film adhered to a rigid substrate. A theoretical analysis is given of an axisymmetric debond ('blister'). Expressions have been derived which describe the critical stress and pressure necessary to rupture oxide blisters which form on aluminum during growth of corrosion pits by Ryan and McCafferty (1995).

Although numerous effects have been made to an understanding of the effect of cracks on the life of TBC coated specimens require special attention. It is now determined that in some TBC systems such as electron beam-plasma vapor deposition (EB-PVD), there is microcrack initiation that coalesce to form major delamination cracks as reported by Newaz, et. al., (1996). Interfacial crack in a stepped-disk specimen is shown in Fig. 1. An important consideration is the nature of crack growth characteristics at the TBC/bond coat interface. In a previous study by Nusier and Newaz (1996), it was shown that a central delamination under pure thermal loading has no stress intensification at the crack tip unless the delamination is large enough to promote buckling. By investigating the issue of interfacial crack growth, we will be able to evaluate the condition necessary for their growth under thermo-mechanical loading. This button specimen under consideration is amenable to axisymmetric modeling due to geometry. The importance of this problem is due the fact that in order to achieve realistic prediction of TBC spallation performance, one needs to study the interaction of various layers and interfacial cracks at high temperature.

THEORETICAL AND COMPUTATIONAL ANALYSIS

The TBC coating in a button specimen as studied by Nusier and Newaz (1995) is in a state of biaxial compression. Residual compression stresses has been observed in TBC coating that was applied using Electron Beam-Plasma Vapor Deposition (EB-PVD) technique. This residual compression stress arise because of thermal expansion mismatch. Buckling failure mode has been observed by Newaz, et al. (1996) in the EB-PVD system. Oxidation growth between bond coat and ceramic layer (TBC) can be modeled as volume increase which can be represented as an induced pressure across the interface (TBC/Oxide). Mixed-mode fracture analysis of a thin circular delamination in an-axisymmetrically multi layer circular plate is given as follows.

Theoretical Analysis

Let a circular plate of radius a be clamped at the edge of the delamination and subject to a uniformly distributed pressure p . The clamped edge has a radial displacement $\Delta\epsilon_0$ due to the applied compressive load. The deflection and slope at the clamped edge is zero, also the radial displacement at the center of the plate is zero. For a large deflection, the strain in the radial direction is

$$\epsilon_r = \frac{du}{dr} + \frac{1}{2} \left(\frac{dw}{dr} \right)^2 \quad (1)$$

and the strain in the tangential direction is

$$\epsilon_\theta = \frac{u}{r} \quad (2)$$

where u and w are the radial and vertical components of the displacement vector, respectively. Let N_r and N_θ be the corresponding tensile forces per unit length and applying Hooke's law, we obtain

$$\begin{aligned} N_r &= \frac{Eh}{1-\nu^2} (\epsilon_r + \nu\epsilon_\theta) \\ N_\theta &= \frac{Eh}{1-\nu^2} (\epsilon_\theta + \nu\epsilon_r) \end{aligned} \quad (3)$$

where h is the plate thickness. The strain energy due to bending is given by

$$V = \frac{D}{2} \int_0^{2\pi} \int_0^a \left[\left(\frac{\partial^2 w}{\partial r^2} \right)^2 + \frac{1}{r^2} \left(\frac{\partial w}{\partial r} \right)^2 + \frac{2\nu}{r} \frac{\partial w}{\partial r} \frac{\partial^2 w}{\partial r^2} \right] r dr d\theta \quad (4)$$

where D is the flexural rigidity of the plate, and is given by

$$D = \frac{Eh^3}{12(1-\nu^2)} \quad (5)$$

The strain energy due to stretching of the middle plane is

$$V_1 = 2\pi \int_0^a \left(\frac{N_r \epsilon_r}{2} + \frac{N_\theta \epsilon_\theta}{2} \right) r dr \quad (6)$$

The elastic deformation problem for a circular plate subjected to the boundary conditions indicated earlier was solved using a Rayleigh-Ritz method (an energy method) based on the following polynomial series solution

$$\begin{aligned} w &= \sum_{i=1}^n c_i \left(1 - \frac{r^2}{a^2} \right)^{i+1}, \quad \text{and} \\ u &= r(a^2 - r^2) \left(\sum_{i=1}^n b_i r^{2i-2} \right) - \epsilon_0 r \end{aligned} \quad (7)$$

where C_i and b_i are constants to be evaluated from the condition that the total energy of the plate for a position of equilibrium is a minimum. Hence,

$$\frac{\partial V_1}{\partial b_i} = 0, \quad \text{and}$$

$$\frac{\partial(V + V_1)}{\partial c_i} \delta c_i = 2\pi \int_0^a p \delta w r dr$$

(8)

The first part of Eqn. 8 give us an n-linear equations for the constants b_i , these equations are solved in symbolic form, the second part of Eqn. 8 give us an n-nonlinear equations for the constants c_i , the solution of the constants b_i were used. All of this symbolic calculation are carried out by using Mathematica (1996). The set of nonlinear equations have been solved by IMSL (1989) library subroutine NEQNJ based on Levenberg -Marquardt algorithm with a user-supplied jacobian obtain by Mathematica also. The solution converged after 6 terms ($n=6$) for the case considered.

The compressive strain in the TBC layer can be obtained by applying the equilibrium radial force equation for the three layers. This solution is valid only for thick substrate. The radial stress in each layer is written in the following form

$$\sigma^c = \frac{E^c}{1 - \nu^c} [\epsilon - \alpha^c (T - T_r)]$$

$$\sigma^b = \frac{E^b}{1 - \nu^b} [\epsilon - \alpha^b (T - T_r)]$$

$$\sigma^s = \frac{E^s}{1 - \nu^s} [\epsilon - \alpha^s (T - T_r)]$$

(9)

where σ is the radial stress, α is the thermal expansion coefficient, and T_r is the stress free temperature, the superscript c , b , and s refers to TBC, bond coat and substrate, respectively. The equilibrium radial force equation for the three layers is

$$\sum F = \sigma^c A^c + \sigma^b A^b + \sigma^s A^s = 0$$

(10)

Substituting Eqn. 9 into Eqn. 10, and solving for ϵ gives

$$\epsilon = \frac{(\frac{E^c}{1 - \nu^c} \alpha^c A^c + \frac{E^b}{1 - \nu^b} \alpha^b A^b + \frac{E^s}{1 - \nu^s} \alpha^s A^s)(T - T_r)}{\frac{E^c}{1 - \nu^c} A^c + \frac{E^b}{1 - \nu^b} A^b + \frac{E^s}{1 - \nu^s} A^s}$$

(11)

Now, the compressive strain in TBC is

$$\varepsilon_0 = \varepsilon - \alpha^c(T - T_r) \quad (12)$$

In case of temperature dependent properties, the previous Eqns. 9-12 will be written in incremental form for each dT , then they will add up to get the right value of ε . For example, the variation of ε due to dT change in temperature will be given as

$$d\varepsilon = \alpha|_T(T - T_0) - \alpha|_{T-dT}(T - dT - T_0) \quad (13)$$

where T_0 is the reference temperature and is equal to zero.

Computational Fracture Analysis

Linear elastic fracture mechanics can be used to assess the conditions for crack growth of bimaterial interfaces. The mechanics of interface fracture can be traced back to the earlier works of Griffith (1921) and Irwin (1960) on the general theory of fracture, of Williams (1959) on the elastic stress distribution around an interface crack, of England (1965), Erodogan (1965), and Rice and Sih (1965) on explicit solutions for interface cracks. The classical fracture mechanics concepts enable us to predict, without a detailed description of the crack tip processes, crack growth behavior in a fracture specimen. In recent years, complexity of obtaining closed-form solutions have been circumvented through computational fracture analysis to determine conditions for crack growth at bimaterial interfaces. However, the analytical basis is essential to study the critical parameters that characterize interface fracture.

With the interface on the x_1 -axis, let E_1 , μ_1 and ν_1 be the Young's modulus, shear modulus and Poisson's ratio of material 1 lying above the interface ($x_2 > 0$) with similar quantities, E_2 , μ_2 and ν_2 , for material 2 lying below the interface. For plane problems with traction boundary conditions, only two nondimensional combinations of the four independent material moduli parameters enter into any solution as discussed by Dunders (1969). For plane strain, the moduli mismatch parameters of Dundurs are

$$\alpha = \frac{\bar{E}_1 - \bar{E}_2}{\bar{E}_1 + \bar{E}_2} \quad \text{and} \quad \beta = \frac{\mu_1(1 - 2\nu_2) - \mu_2(1 - 2\nu_1)}{\mu_1(1 - \nu_2) + \mu_2(1 - \nu_1)} \quad (14)$$

where $\bar{E} = E / (1 - \nu^2)$ is the plane strain tensile modulus. Note that α and β both vanish when dissimilarity between the elastic properties of the materials is absent, and α and β change signs when the materials are switched. For each material pair, a universal singular crack tip field exists at the crack tip according to linear elasticity theory for a traction-free line crack. For the plane problems, the normal and shear stresses of the singular field acting on the interface a distance r ahead of the tip can be written according to the "function" form

$$\sigma_{22} + i\sigma_{12} = \frac{(K_1 + iK_2)r^{i\varepsilon}}{\sqrt{2\pi r}} \quad (15)$$

where $i = \sqrt{-1}$ and the oscillation index ε depends on β according to

$$\varepsilon = \frac{1}{2\pi} \ln \left| \frac{1-\beta}{1+\beta} \right| \quad (16)$$

In plane strain, the crack face displacements a distance r behind the tip, $\delta_i = u_i(-r, 0^+) - u_i(-r, 0^-)$, are given by

$$\delta_2 + i\delta_1 = \frac{4}{\sqrt{2\pi}} \frac{(1/\bar{E}_1 + 1/\bar{E}_2)}{(1 + 2i\varepsilon) \cosh(\pi\varepsilon)} (K_1 + iK_2) \sqrt{r} r^{i\varepsilon} \quad (17)$$

The amplitude factors, K_1 and K_2 , depends linearly on the applied loads and on the details of the full geometry of the body, as will be illustrated below. These stress intensity factors are defined to be consistent with corresponding stress intensity factors for cracks in homogeneous problems (Rice, 1988). The energy release rate per unit length of extension of the crack in the interface for plane strain is related to the stress intensity factors by

$$G = \frac{(1/\bar{E}_1 + 1/\bar{E}_2)}{2 \cosh^2(\pi\varepsilon)} (K_1^2 + iK_2^2) \quad (18)$$

which is the generalization of Irwin's result for a homogeneous isotropic material. When $\varepsilon \neq 0$, the relative proportion of normal and shear stresses on the interface in the singular field varies slowly according to $r^{i\varepsilon}$, and this feature complicates the implementation of interfacial mechanics in several respects. When $\varepsilon \neq 0$, the traction-free line crack solution is not fully consistent since the solution (England, 1965) implies that the crack faces interpenetrate behind the tip.

Another approach to characterize fracture at bimaterial interface is via the J-integral. Originally developed by Eshelby (1956), the basic concept of J-integral is a path independent evaluation of the energy release rate. In other words, it is a measure of decrease in potential energy of the system with increase in crack length. In linear elastic fracture mechanics "J" is equivalent to G. The J-integral can be written as (Rice, 1968)

$$J = \int_{\Gamma} W dy - \int_{\Gamma} T \frac{\partial u}{\partial x} ds \quad (19)$$

where W is the strain energy density. Fig. 2 shows the notation and parameters for J-integral for a homogeneous medium. The analysis can be easily extended for a line crack between two materials assuming crack growth along the interface. The essence of J definition and its meaning remains unaltered for a crack at the bimaterial interface.

Following the work done by Yin (1985), the energy release rate associated with uniform-expansion growth of a circular delamination in a compressively loaded plate is obtained by means of the M-integral. The strain energy-release rate per unit increment of the area of delamination is given by

$$G = \frac{1-\nu^2}{2Eh} \left\{ \left[\frac{Eh}{1-\nu} \varepsilon_0 - N_r(a) \right]^2 + 12 \left[\frac{M_r(a)}{h} \right]^2 \right\} \quad (20)$$

where $M_r(r)$ is given by

$$M_r(r) = D(w'' + \nu w' / r) \quad (21)$$

where the prime denote differentiation with respect to r .

For arbitrary combinations of N and M the stress field at the crack tip is governed by both K_I and K_{II} (Thouless, et al., 1987). Dimensional considerations require that the stress intensity factors be related to the load quantities by

$$\begin{aligned} K_I &= d_1 N h^{-0.5} + d_2 M h^{-1.5} \\ K_{II} &= d_3 N h^{-0.5} + d_4 M h^{-1.5} \end{aligned} \quad (22)$$

where the d_i are constants. The energy release rate is given by

$$G = \frac{(1-\nu^2)}{E} (K_I^2 + K_{II}^2) \quad (23)$$

Solving the crack problem for one loading combination and comparison of Eqns. 22 and 23 gives (Thouless, et al., 1987)

$$d_1 = 0.434, \quad d_2 = 1.934, \quad d_3 = 0.558, \quad d_4 = -1.503 \quad (24)$$

There is one idealized condition that we explored related to the specimen geometry. The presence of circumferential crack between the ceramic layer and the bond coat layer is as shown in Fig. 1 which was analyzed using finite element method. The general code ABAQUS (1995) was used for these analyses. The energy release rate G can be estimated by using the virtual crack extension method. The J-integral value can be found directly from ABAQUS.

Within linear elastic fracture mechanics two parameters are generally used to describe the conditions at the crack tip, normally the stress intensity factor(s) and the energy release rate. Evaluation of the stress intensity factor requires a through understanding of the state of stress at the crack tip. Energy release rate evaluation, on the other hand, is based more on an energy criteria and hence more popular.

A procedure for calculating the energy release rate, G , that has gained increasing acceptance over the past decade is the Virtual Crack Extension Method (VCEM). This was originally developed by Hellen and Parks (1975), who subsequently extended the method to cover material nonlinearities, and the evaluation of the J-integral. The method of VCE used to evaluate G is explained in the following few steps. Consider the following Fig. 3(a). The energy release rates in mode I and II are given by

$$G_I = \frac{1}{2A} f_x \Delta u_x$$

$$G_{II} = \frac{1}{2A} f_y \Delta u_y$$
(25)

Where f_x and f_y are the reaction forces, A is the crack surface area corresponding to Δa , and similarly Δu_x and Δu_y are the difference in the displacements of nodes A and B in the x and y directions respectively (Fig. 3(b)).

The reaction forces and the displacements were obtained via two runs. For the first run, we assume a very weak spring, so the opening displacement and sliding displacement can be determined from springs deflection. In the second run the spring stiffness is assumed to be very high compared to the material stiffness, so the reaction forces can be determined. In this study a eight node isoparametric element are used, the energy release rates in mode I and mode II are given by

$$G_I = \frac{1}{2A} [f_{x1} \Delta u_{x1} + f_{x2} \Delta u_{x2}]$$

$$G_{II} = \frac{1}{2A} [f_{y1} \Delta u_{y1} + f_{y2} \Delta u_{y2}]$$
(26)

Hence

$$G_{total} = G_I + G_{II}$$
(27)

RESULTS AND DISCUSSION

The presence of circumferential crack between the ceramic layer and the bond coat layer as shown in Fig. 1 was analyzed using A Rayleigh-Ritz method and finite element method. The general code ABAQUS was used for finite element analysis. The energy release rate G was estimated by using the virtual crack extension method.

Finite element method was used in order to determine the J-integral value and the energy release rate. Virtual crack extension method was used to evaluate the energy release rate for both Mode I and Mode II crack growth. For stepped-disk specimen, the disk radius is 12.7 mm, the bond coat layer thickness is 0.04826 mm, the TBC thickness is 0.127 mm, and the uncoated Nickel based superalloy had a thickness of 3.175 mm. These dimensions are shown in Fig. 4. The properties of these three layers are given in Table 1. We analyzed a model case where the specimen was plasma sprayed in air with a thin zirconia-yttria

($\text{ZrO}_2 - 8\text{wt}\%\text{Y}_2\text{O}_3$) layer on a nickel-chromium-aluminum-zirconium bond coat, as in Ref. 1. The specimen was cooled down from a processing temperature of 1000°C to a temperature of 0°C . Half model for stepped-disk specimen was used since the specimen is axisymmetric. Eight node isoparametric element type was used; the total number of element was 1380. Along the longitudinal axis, the nodes can move in the axial direction only. The mesh was very fine close to the crack tip, and to make sure that the mesh is fine enough, another model with the same number of element but has one tenth of element size near to the crack tip, the difference in the results was less than 1%. Details of the finite element mesh near the crack tip is shown in Fig. 5.

Figure 6 shows the variation of maximum deflection versus pressure ratio for a delamination radius of 20 times the TBC thickness. For zero pressure load the deflection has a value greater than zero due to buckling. It is clear that the use of temperature dependent properties in contrast to constant properties provide significantly different values of maximum deflection. The finite element results compare to numerical results correlate very well. The variation of the maximum deflection versus pressure ratio is non-linear compare to linear variation as in the case of no geometrical nonlinearity. Using temperature dependent properties gives a 20-30% higher maximum deflection and energy release rate as seen in Figs. 6 and 7. The variation of J and G_I versus pressure ratio from finite element method and virtual crack extension method (VCEM) are shown in Fig. 7. Comparison between the energy release rate evaluated by energy method and by finite element method (J -integral) is shown in Fig. 8, finite element method and numerical method are very good agreement.

Figure 9 shows the variation of G_I and G_{II} versus pressure ratio for a delamination radius of twenty times the TBC thickness. This figure shows good agreement between finite element method results based on VCEM and numerical results. Mode I is dominant in this case. Figure 10 is same as Fig. 9, but temperature dependent properties were used. In Fig. 10, we observe that Mode II energy release rate component is much smaller compared with the mode I component for both numerical and VCEM analyses. In either case, results match well. Figure 11 shows the variation of J -integral delamination radius from numerical analysis. From this figure one can obtain the conditions when the crack will propagate. From literature the critical energy release rate is varied between $100\text{--}300\text{ J.m/m}^2$ for this system configuration. For a value of 300 J.m/m^2 , and a delamination radius of four times the TBC thickness, the crack will propagate at induced pressure value equivalent to 500 atmosphere ($\approx 50\text{ MPa}$). This value is easy to develop due to volume increase because of oxide layer growth. Also, based on finite element analysis conducted by the authors for this system with a wavy interface, the results shows that an axial stress of 250 MPa can be developed for a sine wave interface with amplitude of $2.4\text{ }\mu\text{m}$ and wave length of $127\text{ }\mu\text{m}$. These values are practical for this system (Newaz, et al., 1996).

CONCLUSIONS

Effect of interfacial microcracks were investigated using fracture mechanics approach under thermo-mechanical loading. Thermal load was used in conjunction with internal surface pressure due to oxide scale buildup to analyze interfacial cracks. The use of temperature dependent properties in contrast to constant properties provide significantly different values of J -integral and G values. Stepped-disk type specimen with a central crack has mixed mode conditions under pure thermo-mechanical loading. The total energy release rate evaluated by the virtual crack extension method and the J -integral value evaluated directly by ABAQUS agree quite well. The maximum deflection and total energy release rate evaluated by finite element method and energy method are in very good agreement. For a TBC toughness value of 300 J.m/m^2 , and a delamination radius of four times the TBC thickness, the crack will propagate at induced pressure value equivalent to 500 atmosphere

(≈ 50 MPa). The results clearly indicate that small internal pressure due to oxidation induced volume change may create the necessary conditions for crack growth during thermal cycling.

ACKNOWLEDGMENT

Funding for this research was provided through a grant (# F49620-95-1-0201) from the Air Force Office of Scientific Research (AFOSR). Dr. Walter Jones is the program monitor. Discussion and interaction with Dr. P. K. Wright of GEAE is gratefully acknowledged.

REFERENCES

- Ahmad, J., 1993, "A Micromechanics Based Representation of Combined Mode I and Mode II Toughness of Brittle Materials and Interfaces," *ASME J. of Engineering Materials and Technology*, vol. 115, 101-105.
- ABAQUS, 1995, Hibbitt, Karlsson and Sorensen, Inc.
- Aravas, N., and Sharma, S. M., 1991, "An Elastoplastic Analysis of the Interface Crack with Contact Zones", *J. Mech. Phys. Solids* Vol. 39, No. 3, 311-344.
- Blanchard, J. P., and Ghoniem, N. M., 1989, "Relaxation of Thermal Stress Singularities in Bonded Viscoelastic Quarter Planes", *Transactions of the ASME*, 56, 756-762.
- Bottega, W. J., and Maewal, A., 1983, "Delamination Buckling and Growth in Laminates", *Transactions of the ASME*, Vol. 50, 184-189.
- Bottega, W. J., and Maewal, A., 1983, "Dynamics of Delamination Buckling", *Int. J. Non-Linear Mechanics*, Vol. 18, No. 6, 449-463.
- Chai, H., 1990, "Three-Dimensional Fracture analysis of Thin-Film Debonding", *Int. J. Fracture*, Vol. 46, 237-256.
- Chang, G. C., and Phucharoen, W., Miller, R. A., 1987, "Finite Element Thermal Stress Solutions for Thermal Barrier Coatings", *Surface and Coatings Technology*, 32, 307-325.
- Dattaguru, B., Venkatesha, K. S., Ramamurthy, T. S., and Buchholz, F. G., 1994, "Finite Element Estimates of Strain Energy Release Rate Components at the Tip of an Interface Crack Under Mode I Loading", *Engineering Fracture Mechanics*, Vol. 49, No. 3, 451-463.
- Dundurs, J., 1969, Discussion, *J. Appl. Mech.*, 36, p. 650.
- England, A. H., 1965, "A Crack Between Dissimilar Media", *J. Appl. Mech.* 32:400-402
- Erdogan, F., 1965, "Stress Distribution in Bonded Dissimilar Materials With Cracks", *J. Appl. Mech.* 32:403-410.
- Eshelby, J. D., 1956, "The Continuum Theory of Lattice Defects, in *Solid state Physics*, 3, 79-141.
- Evans, A. G., Crumely, G. B., and Demaray, R. E., 1983, "On the Mechanical Behavior of Brittle Coatings and Layers", *Oxidation of Metals*, Vol. 20, No. 5/6.
- Evans, A. G., and Hutchinson, J. W., 1984, "On the Mechanics of Delamination and Spalling in Compressed Films", *Int. J. Solids Structures*, Vol. 20, No. 5, 455-466.
- Griffith, A. A., 1921. *Phil. Trans. Roy. Soc. Lond.* A221:163-197.
- Hellen, T. K., 1975, "On the Method of Virtual Crack Extensions", *Int. J. Num. Meth.* 9, 187-207.
- Imsl, 1989, User's Manual, Houston, Texas, version 1.0.
- Irwin, G. R., 1960. In: *Structural Mechanics*. (J. N. Goodier and N. J. Hoff, eds.), 557-591, Oxford: Pergamon Press.
- Jin, Z., and Noda, N., 1994, "Crack-Tip Singular Fields in Nonhomogeneous Materials", *Transactions of the ASME*, 61, 738-740.
- Kokini, K., and Hornack, T. R., 1988, "Transient Thermal Load Effects on Coatings Bonded to Cylindrical Substrates and Containing Circumferential Cracks", *J. of Eng. Mat. and Tech.*, 110, 35-40
- Mathematica, 1996, Wolfram Media, Inc., version 3.
- Nahta, R., and Moran, B., 1993, "Domain Integrals For Axisymmetric Interface Crack Problems", *Int. J. Solids Structures*, Vol. 30, No. 15, 2027-2040.

Newaz, G. M., Nusier, S. Q., Chaudhury, Z. A., and Wright, K. P., 1996, "Damage Accumulation Mechanisms in Thermal Barrier Coatings", To be presented at IMECE'96, Atlanta.

Nusier, S. Q., Newaz, G. M., 1996, "Analysis of Interfacial cracks in a TBC/Superalloy System under Thermal Loading", submitted to J. of Engineering Fracture Mechanics.

Oneil, D. A., and Wayne, S. F., 1994, "Numerical Simulation of Fracture in Coated Brittle Materials Subjected to Tribo-Contact", J. of Eng. Mat. and Tech. 116, 471-478.

Rice, J. R., 1988, "Elastic Fracture Mechanics Concepts of Interfacial Cracks", J. Appl. Mech., 55, p. 98-103.

Rice, J. R., 1968, "Mathematical Analysis in the Mechanics of Fracture, in Fracture", An Advanced Treatise (editor H. Leibowitz), Academic Press, New York, 2, pp. 191-311.

Rice, J. R., and G. C. Sih., 1965, "Plane Problems of Cracks in Dissimilar Media", J. Appl. Mech. 32:418-423.

Ryan, R. L., and McCafferty, E., 1995, "Rupture of an Oxide Blister", J. Electrochem. Soc., Vol. 142, No. 8, 2594-2597.

Suo, Z., 1995, "Wrinkles of the Oxide Scale on an Aluminum-Containing Alloy at High Temperature", J. of Mechanics of Physics and Solids, Vol. 43, No. 6, 829-846.

Takeuchi, Y. R., and Kokini, K., 1994, "Thermal Fracture of Multilayer Ceramic Thermal Barrier Coatings", J. of Eng. for Gas Turb. and Power. Transactions of the ASME, 116, 266-271.

Thouless, M. D., Evans, A. G., Ashby, M. F., and Hutchinson, J. W., 1987, "The Edge Cracking and Spalling of Brittle Plates", Acta Metall. Vol. 35, No. 6, 1333-1341.

Van der Zande, H. D., and Grootenboer, H. J., 1986, "A Finite Element Approach to Interface Cracks", J. of App. Mech., 53, 573-578.

Wan, K. and Mai, Y., 1995, "Fracture Mechanics of a Shaft-Loaded Blister of Thin Flexible Membrane on Rigid Substrate", Int. J. Fracture, Vol. 74, 181-197.

Williams, M. L., 1959, "The Stresses Around a Fault or Crack in Dissimilar Media", Bull. Seismol. Soc. Am. 49:199-204.

Yin, W., 1985, "Axisymmetric Buckling and Growth of a Circular Delamination in a Compressed Laminate", Int. J. Solids Structures, Vol. 21, No. 5, 503-514.

TABLE 1
Material properties at 22 & 566 & 1149 °C

Material	Young's modulus (GPa)	Poisson's ratio	Coefficient of thermal expansion (°C ⁻¹)
Substrate	175.8	0.25	13.91 x10 ⁻⁶
	150.4	0.2566	15.36 x10 ⁻⁶
	94.1	0.3224	19.52 x10 ⁻⁶
Bond coat	137.9	0.27	15.16 x10 ⁻⁶
	121.4	0.27	15.37 x10 ⁻⁶
	93.8	0.27	17.48 x10 ⁻⁶
TBC	27.6	0.25	10.01 x10 ⁻⁶
	6.9	0.25	11.01 x10 ⁻⁶
	1.84	0.25	12.41 x10 ⁻⁶

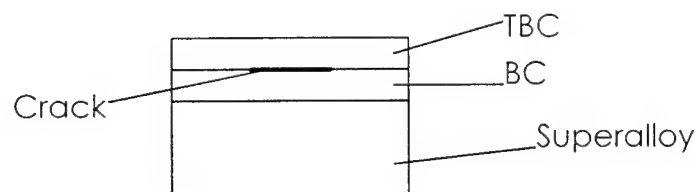


Figure 1. Circumferential crack between the ceramic layer and the bond coat layer in a stepped-disk specimen.

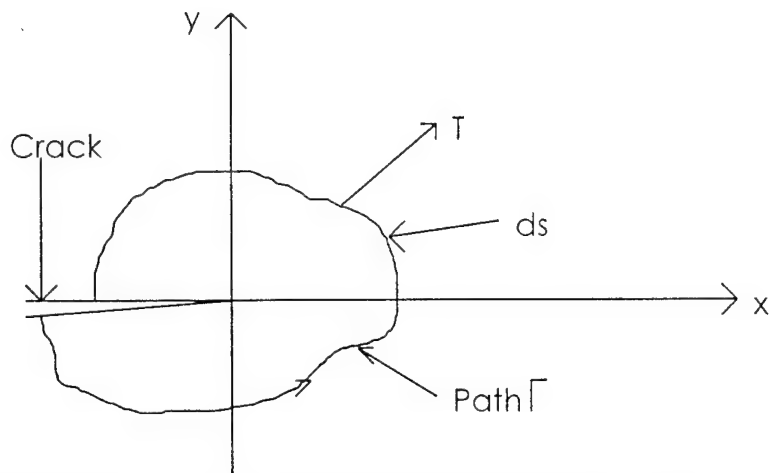


Figure 2. Notation and parameters used for J-integral.

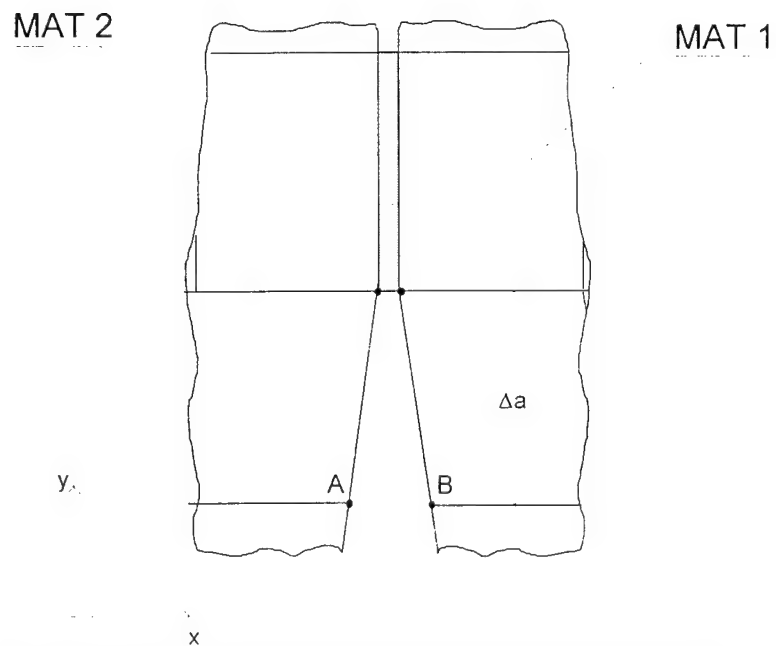


Figure 3a. Interfacial crack between bond coat and TBC.

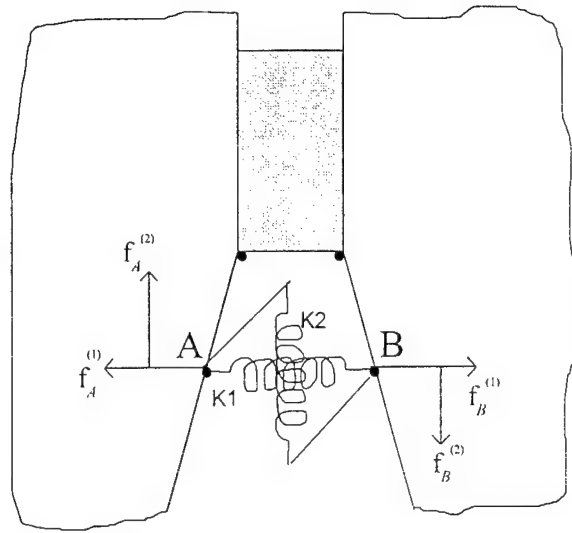


Figure 3b. Forces and displacement illustrations for a crack.

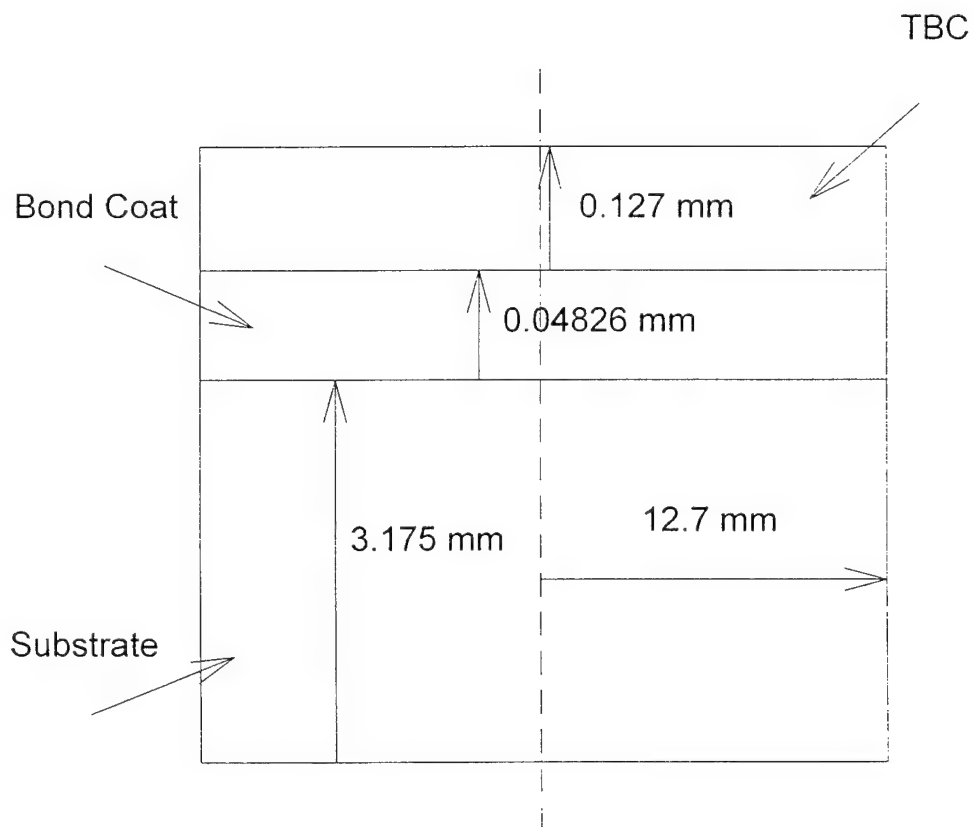


Figure 4. Dimension of TBC layer in relation to bond coat and superalloy substrate.

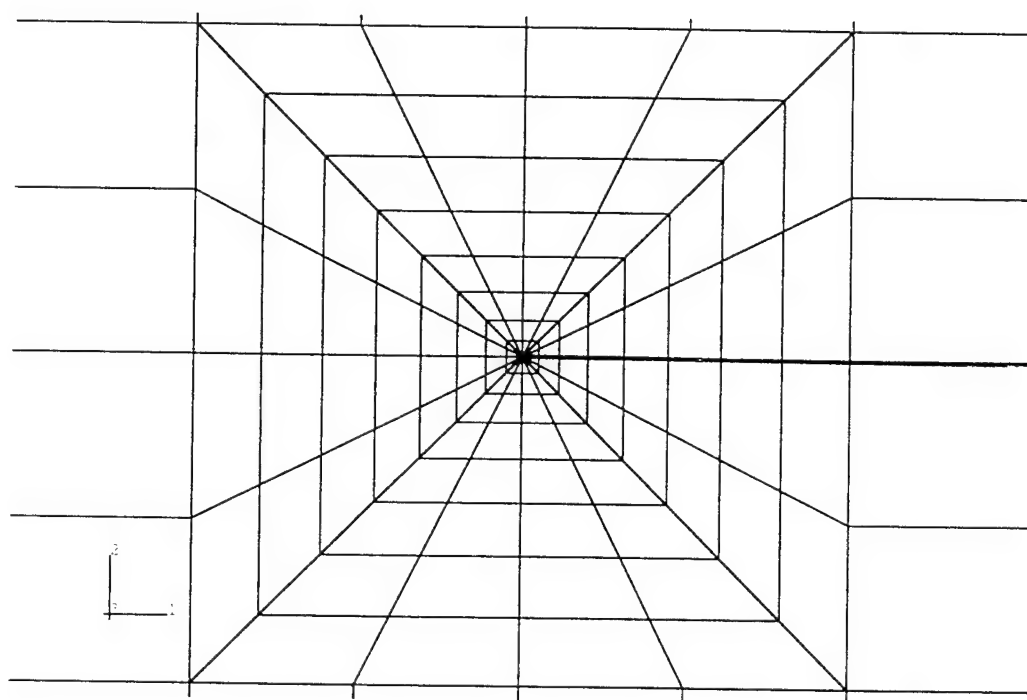


Figure 5. Details of near crack-tip finite element mesh

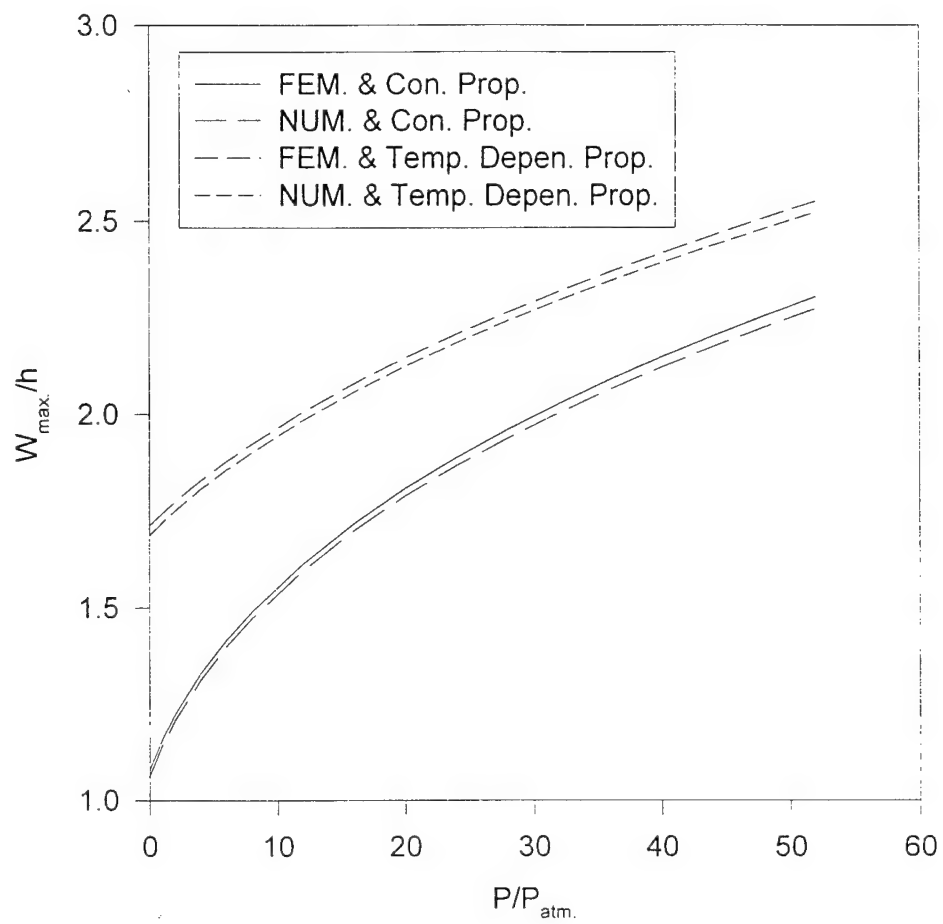


Figure 6. Variation of maximum deflection versus pressure ratio, for both constant and temperature dependent properties, $a=20h$.

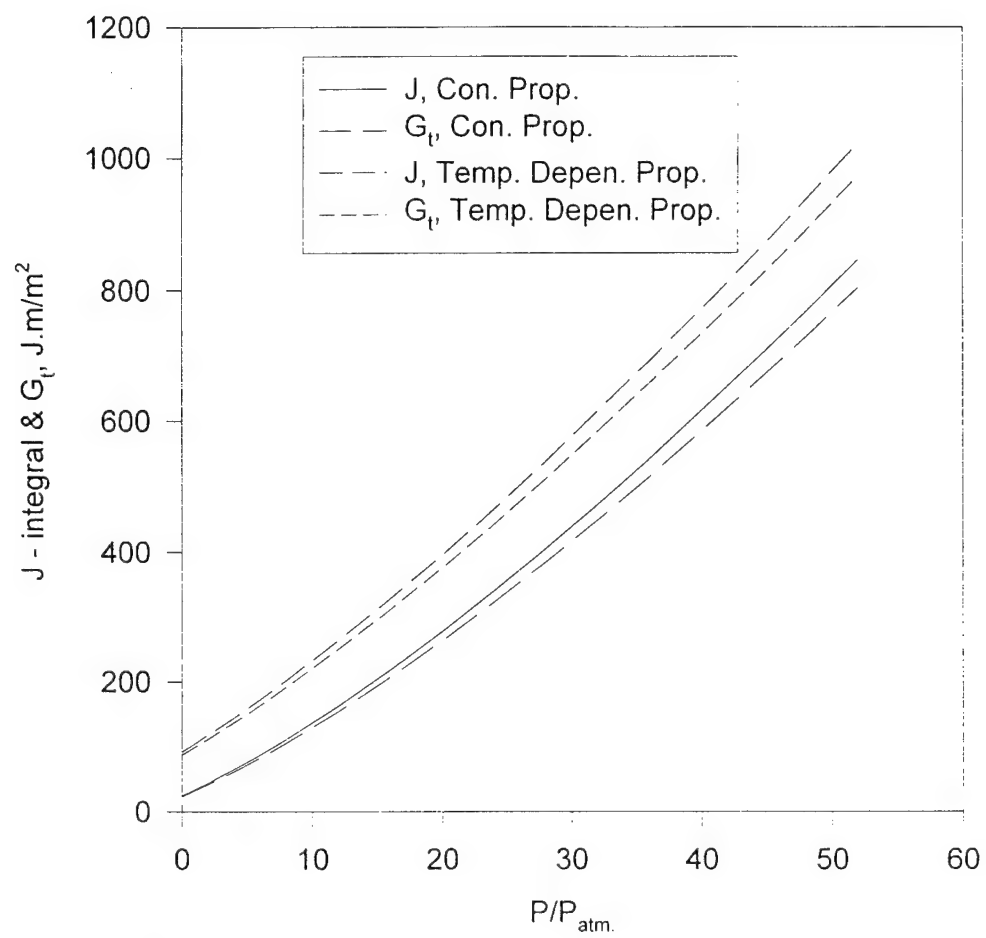


Figure 7. Variation of the J & G versus pressure ratio, for both constant and temperature dependent properties, $a=20h$.

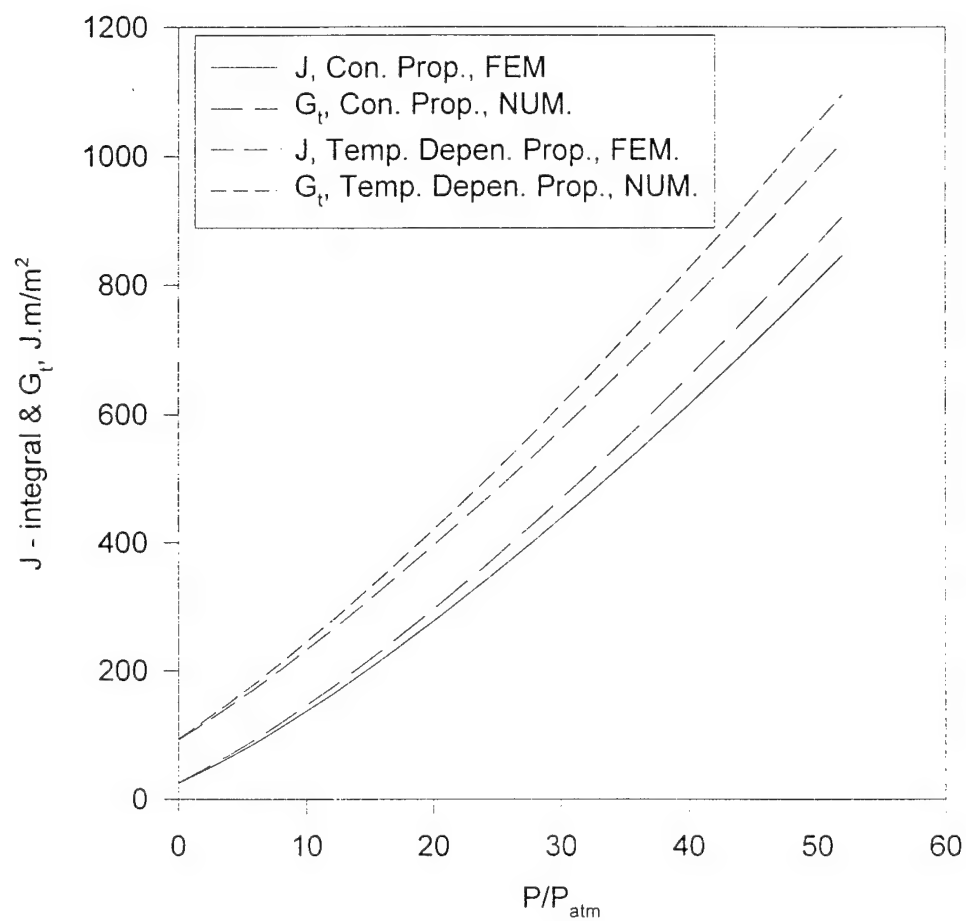


Figure 8. Variation of J & G versus pressure ratio, numerical and finite element method are used, for both constant and temperature dependent properties, $a=20h$.

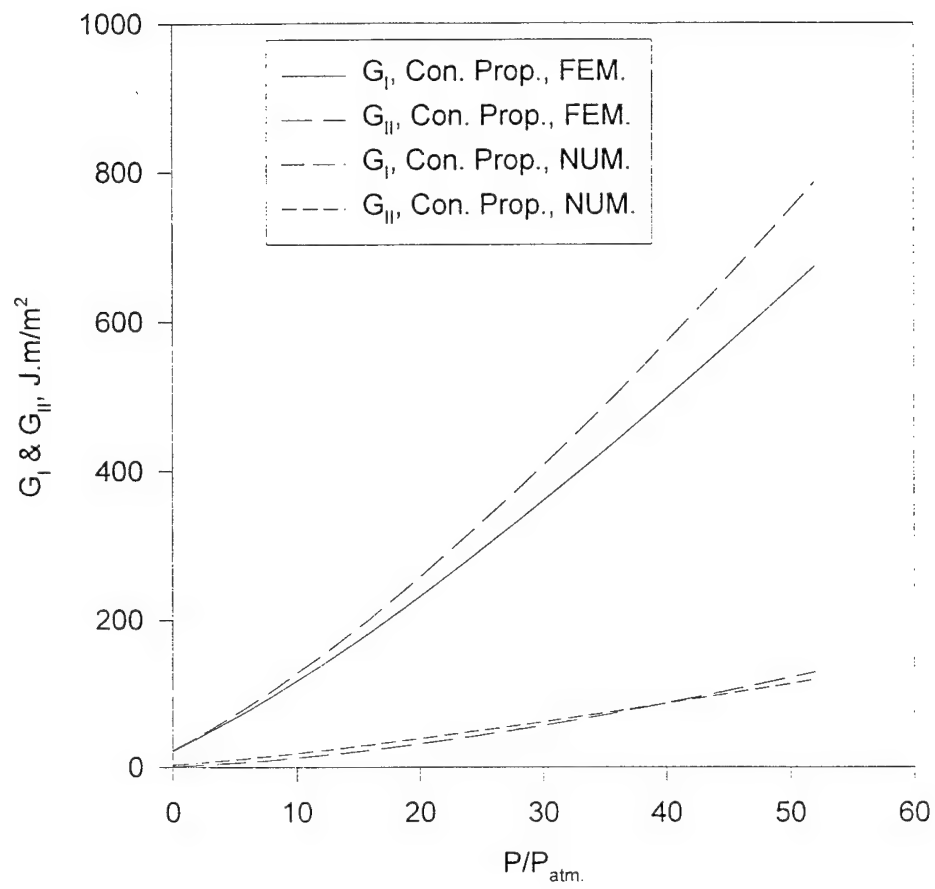


Figure 9. Variation of G_I & G_{II} versus pressure ratio, numerical and finite element methods are used, constant properties, $a=20h$.

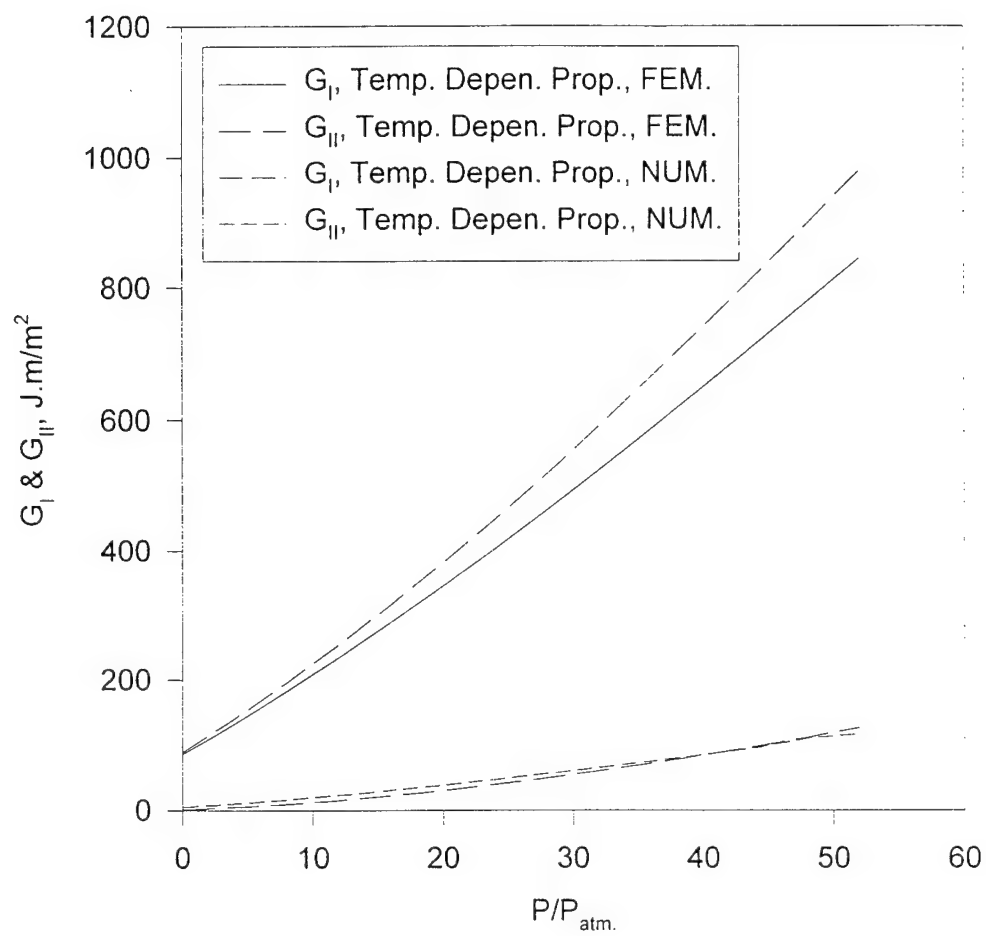


Figure 10. Variation of G_I & G_{II} versus pressure ratio, numerical and finite element method are used, temperature dependent properties, $a=20h$.

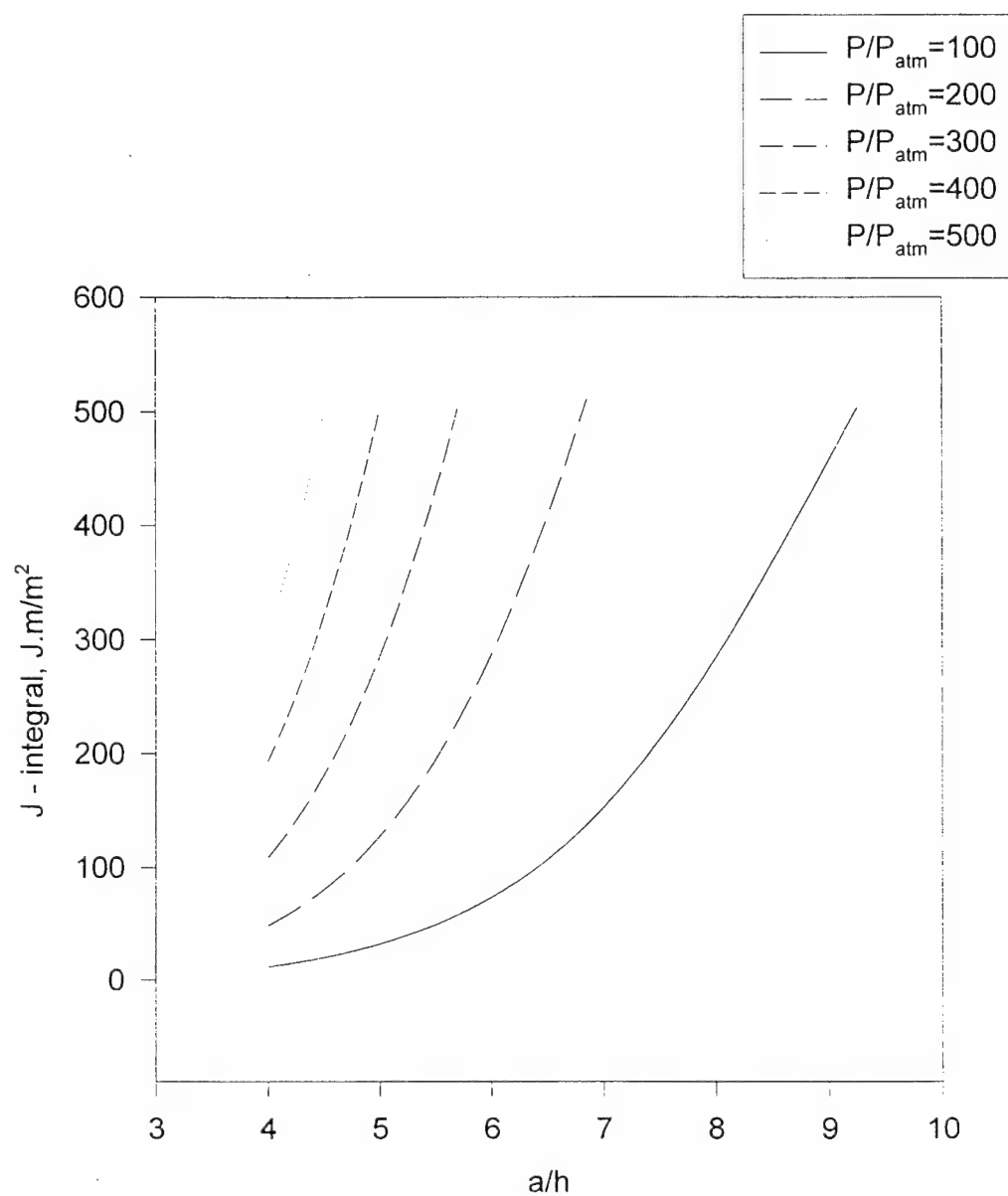


Figure 11. Variation of G versus delamination radius at different pressure ratio, numerical and temperature dependent properties are used.

Submitted to the J. Materials Science, U.K. October, 1996. *Accepted July, 1997*

**CHRONOLOGICAL EVALUATION OF INTERFACIAL DAMAGE
IN TBC DUE TO THERMAL CYCLING**

Z. A. Chaudhury¹, G. M. Newaz¹, S. Q. Nusier¹, T. Ahmed² and R. L. Thomas²

Mechanical Engineering Department¹, Institute of Materials Research²

Wayne State University, Detroit, MI 48202, USA

and

K. P. Wright

General Electric Aircraft Engines

Evendale, OH 45215, USA

ABSTRACT

A two layer Electron Beam-Physical Vapor Deposited (EV-PVD) Thermal Barrier Coating (TBC) on a single crystal superalloy (Rene' N5) substrate was characterized prior to and after thermal cycling at 2, 18, 25, 44, 50, 75, 100, 110, 150 and 175 cycles in between 200 C-1177 C. Optical microscopy, scanning electron microscopy and thermal wave imaging techniques were used to characterize the interfacial damage. Pt-Al was used as bond coat and 8 wt.% YSZ was used as outer top layer. Interfacial cracking was observed even at 2 thermal cycles. Thermally Grown Oxide (TGO) layer increased with the number of thermal cycles. After numerous cycles over 100, interfacial separation was observed to be higher at the middle than at the edges of the sample. This observation is consistent with buckling induced delamination - a possible mechanism for spallation.

CHRONOLOGICAL EVALUATION OF INTERFACIAL DAMAGE IN TBC DUE TO THERMAL CYCLING

Z. A. Chaudhury¹, G. M. Newaz¹, S. Q. Nusier¹, T. Ahmed² and R. L. Thomas²

Mechanical Engineering Department¹, Institute of Materials Research²

Wayne State University, Detroit, MI 48202, USA

and

K. P. Wright

General Electric Aircraft Engines

Evendale, OH 45215, USA

1. Introduction

Different turbine engine components are using thermal barrier coatings(TBCs) in order to increase the life of the metal parts and to improve the operating temperature. TBCs offer a number of benefits including up to 145 C metal temperature reduction, significant fuel savings and improved durability [1, 2]. Other advantages and improvements of TBCs on the turbine blades are to increase the turbine thermal efficiency due to a higher stator outlet temperature, increase the compressor efficiency due to a reduced air flow for the turbine cooling, longer service life of the metallic substrate due to a decreased thermal fatigue load. TBCs consist of a thermally insulating zirconia ceramic overlayer applied over a metallic bond coat which protects the substrate from oxidation and hot corrosion during high temperature operations.

Several coating methods are available. Of them Plasma Spray and Electron-Beam Physical Vapor Deposition (EB-PVD) processes are very popular for their various advantages. EB-PVD has been successfully used to coat turbine airfoils [3]. EB-PVD ceramic structure is highly columnar with the columns aligned perpendicular to the metal-ceramic interface. Due to columnar microstructure in EB-PVD system, the coatings become strain tolerant. The reason for this is that the coatings can accommodate the applied thermal strain by movement between the columnar growth structures [2]. In EB-PVD technique a small piece of ceramic material such as 8 wt.% YSZ is evaporated by an electron beam in a vacuum chamber. The ceramic vapor cloud condenses on the surfaces of the component, which is rotated and controlled in the vapor cloud to form the coating. Power to evaporate the ceramic coating material is provided by a high-energy electron beam gun. Feeders, electron beam gun, temperature and gas should be controlled very carefully.

Calculations indicate that 0.25 mm thick layer of zirconia can reduce metal temperature by as much as 170 C depending on local heat flux [1, 4]. This relative temperature reduction can provide significant benefits [1, 2] in the form of either component durability extension or system performance improvement. The most widely used TBCs are based on zirconia (zirconium dioxide), which shows thermal expansion characteristic similar to superalloys. Zirconia offers a good compromise with a low thermal conductivity about (2 W/mK like 3 to 7% of superalloy) and a high thermal expansion coefficient ($\sim 10 \times 10^{-6} \text{K}^{-1}$) [5]. Yttria Stabilized Zirconia (YSZ) coatings constitute the current state of the art of TBCs [6].

Bond coat compositions started from early Ni-Cr and Ni-Al compositions to the presently used MCrAlX (M=Ni or Cr or both, X=Hf, Zr or Al) and Pt-Al compositions. Pt-Al diffusion coating has been developed due to demands on coatings for gas turbine engines, that must operate at significantly higher temperatures than required previously. Pt-Al is also cheaper in the long run process. Oxidation behavior of platinum-modified aluminide coating and platinum -aluminum alloys has been reported by other investigators [7, 8].

The function of the bond coat in a TBC system is to provide good adhesion between the metal substrate and the ceramic top coat while providing good oxidation protection to the underlying substrate alloy. During thermal exposure, this bond coat oxidizes and forms an aluminum oxide layer between the ceramic and the bond coat. Oxidation plays a dominant role in the failure of graded thermal barrier coatings as confirmed by many researchers [9-12]. Oxidation of the bond coat has been proposed [13] as a life limiting factor of TBCs. Numerous studies have shown that oxidation of bond coat can significantly affect spalling [14-17].

Depending on the temperature range to which thermal barrier coatings are exposed, different types of failure modes have been observed. Bond coat oxidation and damage initiation is common for high temperature applications [18-20]. On the other hand for low temperature applications thermal cyclic stresses which occur during engine operation is believed to be responsible for coating delamination and spallation [21]. For long term successful use of the turbine components, the durability of the TBC must be maintained. Due to improvements in processing condition and coating materials,

significant advances in coating durability have been realized [22-28]. Stress calculations have indicated that high rates of heating and cooling has a more destructive influence on ceramic coating life than isothermal exposure at temperature [29]. Substrate temperature is important in TBC behavior. Thermal cycle life of TBC decrease dramatically due to higher substrate temperature [30-31]. Compressive stresses are also believed to be responsible for TBC failure which occur in the ceramic layer during cooling [14, 29]. The mechanism involves buckling of TBC due to compressive residual stress which results in spallation. These stresses can be attributed to the thermal expansion mismatch between the ceramic top coat and the metal bond coat[32-35]. Extensive research work on TBCs have been reported in the literature [36-46]. The basic causes of TBC failure and the effect of TGO on delamination is still not clear. As a part of our continued research program on an investigation with focus on damage accumulation mechanisms in thermal barrier coated single crystal substrate [47-49], a number of thermal cycling tests have been carried out, evaluated and analyzed to determine the causes of coating failure and delamination. In this article, we present a chronological sequence of damage and oxidation evolution at the bond coat and TBC interface.

2. Experimental Procedure

The TBC specimens were 25.4 mm diameter by 3.17 mm thick button samples of nickel base superalloys Rene' N5. There are two coats. One is the top coat which is the EB-PVD thermally insulating outer ceramic layer and the other is the bond coat which is a

diffusion aluminide Pt-Al alloy. This bond coat protects the alloy substrate from oxidation and bonds very well to both the alloy substrate and the outer EB-PVD thermally insulating layer. The outer layer TBC has been the 8 wt.% YSZ. The thickness of the outer top coat is 0.127 mm and that of bond coat is 0.0482 mm. The outer ceramic top coat is used for its chemical and thermal stability as well as low thermal conductivity and relatively high coefficient of thermal expansion. Several researchers have worked on this material systems between 150 C-1200 C. A number of coated specimens were placed in a muffle-type rapid heating/cooling furnace and thermally cycled to 2, 18, 25, 42, 50, 75, 100, 110, 150, and 175 cycles in the range of (200 C- 1177 C). The holding time was 45 minutes at the peak temperature in each cycle. The rate of heating was 9 minutes to reach to the peak temperature and the rate of cooling was 10 minutes to reach to the lower temperature of the cycles. Figure 1 shows the temperature profile of the thermal cycle tests.

A number of samples were taken out after a certain number of thermal cycles. These samples did not fail. The thermally cycled samples were potted by using cold mounting epoxide resin. After curing for one day, the specimens were cut by using a Buheler Isomet 2000 diamond cutter. The samples were then grinded and polished by using normal metallurgical procedures. The polished samples were observed under Olympus BX 60 optical microscope. Scanning Electron Microscopy was carried by using a Hitachi 2000 SEM on the polished samples to observe interfacial damage/crack propagation at the ceramic top coat and bond coat interface and morphology of the thermally grown oxide (TGO) layer at higher magnification. Thermal wave images were taken on the surface of

the thermally cycled and untested samples in order to identify any damage at the ceramic top coat and bond coat interface.

3. Results and Discussions

3.1 Thermal Cycling of TBC samples

Figure 2 shows the photomicrograph of a thermal barrier coated sample without any thermal cycling. No interfacial cracking and oxidation product (TGO) were observed at the bond coat/top coat (TBC) interface. Thermally cycled TBC samples in air leads to the formation of a reaction product layer and interfacial cracking/damage at the bond coat/top coat interface. This oxidation product (TGO) is Al_2O_3 and has been confirmed by many researchers [47, 48, 51, 52]. Interdiffusion of bond coat and substrate elements at elevated temperature does occur [53] and their effect on TBC failure is still not clear. Migration of aluminum from bond coat into the substrate can change the oxidation behavior of the bond coat and sometimes may be responsible for the formation of less adherent oxide species. A few number of thermal cycles leads to the formation of interfacial cracking at the bond coat/top coat interface and with increasing the number of cycles leads to the formation of both interfacial cracking and TGO layer. Figures 3 (a) and 3 (b) show the photomicrographs of the interfacial cracking at the bond coat/top coat interface taken after 2 and 18 thermal cycles. TGO layer just started growing at 18 thermal cycles. The length of the interfacial crack was typically 600 μm and the thickness of the crack was 3 μm . The TGO layer starts growing with increasing the number of thermal

cycles. Figures 3(c)-(d), 4 (a)-(c), 5 and 6(a)-6(b) show the chronological evaluation of interfacial damage in TBC due to thermal cycling at 25, 42, 50, 75, 100, 110 and 175 cycles. The thickness of the TGO layer grows with increasing the number of cycles. Figure 4 (c) shows separation through the TGO layer. In figure 5, interfacial cracking at the bond coat/top coat interface are increased and TGO layer is quite visible through the interfacial cracking. Interfacial cracking is showing a sinusoidal nature. In Figures 6 (a)-6 (b), complete separation through TGO layer is observed. This TGO layer/separation is very high at the center and small at the edges of the TBC sample. The thickness of this separation at the center is roughly double than at the edges which is $\sim 85.5 \mu\text{m}$ at the center and $\sim 42.9 \mu\text{m}$ at the edges. Figure 7 shows the schematic cross-section and photomicrographs of TBC specimen showing interfacial separation through TGO layer after 150 thermal cycles. The TGO layer is thicker at the middle and thinner at the edges of the specimen. A large interfacial delamination crack is needed for buckling induced spallation to occur. Current understanding [9, 12] and from the Figures 5, 6 (a)-6 (b), and 7 it is now clear that buckling induced delamination is a possible mechanism for spallation.

3.2 Scanning Electron Microscopy (SEM)

Scanning Electron Microscopy is a very good tool for materials characterization at higher magnifications. Sample preparation for SEM is simple. SEM was done on all the thermally cycled samples. Figures 8(a)-(c) show the high magnification SEM micrographs taken from the specimens thermally cycled at 25, 50 and 150 cycles. At 25 thermal cycles, separation through TGO layer is quite prominent as shown in the micrograph 8(a). In

micrograph 8(b), voids and microcracks are seen and TBC seems to be spalling out. Figure 8 (c) shows the microcrack and big separation. Interfacial damage is very large in this situation.

3.3 Nondestructive Evaluation Using Thermal Wave Imaging (TWI)

Microscopy is a destructive technique and time consuming. TWI on the other hand can provide a good assessment of damage due to thermal loading without any destruction of the samples. It is clean, cheap and much faster than microscopy.

The thermal wave imaging method is based on the idea in which a time-dependent heat source at the surface of an object launches waves of heat into the object in the form of heat diffusion, called thermal waves. The thermal waves are scattered from subsurface defects or anomalies in much the same way that sound waves reflect from such defects and, upon returning to the surface of the object, modify the temperature of the surface map. Figure 9 shows the schematic experimental setup for thermal wave imaging[54]. In the usual configuration, high power flash lamps are used to pulse-heat the surface of the object under inspection. This causes a plane thermal wave pulse to propagate into the material from the heated surface. As this pulse encounters subsurface material defects, each defect scatters a fraction of the pulse back towards the surface. When these scattered pulses or thermal waves arrive back at the surface, they modify the time dependent temperature distribution on the surface, with signal from defects at different depths affecting the surface temperature at different times. During the process, the evolving surface temperature distribution is imaged by an infrared video camera as function of time.

Through the use of fast image processing hardware and software, the system's computer memory stores a sequence of gated images corresponding to the various times after the flash heating. The result is a series of thermal wave images corresponding to various depths beneath the surface. The time after the onset of the flash heating at which defects from various depths beneath the surface can be observed depends on the depth and the thermal diffusivity of the specimen under inspection.

Figure 10 (a) shows the thermal wave image of four samples at 0, 25, 50 and 100 thermal cycling respectively from left to right. In this image the color map representation is as follows: blue is low thermal wave signal amplitude, followed by green and yellow indicating increasing thermal wave signal amplitude respectively and red being the higher thermal wave signal amplitude. The corresponding surface temperature profile plots shown on the right hand side of the figure represents the relative amplitude plotted as function of position or distance across the center of the samples. The plot indicates that the thermal wave signal amplitude increases 100% from 0 thermal cycling to 25 thermal cycling, while the change in the thermal wave signal amplitude from 25 thermal cycling to 50 thermal cycling is only 10% for each case. Figure 10 (b) shows the thermal wave image of a second set of samples at 0, 150 and 175 thermal cycling respectively from left to right. The color map used is identical to the one in figure 10(a). The corresponding surface temperature profile shows that the thermal wave signal amplitude increases 150% from 0 thermal cycling to 150 thermal cycling, however, the thermal wave signal amplitudes of the 150 thermal cycling and 175 thermal cycling samples are identical. As the number of thermal cycles increases, the damage at the bond coat/top coat interface are

also increased. The damage thickness may also change depending on the number of thermal cycles. This damage thickness may be responsible for the thermal wave signal amplitude to vary.

4. Conclusions

Based on our present investigation, the following conclusions may be drawn:

- (1). Microcracks may occur early due to thermal cycles. A number of microcracks were observed only after 2 cycles (200 C-1177 C) in the bond coat near the TBC/bond coat interface.
- (2). The TGO layer continues to grow with higher the number of thermal cycles. However, there is a substantial interaction of TGO layer and damage at higher number of cycles.
- (3). There appears to be a transition from low scale distribution damage (microcracks that are separate) to more extensive interlinked damage (microcracks that have connected) around 100 cycles.
- (4). Interfacial separation between bond coat and TBC increases with increasing the number of thermal cycles. This separation is higher at the center and lower at edges of the sample. The separation has been estimated to be 85 μm for 175 thermal cycles. This separation is twice the separation measured at the edges of the sample.

(5). Based on current evidence and from our previous investigation [50], it can be concluded that buckling induced delamination is a possible mechanism for spallation.

(6). Thermal wave imaging technique is potential NDE tool to assess the degradation in TBC system.

Acknowledgements

This program was funded by Air Force Office of Scientific Research - grant # F 49620-95 -1-0201 (Dr. Walter Jones is the Program Monitor).

References

1. R. A. Miller, and C. E., Lowell, Thin Solid Films, 99, (1982) 265.
2. K. D. Sheffler, and D. K. Gupta, The American Society of Mechanical Engineers, 88-GT-286
3. E. Demaray, DOE Contract DE-AC-06-76RL01830, 1982 (Department of Energy).
4. D. S. Duvall, 1982, Proceedings from the Second Conference on Advanced Materials for Fuel Capable Heat Engines, Electric Power Research Institute, Palo Alto, CA EPRI-RD-2396-SR, pp 6-102.
5. M. F. Stroosnijder, M. J. Bennet, R. Mevrel, Advanced Technologies for Surface Engineering (1992), 335.
6. C. Mertens, D. Muck, and J. Garcia, Materials for Advanced Power Engineering, Part II, 1994, 1313.
7. M. Gobel, A. Ramel, M. Schutze, M. Schorr and W. T. Wu, Materials at High

- Temperature, 12, No. 4, (1994) 301.
8. E. J. Felten and F. S. Pettit, Oxidation of Metals, 10, No. 3, (1976) 189.
 9. H. E. Evans, Materials Science and Engineering, A120 (1989), 139.
 10. R. A. Miller and C.E. Lowell, Thin Solid Films, 95 (1982), 265.
 11. W. R. Sevick and B.L. Stoner, NASA Contractor Report, CR-135360, 1978.
 12. A. G. Evans, G. B. Grumley and R. F. Demary, Oxidation of Metals, 20, 5-6 (1983), 193.
 13. J. R. Springaran, B. E. Jacobson and W. D. Nix, Thin Solid Films, 45, (1977), 507.
 14. R. A. Miller, and C. E. Lowel, NASA TM-82905 (1982).
 15. S. Stecura, NASA TM-79206, (1979).
 16. M. A. Gedwill, NASA TM-81567, (1980).
 17. R. A. Miller, and C. Berndt, NASA TM-83663, (1984).
 18. C. H. Liebert and R. Miller, I & EC Product Research and Development, Sept. (1984), 334.
 19. S. R. Levine, R. Miller, and P. E. Hodge, Sampe Quarterly, 12, Oct. (1980), 20.
 20. S. R. Levine and R. Miller, Research and Development, 26, Mar. (1984), 122.
 21. Y. R. Takeuchi, and K. Kokini, Transactions of the ASME, 116, Jan. (1994), 266.
 22. Proceedings of the Coatings for Advanced Heat Engines workshop, US DOE, Castine, Maine, (1987).
 23. Proceedings of the 1992 Coatings for advanced Heat Engines Workshop, US DOE Monterey, California, (1992).
 24. J. T. DeMasi, K. D. Sheffler and M. Ortiz, NASA Contractor Report 182230, prepared for NASA under contract NAS3-239544, December, (1989).

25. S. M. Meier, D. M. Nissley and K. D. Sheffler, NASA Contractor Report 189111, prepared for NASA under Contract NAS3-23944, July (1991).
26. R. A. Miller, W. J. Brindley, J. G. Goedjen, R. Tiwari, D. Mess, Proceedings of the 7th National Thermal Spray Conference, Boston, Massachusetts, June 20-24, (1994).
27. R. A. Miller, R. G. Garlick, J. L. Smialek, American Ceramic Society Bulletin, 62(12), December 1983.
28. R. A. Miller and W. J. Brindley, Proceedings of the International Thermal Spray Conference & Exposition, Orlando, Florida, May 28 - June 5, (1992).
29. G. McDonald, and R. C. Hendricks, NASA TM-81480, (1980).
30. J. W. Watson, and S. R. Levine, NASA TM 83670, (1980).
31. 1983 Independent Research and Development Plan, General Electric Company, Aircraft Engine Business Group, R83 AEB263, Vol V, (1983).
32. S. Rangaswamy, H. Herman and S. Safi, Thin Solid Films, 73, (1980), 43.
33. P. F. Becher, R. W. Rice, C. C. Wu, and R. L. Jones, Thin Solid Films, 53, (1978) 225.
34. R. C. Bill, NASA TM-81732, (1981).
35. R. L. Mullen, G. McDonald, R. C. Hendricks, and M. Hofle, NASA TM-83460, (1983).
36. J. R. Springaran, B. E. Jacobson and W. D. Nix, Thin Solid Films, 45, (1977), 507.
37. C. A. Anderson, R. J. Bratton, S. K. Lau and S. Y. Lee, International Conference on Metallurgical Coatings, San Diego, California, Elsevier Sequoias, Laussane, April, (1980).
38. R. A. Miller, S. R. Levine and P. E. Hodge, Proc. 4th Intl. Symp. on Superalloys, Seven Springs, PA, September, 1980, ASM, Metals Park, OH, (1980), 473.
39. R. A. Miller, S. R. Levine and S. Stecura, AIAA Meeting, Pasadena, CA, Jan., (1980),

Paper # AIAA 80-0302.

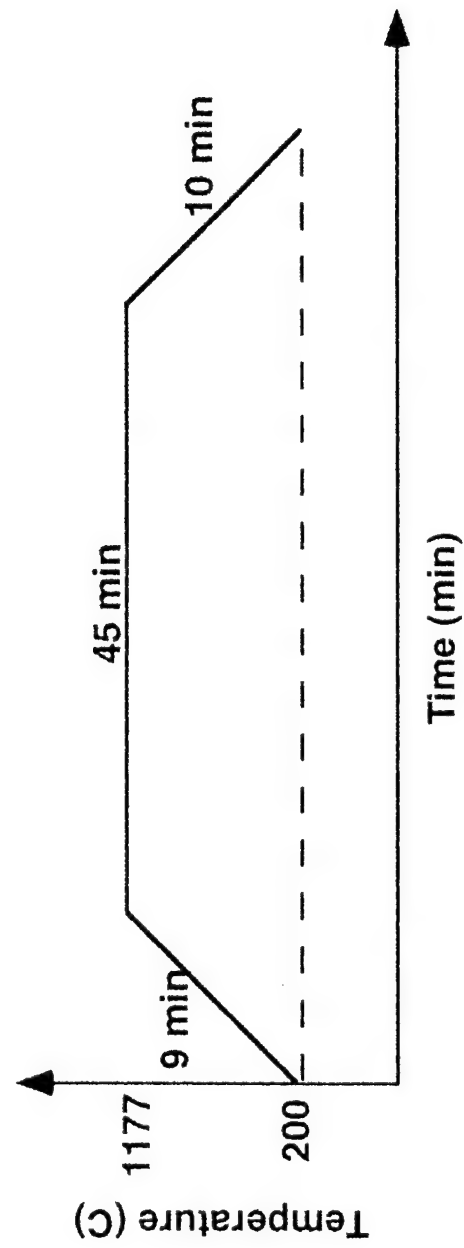
40. S. Stecura, Intl. Conf. on Metallurgical Coatings, San Diego, Elsevier Sequoia, April, (1980), 481.
41. N. R. Sankar, C. C. Brendt, H. Herman, Ceramic Eng. Sci. and Proc., 4, (1983), 784.
42. C. H. Liebert, Thin Solid Films, 64, (1979), 329.
43. R. C. Hendricks, G. McDonald and R. L. Mullen, Ceramic Eng. Sci. and Proc., 4, (1983), 802.
44. Proceedings of the 1987 Coatings for Advanced Heat Engines Workshop, US DOE, Castine, Maine, (1987).
45. Proceedings of the 1992 Coatings for Advanced Heat Engines Workshop, US DOE, Monterey, California.
46. R. V. Lang, F. Jamarni, K. L. Yan and M. N. Korotkin, 3rd Intl. SAMPE Metals Conference, October, (1992).
47. Z. A. Chaudhury, G. M. Newaz, and T. Ahmed, J. of Materials Letters, (1996) (submitted)
48. Z. A. Chaudhury, G. M. Newaz, S. Q. Nusier and T. Ahmed, J. of Materials Science and Engineering, (1996), (submitted).
49. Z. A. Chaudhury and G. M. Newaz (unpublished work).
50. G. M. Newaz, S. Q. Nusier, Z. A. Chaudhury and K. P. Wright, J. Eng. Mat. and Tech., (1996), (submitted).
51. L. Lelait, S. Alperine, R. Mevrel, J. Mat. Sci., 27, (1992) 5.
52. E. Y. Lee, R. R. Biederman, R. D. Sisson, J., Mat. Sci. Eng., A 121 (1989) 467.
53. Siemers, P. A. , and Hillig, W. B., NASA CR-165351, (1981).

54. A. C. Ramamurthy, T. Ahmed, L. D. Favro, R. L. Thomas, David K. Hsu, Review of Progress in Quantitative Nondestructive Evaluation, Vol. 13, Edited by D. O. Thompson and D. E. Chimenti, Plenum Press, New York, (1994).

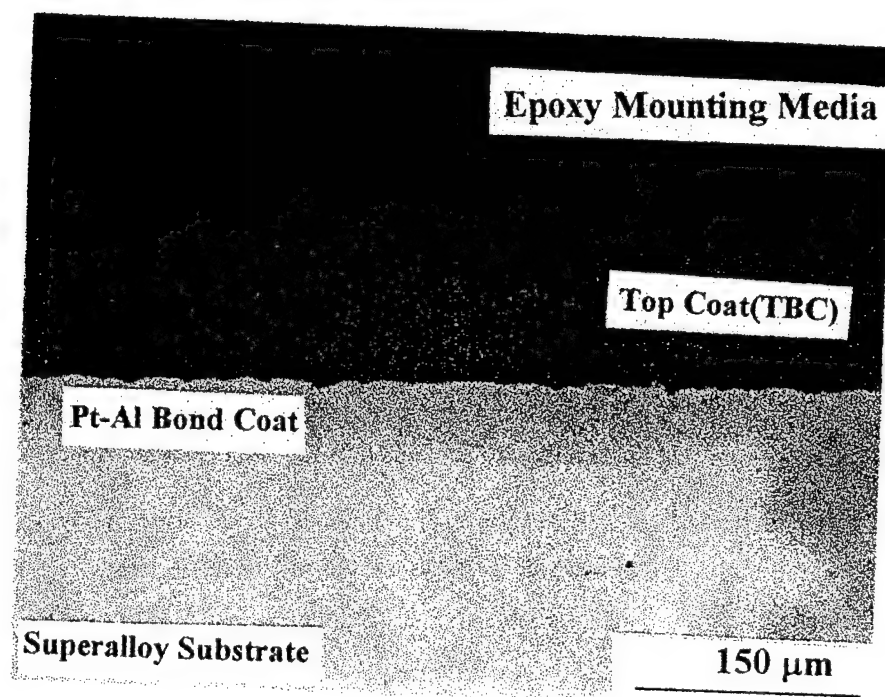
FIGURE CAPTIONS

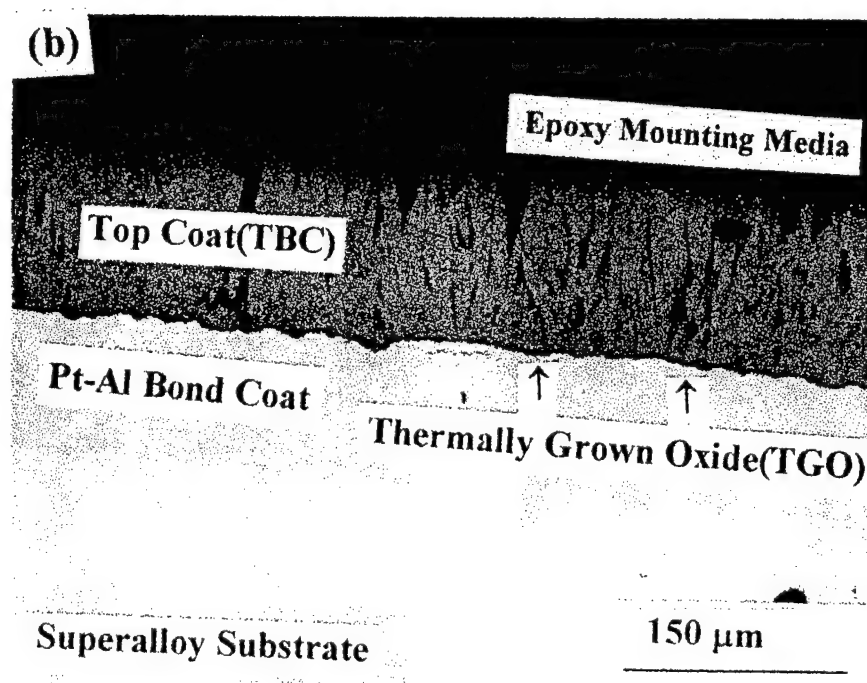
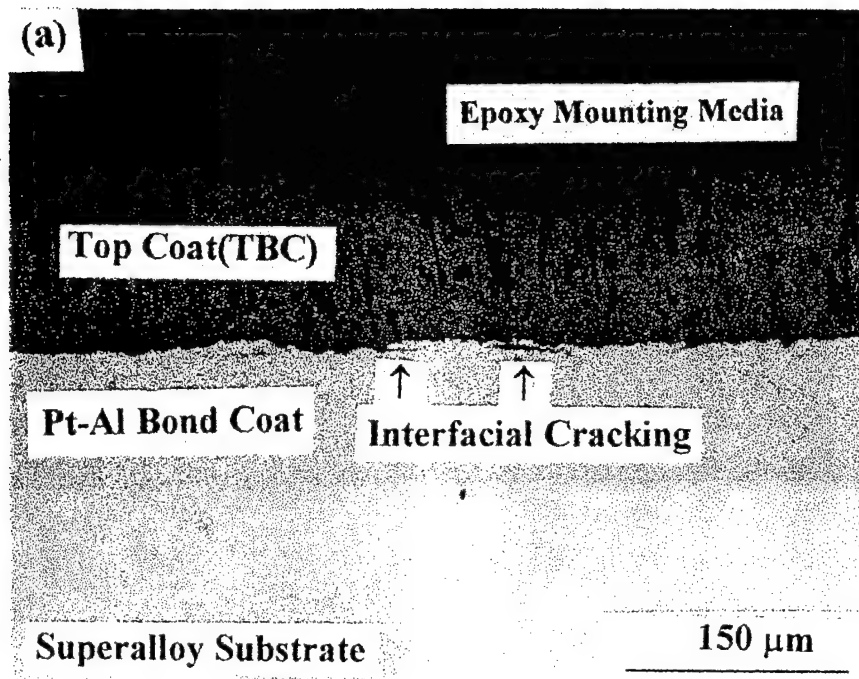
1. Figure 1 shows the temperature profile of the thermal cycle tests conducted in the present investigation.
2. Figure 2 shows an optical micrograph of an untested thermal barrier coated sample. Thermally Grown Oxide (TGO) layer and/or interfacial separation were absent at the bond coat/top coat (TBC) interface.
3. Figures 3.(a) and (b) show the photomicrographs of interfacial cracking at the bond coat/top coat interface taken after 2 and 18 thermal cycles. TGO layer started growing at 18 cycles. Figures 3 (c) and (d) show the chronological evaluation of interfacial damage in TBC due to thermal cycling at 25 and 42 cycles.
4. Figures 4(a), (b) and (c) are the optical micrographs showing the chronological evaluation of interfacial damage in TBC due to thermal cycling at 50 and 75 and 100 cycles. Separation through TGO layer is quite visible.
5. Figure 5 shows the photomicrograph of bond coat cracking in between bond coat and TBC after thermal cycled at 110 cycles. TGO layer is visible through the bond coat cracking. This bond coat cracking is sinusoidal nature.
6. Figure 6 (a) and (b) are the optical micrographs showing complete separation through the TGO layer after thermal cycled at 175 cycles. Figure 6 (a) shows the separation at the edge of the specimen and Figure 6(b) shows the separation at the center of the specimen.

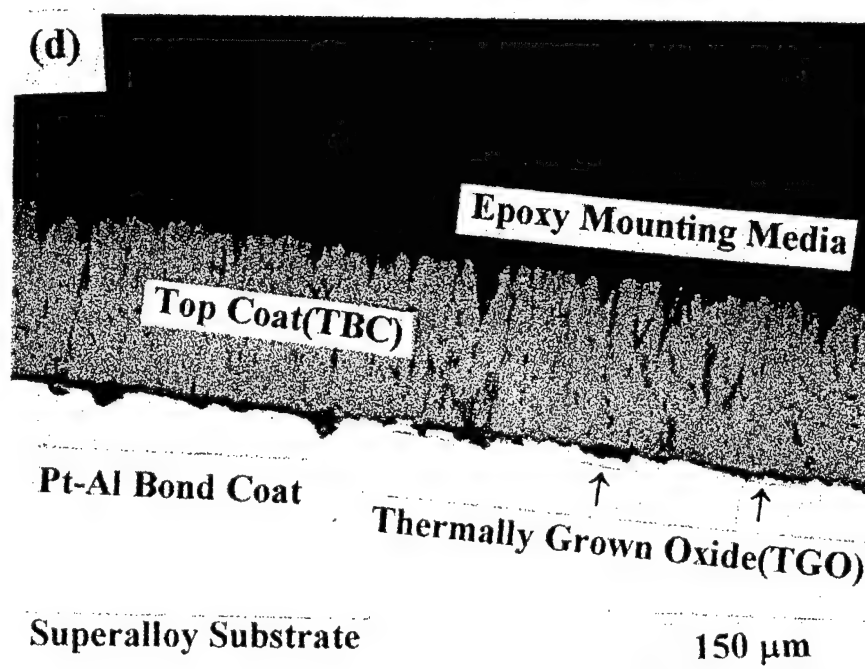
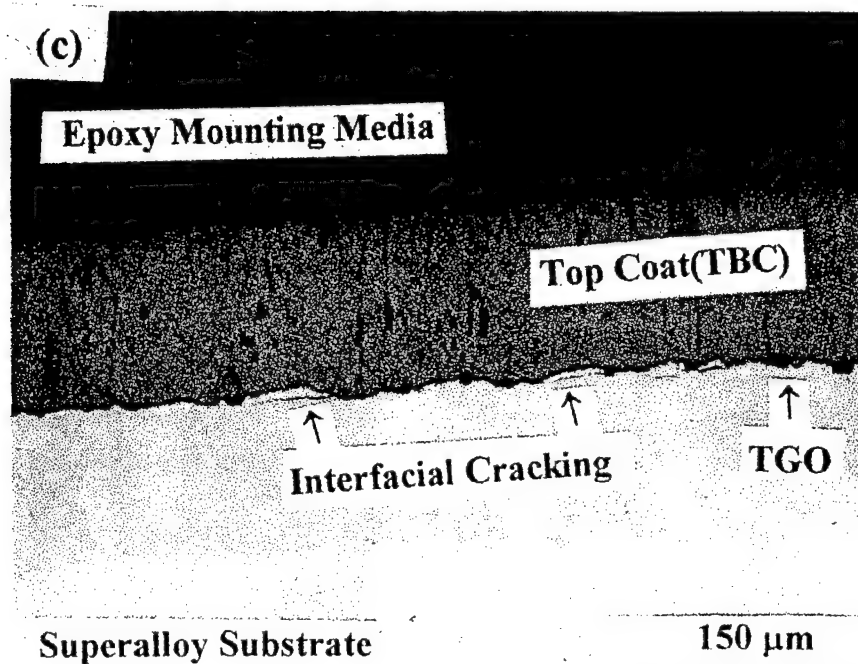
7. Figure 7 show the schematic and photomicrographs of TBC specimen showing interfacial separation through TGO layer after thermal cycled at 150 cycles. The photomicrographs were taken from two edges and center of the specimen.
8. Figure 8 show the scanning electron micrographs taken from the polished TBC specimens after thermal cycled at 25, 50 and 150 cycles. TGO layer, microcracks, voids and separation through TGO layer are observed in those specimens.
9. Figure 9 shows a schematic experimental setup for thermal wave imaging.
10. Figure 10 (a) shows the thermal wave image of four samples at 0, 25, 50 and 100 thermal cycles and their corresponding surface temperature profile plots respectively. Figure 10 (b) shows the thermal wave image of other set of samples at 0, 150 and 175 cycles and their corresponding surface temperature profile plots.

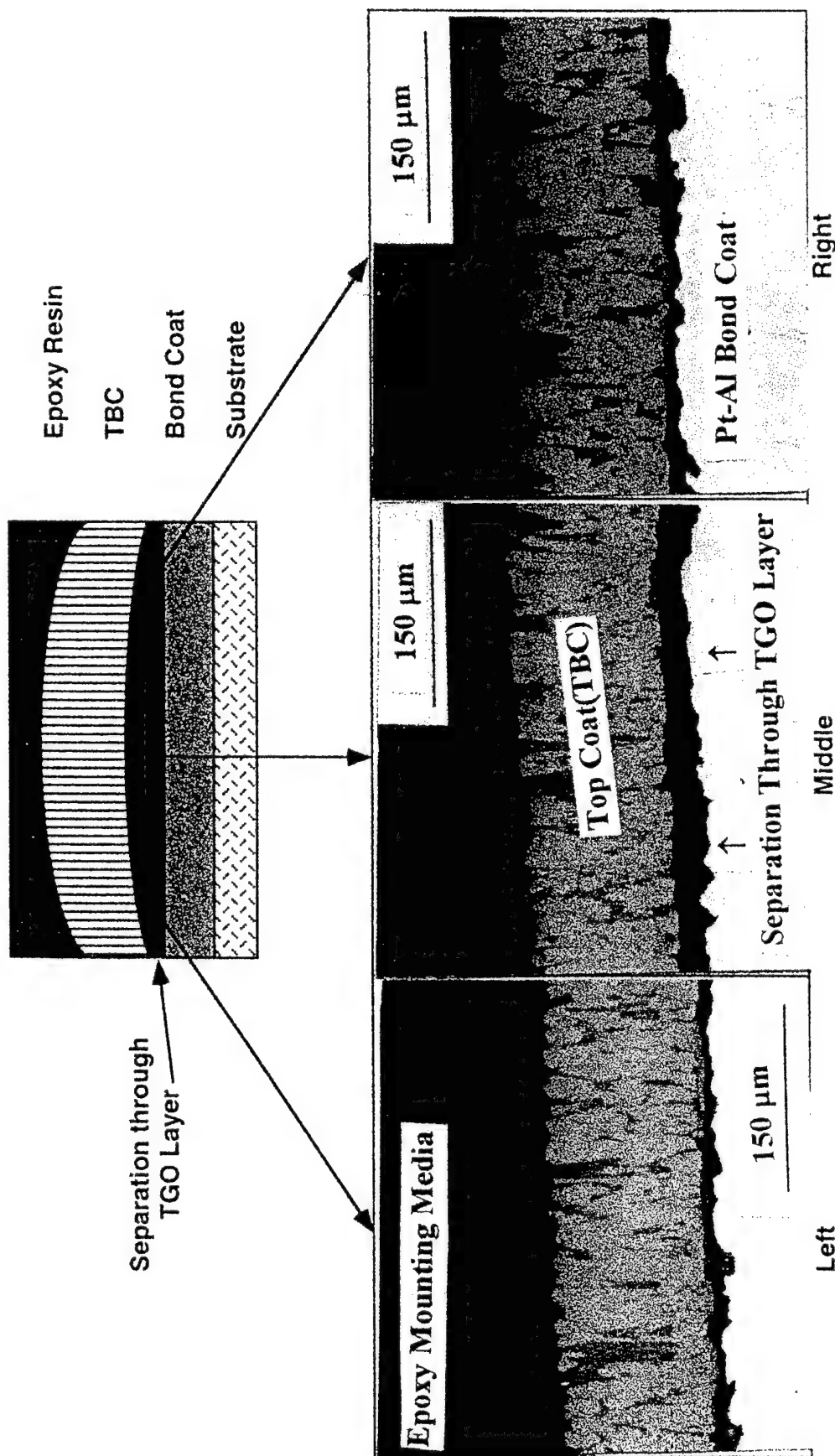


Thermal Cycling Profile

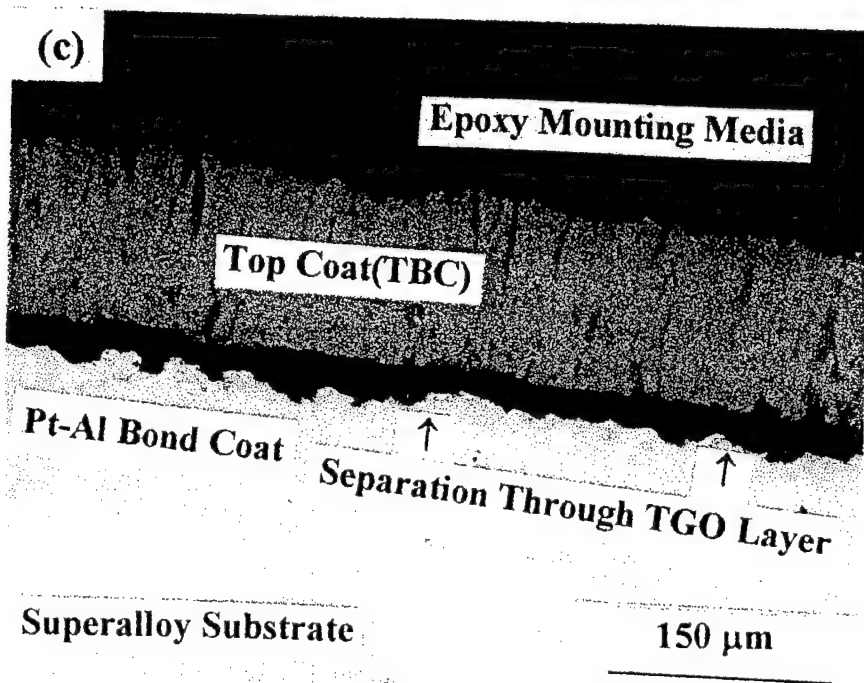








Schematic and photomicrographs of TBC specimen showing interfacial separation through TGO layer



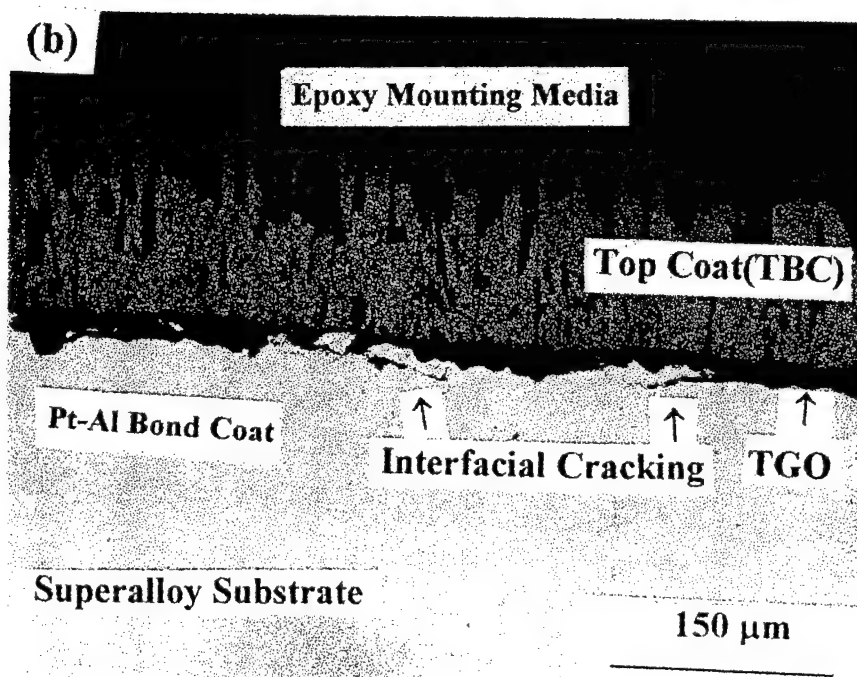
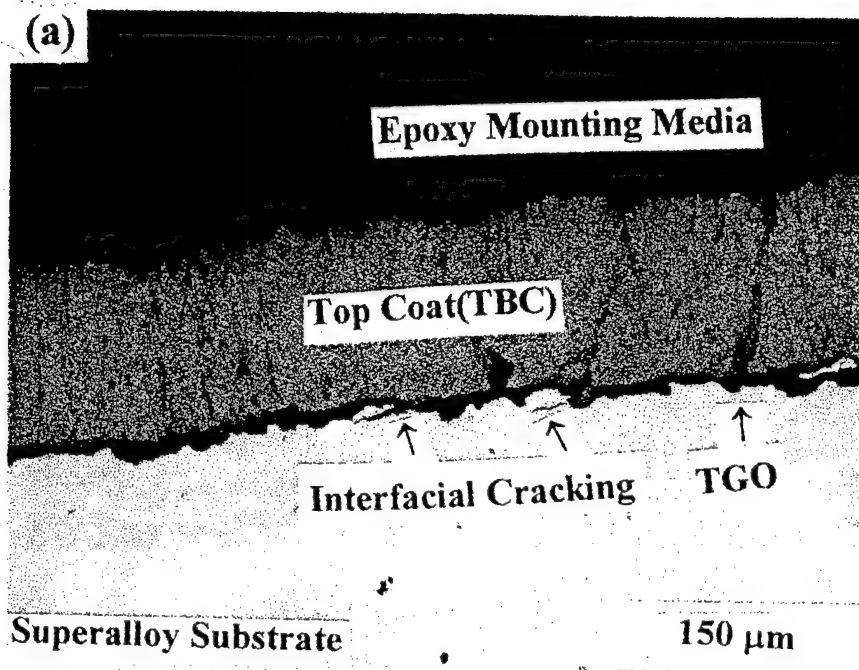
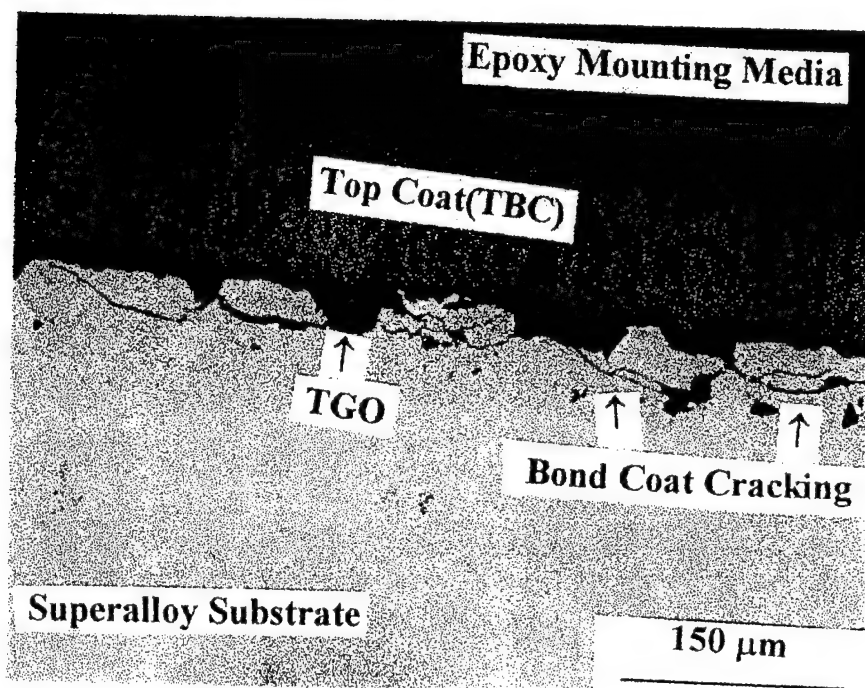
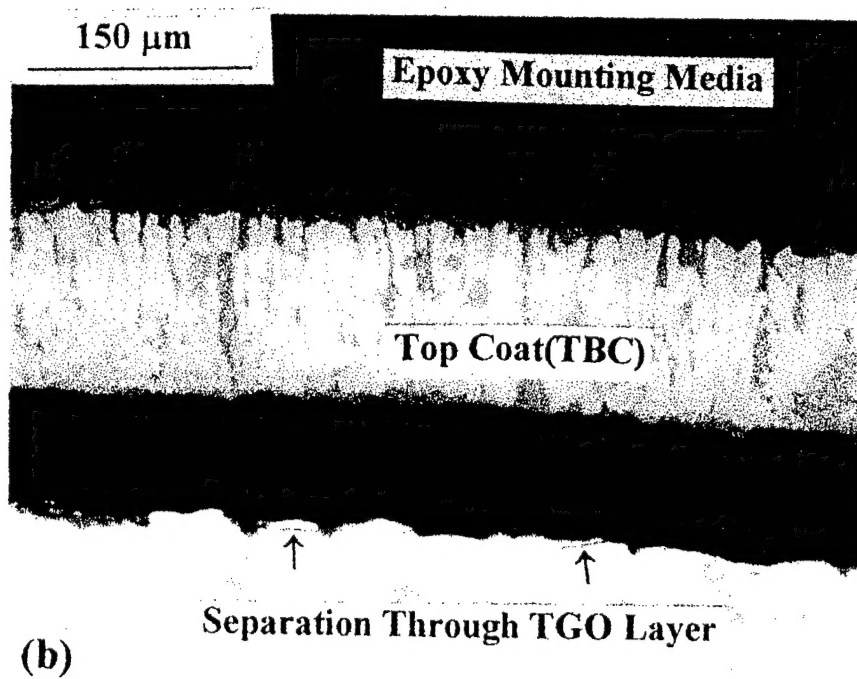
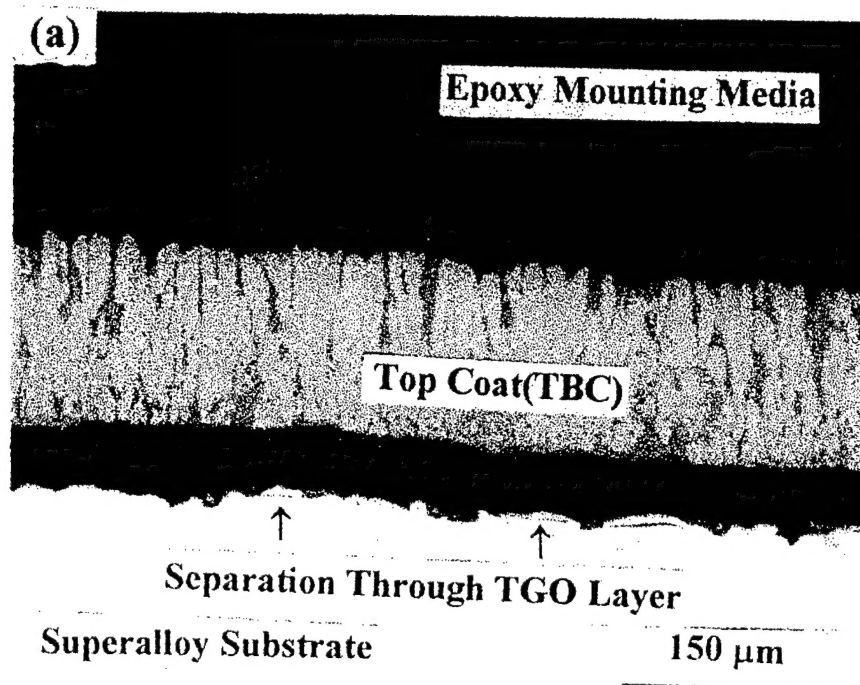
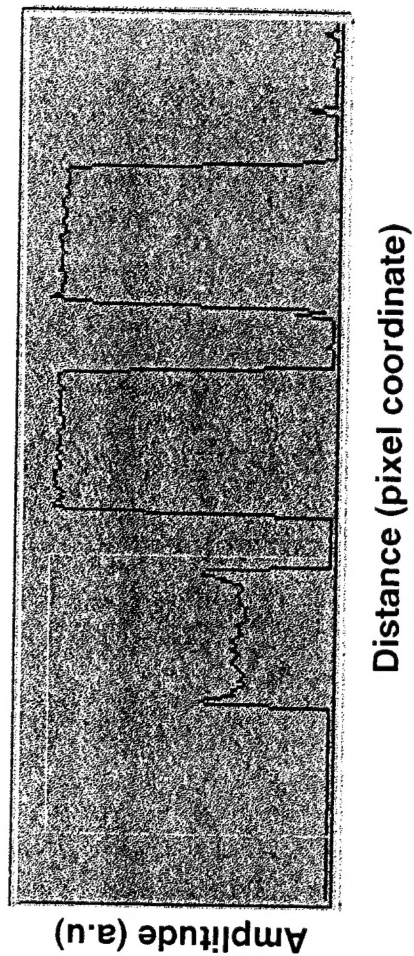
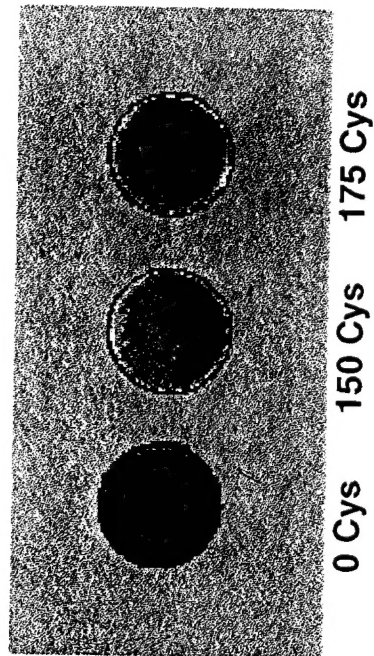
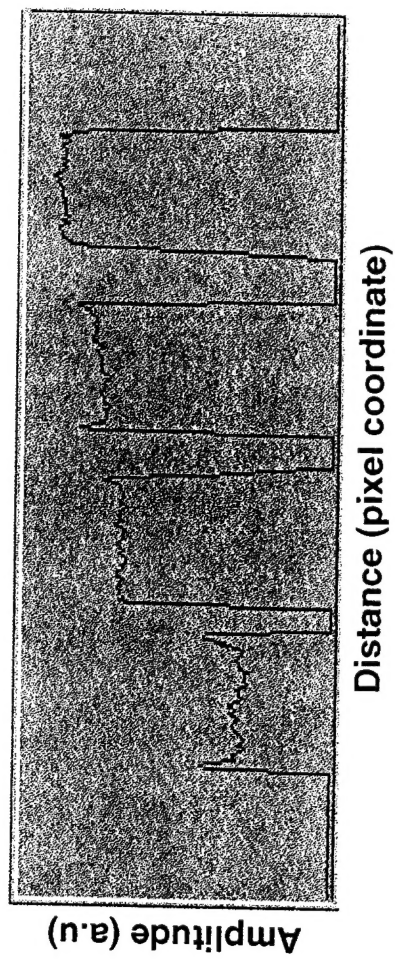
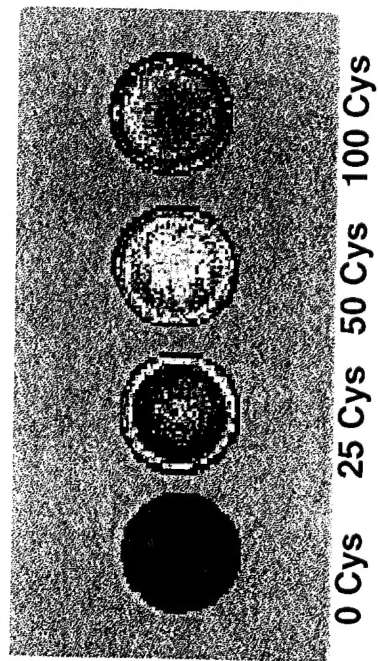


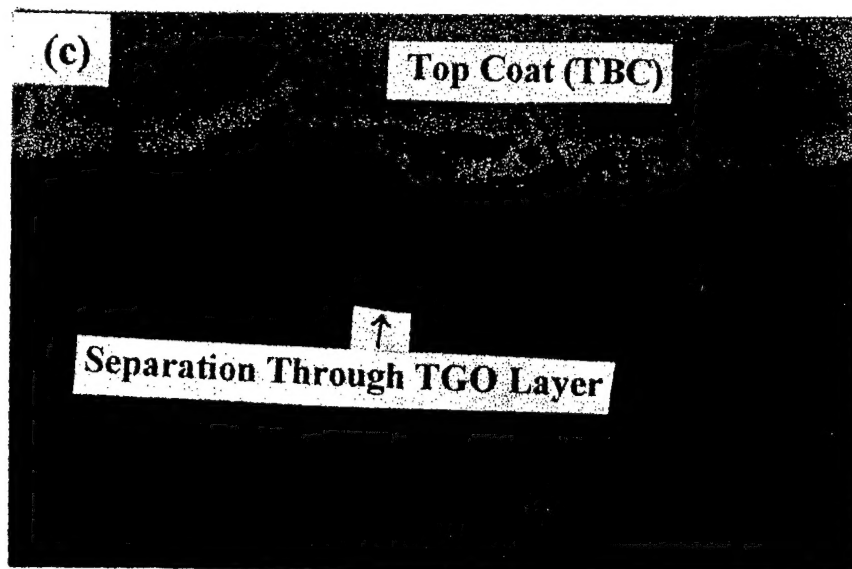
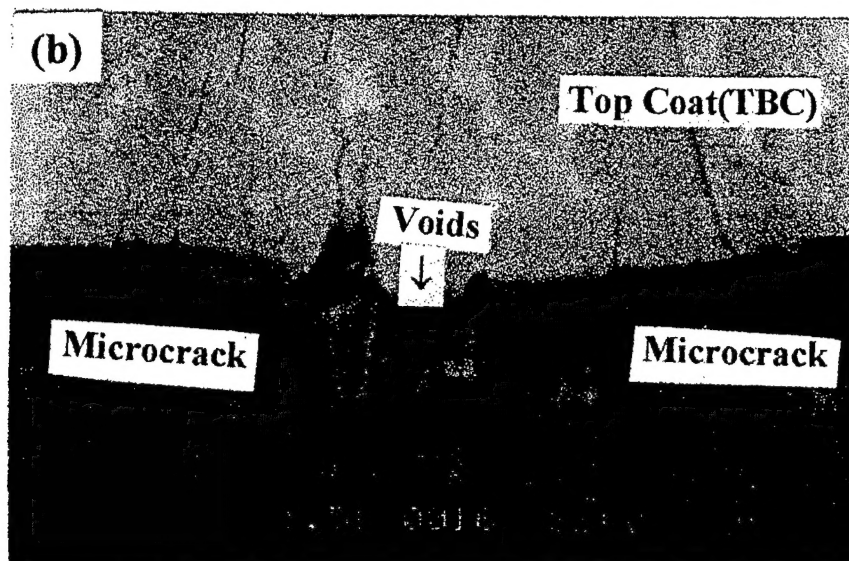
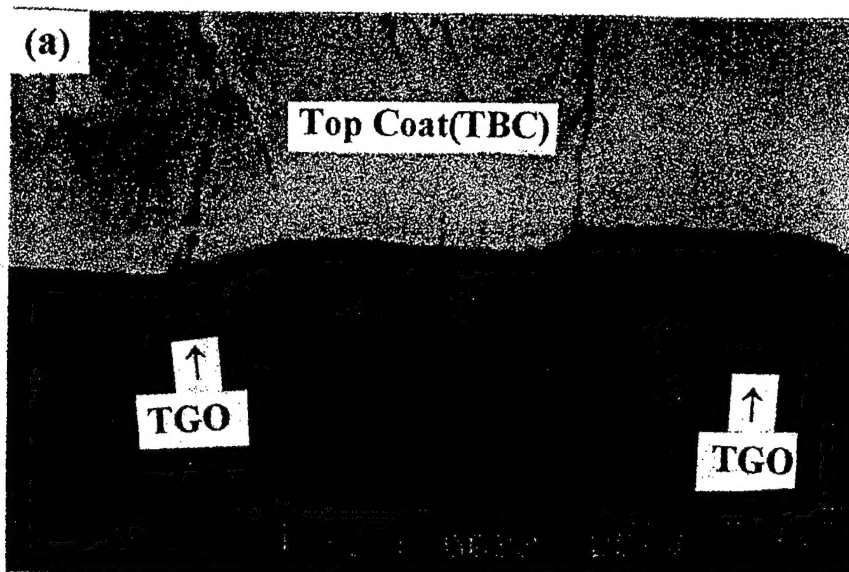
Fig. 4

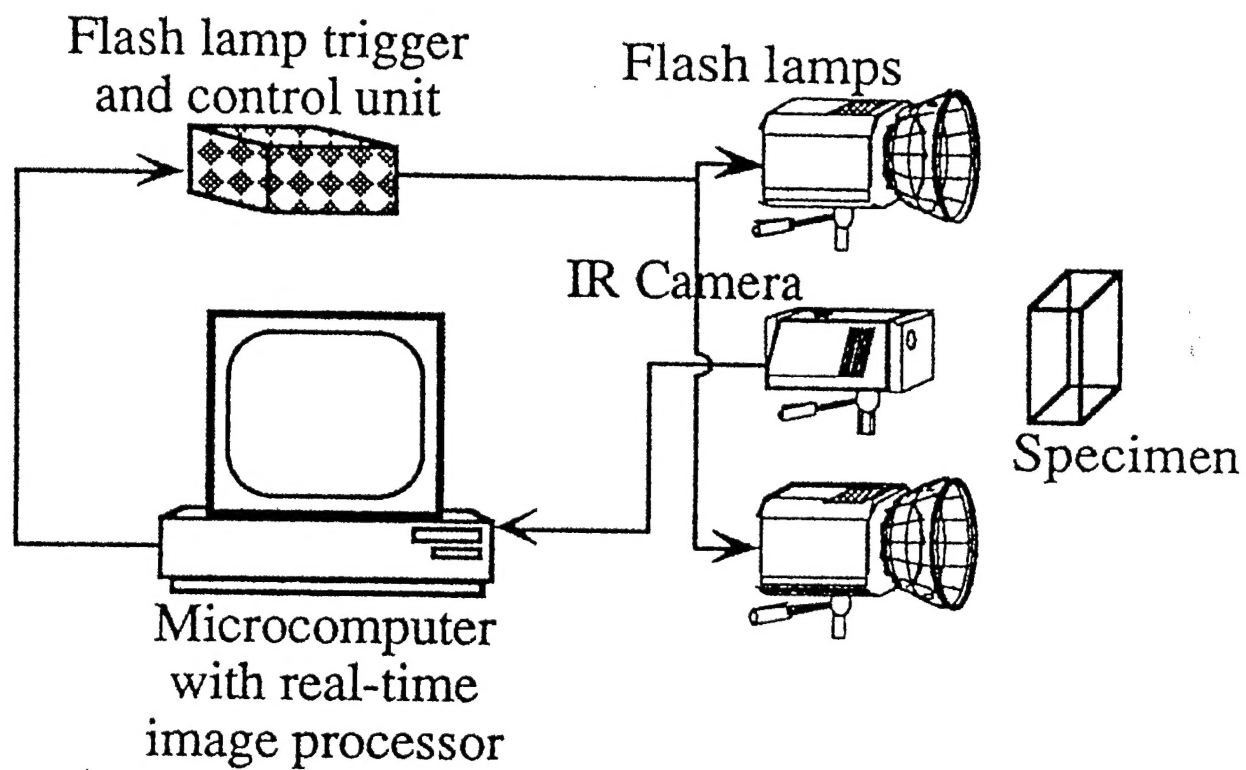




Comparison of thermal wave images at various thermal cycling and corresponding surface temperature profile across the specimens







Experimental setup for thermal wave imaging.